

Si-based anode on three-dimensional carbonaceous substrates for lithium batteries

三次元炭素質基板を用いたリチウム電池用 Si 系負極

February 2017

Seongki AHN

アン ソンギ

Si-based anode on three-dimensional carbonaceous substrates for lithium batteries

三次元炭素質基板を用いたリチウム電池用 Si 系負極

February 2017

Waseda University
Graduate School of Advanced Science and Engineering
Department of Nanoscience and Nanoengineering
Research on Electrochemical Nano-systems

Seongki AHN

アン ソンギ

Supervisor: Prof. Dr. Toshiyuki Momma (Waseda University)

Referees: Prof. Dr. Yoshiyuki Sugahara (Waseda University)
Prof. Dr. Takayuki Homma (Waseda University)
Prof. Dr. Tetsuya Osaka (Waseda University)

Contents

Chapter 1 Geranial introduction

1.1 Background	2
1.2 Lithium ion batteries	4
1.2.1 Components of lithium ion batteries	4
1.2.1.1 Cathode materials	5
1.2.1.2 Separators	9
1.2.1.3 Electrolytes	11
1.2.1.4 Anode materials	
13	
1.3 Anode materials for lithium ion batteries	16
1.3.1 Insertion/de-insertion materials	16
1.3.2 Conversion materials	18
1.3.3 Alloy/de-alloy materials	19
1.4 Si-O-C composites as anode for lithium ion batteries	
23	
1.4.1 Synthesis of Si-O-C composites and its features	
23	
1.4.2 Requirement of Si-O-C composites	
27	
1.5 Strategies of this dissertation	
28	
1.6 References	

Chapter 2 Synthesis of Si-O-C composites using 3D structured carbon paper substrate for high areal capacity lithium secondary battery

2.1 Introduction	34
2.2 Experimental	
35	
2.2.1 SPM treatment of carbon paper	35
2.2.2 Electrodeposition of Si-O-C composites on carbon paper	35
2.2.3 Material measurement of Si-O-C composites	36
2.2.4 Electrochemical measurement of Si-O-C composites	37
2.3 Results and discussions	
37	
2.3.1 Effect of SPM treatment for electrodeposition of Si-O-C composites	37
2.3.2 Evaluation of suitability of PC or EC/DEC as electrolyte	44
2.4 Summary	
50	
2.5 References	
51	

Chapter 3 Preparation of carbon nanotube anchor layer to improve adhesion strength for Si-O-C composite as anode for lithium ion batteries

3.1		Introduction
54		
3.2		Experimental
56		
3.2.1	Fabrication of CNTs anchor layer	
56		
3.2.2	Electrodeposition of Si-O-C composites on carbon paper	
56		
3.2.3	Material characteristics of CNTs anchor layer and Si-O-C composites	57
3.2.4	Electrochemical characteristics of Si-O-C composites	
57		
3.3	Results and discussions	
58		
3.3.1	Evaluation of CNTs/Cu substrate for Si-O-C composites	58
3.3.2	Effect of CNTs anchor layer for Si-O-C composites	
62		
3.3.3	Effect of enhanced adhesion strength by CNTs anchor layer	
74		
3.3.4	Electrochemical properties of LIBs full cell using Si-O-C anode	
81		
3.4		Summary
84		
3.5		References
85		

Chapter 4 Application of Si-O-C as anode for high rate lithium ion capacitor

4.1		Introduction
88		
4.2		Experiment
91		
4.2.1	Fabrication of CNTs cathode by electrophoretic deposition	
91		
4.2.2	Synthesis of Si-O-C composites as anode by electrodeposition	
91		
4.2.3	Material characteristics of Si-O-C composites	
92		
4.2.4	Electrochemical characteristics of Si-O-C composites	
92		
4.3	Results and discussions	
92		
4.3.1	CNTs cathode prepared by electrophoretic deposition	
92		
4.3.2	Si-O-C anode deposited on copper substrate by electrodeposition	99
4.3.3	Electrochemical investigation of LIC full cell	
102		
4.4		Summary
105		
4.5		References
106		

Chapter 5 Geranial conclusion

5.1	Conclusion
108	

<i>List of achievements</i>	111
<i>Acknowledgement</i>	113

Chapter 1

General introduction

1.1 Background

For countless decades, fossil fuels such as natural gas, coal, and petroleum are widely used as energy source for vehicles, industry fields, home electronic appliances, and portable electronics stuff. However, these resources are finite and also cause problems of environmental pollution owing to combustion of fossil fuels. Especially, global warming became a hot topic in the world due to its bad effect on the earth's ecosystem- rising sea levels, expanding the desert area, international climate change, and so on. These kinds of problem are too frightening and too important to ignore any longer for future generation. For this reason, renewable energies such as solar energy, wind power, biomass have been attracting attention from researchers. Accordingly, energy storage devices like lead–acid battery, a nickel-cadmium battery, nickel-metal hydride battery, lithium ion batteries (LIBs), also have been attracting attention for effective usage of renewable energies [1-7]. Batteries are categorized into primary battery and secondary battery depending on rechargeability. The earliest recorded usage of the battery is in the 1800s by Volta from Pavia University. He discovered the electricity flows between zinc and copper electrodes through alkaline solutions, reporting “Voltaic pile”, which is the first energy storage device in Fig. 1.1.1 [59].

In 1976, preliminary achievement of rechargeable batteries consists of titanium disulfide cathode and lithium metal anode was reported by M. S. Whittingham. Since then, a lot of follow-up studies have been extensively researched to realize high performed rechargeable batteries [8]. The commercially rechargeable battery consists of lithium cobalt oxide as a cathode and carbon coke as an anode was developed by Sony Corp. in 1997. Ever since commercial LIB have been reported, it is widely used as power source for home appliances, mobile devices, and medical equipment because of its advantages such as no memory effect, higher energy density, high working voltage, and so on [9-11]. Figure 1.1.2 shows the comparison of energy density and power density of various energy storage devices, as see this figure, it was confirmed that LIB has higher volumetric and gravimetric energy density than other devices. To develop the higher performance of lithium batteries, there have been many attempts related to each component of LIB.

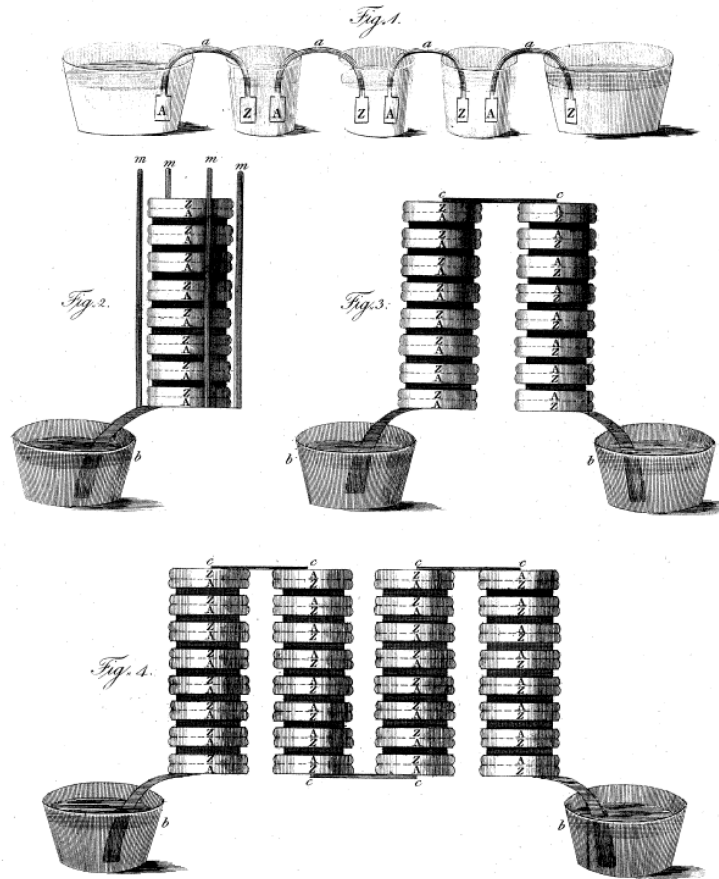


Figure 1.1.1 Schematic of Voltaic pile and its utilization depending on required voltage [59]
 Copyright © The Royal Society 2017 Partner of Research4Life, PERii-INASP, CrossRef & LOCKSS.

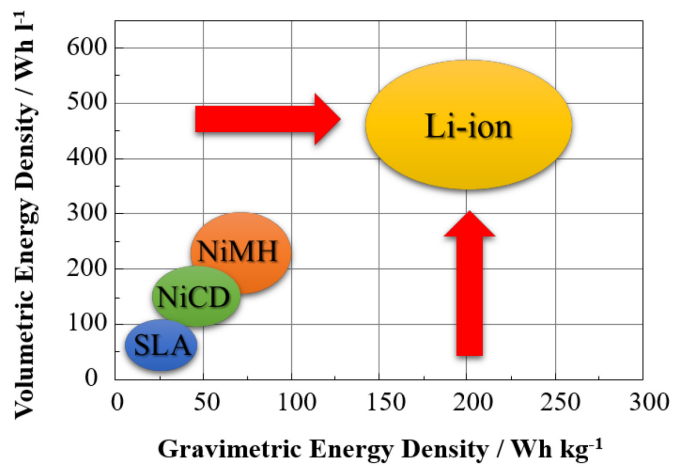


Figure 1.1.2 Comparison of energy storage devices and its volumetric and gravimetric energy density.

1.2 Lithium ion batteries

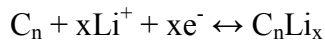
1.2.1 Components of lithium ion batteries

The battery is a device to convert chemical energy into electrical energy or vice versa through oxidation and reduction reaction of electrodes with an electrolyte. LIBs are composed of cathode and anode in an electrolyte. In addition, to prevent a short circuit of both electrodes, separate, which can pass ions during charge/discharge process, is located between electrodes. During charge process, ions migrate from anode to cathode through an electrolyte, in the case of the discharge process, ions are de-intercalated from a cathode and intercalated into an anode in Fig. 1.2.1. As an example, the reaction formula for the charge/discharge process of LIBs can be written as follows:

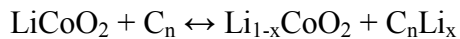
- Cathode (in case of LiCoO_2):



- Anode (in case of graphite):



- Overall reaction (in case of LiCoO_2 // graphite full cell):



As mentioned above, lithium ions are de-intercalated from cathode to anode in charge process, at the same time, electrons are moving toward cathode via connected lead between both electrodes. For this reason, a capacity of a cell is determined by cathode materials. Thus, research related to the development of cathode materials are widely carrying out all over the world. However, for stable cycle life of LIBs, it is needed that anode materials can be reversibly reacted respond to lithium ions from a cathode. Moreover, the cell voltage is decided by a potential difference between cathode and anode. As such, a lower potential of an anode material is an important factor for high voltage LIBs. In this respect, studies on the Improvement of anode materials must also continue to realize the high-performance LIBs. Lithium metal has been in the

spotlight because of its lightweights than other metal and low standard reduction potential of ca. -3 V ($\text{Li}^+ + \text{e}^- = \text{Li} \rightarrow E^\circ = -3.040 \text{ V}$). However, in the case of pure lithium metal as anode, lithium seeds sprout from lithium anode, called “lithium dendrite”, and it grows up and reaches cathode during charge/discharge cycle, causing a short circuit. To prevent this issue, research on alternative anode materials and stable separator should be focused.

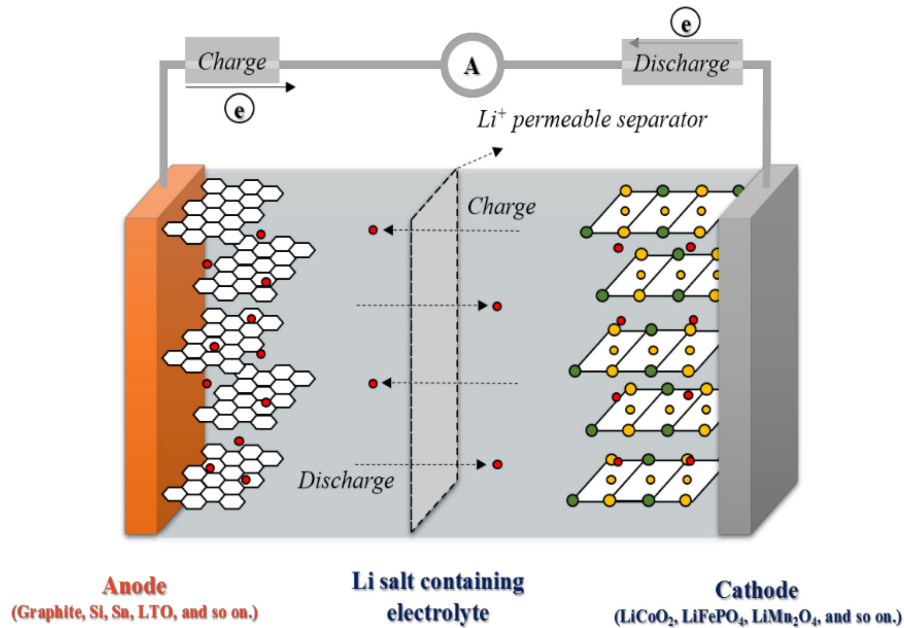


Figure 1.2.1 Mechanism of lithium ion batteries during charge and discharge process.

1.2.1.1 Cathode materials

A cathode provides lithium ions in charge process of LIBs and releases electrons through connected lead by an oxidation reaction of active material. On the contrary, a cathode receives electrons, lead to reduction of active material and intercalated of lithium ions into cathode as shown in Fig. 1.2.1. As such, a cathode is the main role in the operation of LIBs. For a high performance of LIBs, demands as cathode materials are as follows:

- a. Large storage capacity amounts of lithium ions with reversible reaction and constant potential.
- b. Light weights for higher gravimetric capacity, high electron, and ion conductivity.
- c. Chemically, thermal, and electrochemically stability with electrolyte.
- d. Homogeneous morphological properties for high contact efficiency and electric conductivity with each particle.

As active material for the cathode, 3D- transition metals is usually used because of its higher potential than 4D and 5D- transition metals, relatively lightness. Typical cathode materials include the Layered, Spinel, and Olivine structure compound, i.e. LiCoO_2 , LiMn_2O_4 , and LiFePO_4 .

LiCoO_2 which has R-3m rhombohedral structure is widely employed as cathode material despite its high price owing to easy manufacturing methods, resulting in mass production. LiCoO_2 is categorized into two structure, layered LiCoO_2 (over 800 °C) and spinel LiCoO_2 (ca. 400 °C), depending on heat-treatment temperature [60]. However, spinel LiCoO_2 is not used as active material due to its low crystallinity and inner defects in the crystal structure. Layered LiCoO_2 has the theoretical capacity of 274 mA h g^{-1} , but, it shows lower capacity of ca. 140~145 mA h g^{-1} in practice. The reason of this is that the structure of LiCoO_2 , which has mixture state with O3 and P3 type structure, occurs partly phase transition into monocline structure, leading to irreversible charge/discharge process. Despite this structural defect, the LiCoO_2 cathode has stable charge/discharge cycle with good columbic efficiency. For these reasons, a lot of researches are carrying out and reporting [12].

As previously mentioned, it has some problems such as high cost and structural instability [13, 14]. Therefore, spinel LiMn_2O_4 , which has cubic system structure, was reported as alternative cathode material instead of LiCoO_2 due to its merits such as high energy density, low cost than LiCoO_2 , low toxicity, and easy to preparation [15-17]. An Oxidation number of Mn can be transformed from +2 to +4 depending on a ration of a reactant, reaction condition, temperature of reaction, and so on. Thus, synthesis of LiMn_2O_4 is complicated and a variety of phase transition is occurred such as Li_2MnO_3 , LiMnO_2 , $\text{Li}_{6.5}\text{Mn}_5\text{O}_{12}$, LiMn_3O_4 , and so on. Generally, an electrochemical characteristic transformation of LiMn_2O_4 takes two steps. In a case of $\text{Li}_{1-x}\text{Mn}_2\text{O}_4$ of well-defined composition ($0 \leq 1-x \leq 1$), lithium ions located in tetrahedral

intercalate/de-intercalate at ca. 4 V, maintaining the cubic structure. On the other hand, in the case of $\text{Li}_{1+x}\text{Mn}_2\text{O}_4$ of well-defined composition ($1 \leq 1+x \leq 2$), lithium ions located in octahedral site intercalate/de-intercalate at ca. 3 V by a phase transition between cubic and tetragonal phase. This irreversible phase transition leads to a destruction of the LiMn_2O_4 crystal structure. In addition, Mn^{2+} is generated by Mn ion disproportionation ($2\text{Mn}^{3+} = \text{Mn}^{2+} + \text{Mn}^{4+}$) on electrode surface during discharge process. This Mn^{2+} decreases the electrochemical performance of LiMn_2O_4 cathode because it plays a role as a catalyst to decompose electrolyte and obstacle for migration of lithium ion.

To replace the LiMn_2O_4 into other cathode material, LiFePO_4 was reported by A. K. Padhi et al. in 1997. This olivine LiFePO_4 has high energy density and good environmental compatibility. Moreover, LiFePO_4 is an appropriate compound than other iron compounds because of its high theoretical capacity of 170 mA h g^{-1} and operation potential of 3.4 V with good energy density. The charge/discharge mechanism of LiFePO_4 is defined by two-step, i.e. diffusional reaction and transportation in phase boundary of lithium ion. In charge process, lithium ion diffusion in crystal structure without phase transition, showing inclined curve in charge/discharge profile. As charge time passed, particle of LiFePO_4 can be divided into FePO_4 and LiFePO_4 , and finally, only FePO_4 is existed. By this non-phase transition reaction, LiFePO_4 has good cycle stability. However, it is not easy to replace LiFePO_4 into LiCoO_2 because of its electronic and ion conductivities. It is a general characteristic of materials which have poly-anion like PO_4^{2-} . Numerous efforts to solve this demerit of LiFePO_4 cathode have been studied by a lot of researchers.

Figure 1.2.2 shows the crystal structure of LiCoO_2 , LiMn_2O_4 , and LiFePO_4 , and comparison of energy density as described in this chapter.

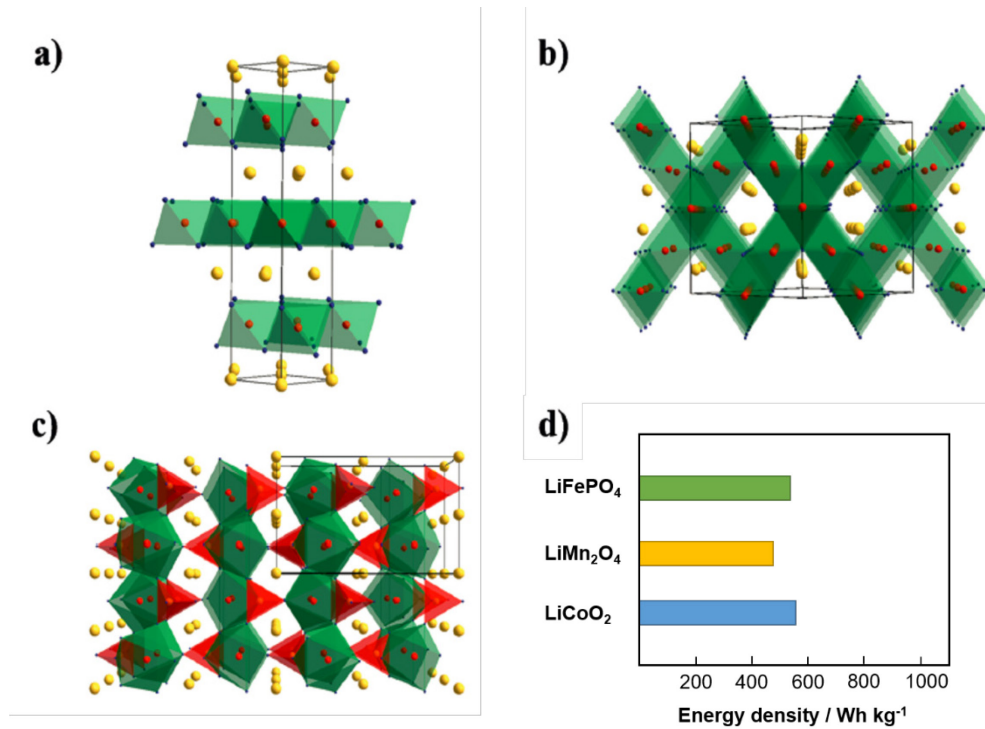


Figure 1.2.2 Three kinds of cathode materials depending on its crystallinity, (a) LiCoO_2 with layered structure, (b) LiMn_2O_4 with spinel structure, (c) LiFePO_4 with olivine structure. (d) Energy density of typical cathode materials [18] Copyright © 2015 WILEY-VCH Verlag GmbH & Co. KGaA, Weinheim.

1.2.1.2 Separators

A separator does not contribute to charge/discharge process of LIBs. As explained in mechanism about lithium batteries, lithium ion dissolved in electrolyte passes through separator which is located between cathode and anode. In other words, a separator is play a role as not only membrane to prevent contact each electrodes but also passageway for lithium salts in electrolyte. For these reason, it is needed to be chemically and physically stable while lithium batteries are operating.

A separator can be categorized as three factor: Porosity polymer membrane, non-woven fabric mats, and inorganic composite membranes depending on its structure and composition of the separator. Porosity polymer membranes are fabricated by semi-crystalline polyolefin materials, including polyethylene (PE), polypropylene (PP), mixture of PE and PP, and so on [19-23]. For suitable of separator, chemical stability, thickness, porosity, permeability, mechanical strength are considered as important factors. Figure 1.2.3 shows the SEM images of three kinds of a separator. The requirements as a separator for LIBs are detailed below and listed in Table 1.2.1.

- a. Thickness: It is important to decrease the gap between cathode and anode for high performance of LIBs. Therefore, thickness of separator should not exceed 25 μm .
- b. Wettability: Low wettability leads to slow reaction rate, resulting in low electrochemical characteristics.
- c. Porosity and permeability: 40 % of porosity is recommended as separator. In addition, it should have appropriate permeability with lithium ion.
- d. Puncture strength: Lithium dendrite and its harmfulness are described above. To prevent any problems caused by lithium dendrite, suitable puncture strength have to be designed.
- e. Thermal and chemical stability: Deformation rate of separate in needed less than 5 % after drying for 1 hour at 90 $^{\circ}\text{C}$. And a separator can be stable in oxidation and reduction in electrolyte.

Table 1.2.1 Requirement parameters of separator for high performance lithium ion batteries [61] Copyright © The Royal Society of Chemistry 2014.

Parameter	Requirement
Thickness	20–25 μm
Wettability	Wet out quickly and completely
Porosity & Permeability (Gurley)	a. 40–60% b. $<0.025 \text{ s } \mu\text{m}^{-1}$
Puncture strength	Strong mechanical property
Thermal & Chemical stability	a. $<5\%$ shrinkage after 1 hour at 90°C b. Stable for a long period of time

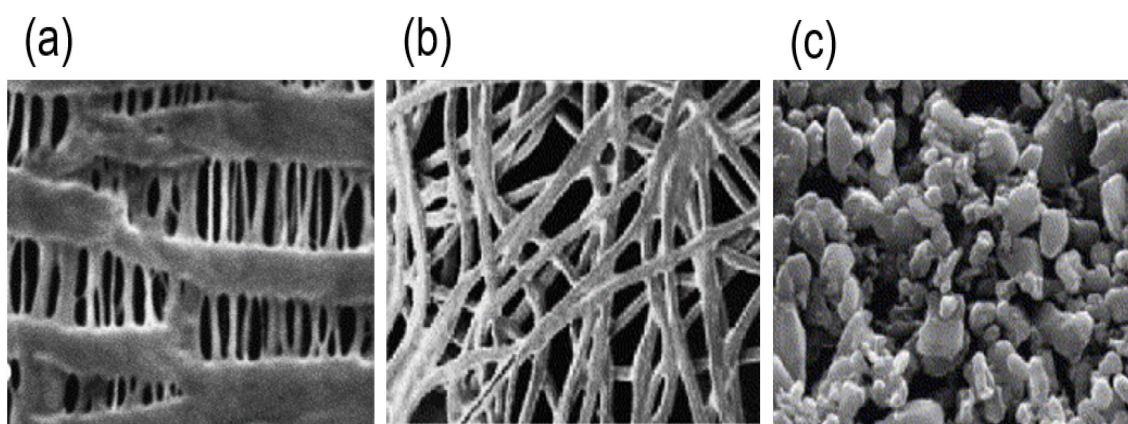


Figure 1.2.3 Three kinds of (a) polyethylene, (b) polypropylene, and (c) mixture of polyethylene and polypropylene [55] Copyright Published by Elsevier B.V..

1.2.1.3 Electrolytes

As an electrolyte for LIBs, the mixed organic solvent including lithium salt is widely used as a non-aqueous electrolyte because LIBs is operating higher potential than electrolysis of water. The important factors of an electrolyte such as thermal safety, operating a potential range, types of lithium salt, a viscosity of the solvent, solvating properties for ions, and low toxicity should be considered. Generally, a mixture of different types aliphatic carbonates such as propylene carbonate and ethylene carbonate are used as electrolyte to use merits from cyclic carbonate which has high dielectric constants, possessing high salt dissociation and linear carbonate which has lower viscosity, and high ion conductivity. Table 1.2.2 shows the various kinds of aliphatic carbonates and their electrochemical and physical properties.

In 1979, E. Paled discovered about ionic conducting interface on the anode as known as solid electrolyte interphase (SEI) [24]. Since charge/discharge test is started, an electrolyte is decomposed with lithium salts to form SEI which has a thickness of ca. 20nm including various organic and inorganic compounds on the anode surface. The total understanding of the mechanism of SEI is not identified yet. However, it develops cycle stability of anode and prevent lithium dendrite in case on lithium metal anode. Figure 1.2.4 depicts the three kinds of model of SEI formation mechanism.

As related research about electrolyte, usage of electrolyte additives such as fluoroethylene carbonate (FEC) and vinylene carbonate (VC) have been attracted as a good way to increase electrochemical properties of lithium batteries [25, 26]. For electrolyte additives, it is now known, are classified depending on its functionality as conditioning agent for forming of SEI, overpotential-retardant, and flame-retardant. Description of each of these parameters is as follows.

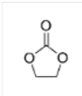
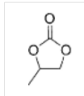
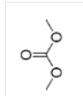
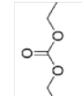
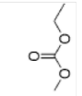
- a. Conditioning agent for forming of SEI: A typically conditioning agent is VC [62, 63]. It form stable SEI on anode surface at initial cycle and prevent exfoliation of graphite layer from graphite, resulting in development of cycle life of LIBs.
- b. Overpotential-retardant: In practice, various parts such as positive temperature coefficient, protection circuit module, and safety vent are used for safe of LIBs. However, it is a major cause of high price of LIBs. For this reason, electrolyte additive

was developed as overpotential-retardant.

- c. Flame-retardant: Almost electrolytes are composed of organic solvent which is highly combustible. To prevent the ignition of electrolyte during charge/discharge process, phosphate-based materials such as trimethyl phosphate (TMP), tris(2,2,2-trifluoroethyl)phosphate (TFP), and hexamethoxycyclotriphosphazene (HMTP) are employed as flame-retardant. The detailed mechanism of ignition protection is not revealed yet. However, it is known that TMP intercalates into a graphitic layer, causing exfoliation of graphite. On the other hand, TFP improves the fire retardant and cycle performance of LIBs.

Overall reaction mechanism of electrolyte additives and influence for LIBs has not yet been identified. Therefore, electrolyte additive has been attracting attention to reveal its electrochemical affection.

Table 1.2.2 Various kinds of electrolytes and their properties [29] Copyright 2015 WILEY-VCH Verlag GmbH & Co. KGaA, Weinheim.

Solvent properties	EC	PC	DMC	DEC	EMC
Structure					
Dielectric constant	+	+	-	-	-
Viscosity	+	+	-	-	-
Melting temp.	+	-	O	-	-
Boiling temp.	+	+	-	-	-
Flash point	+	+	-	-	-
Volatility*	-	-	+	+	+
Contribution to SEI	+	-	-	-	-
Anodic stability	+	+	O	O	O
Σ safety	+	O	-	-	-
+ : High, o : Medium, - : low, * According to NFPA30 (National Fire Protection Association), volatility refers to both flammable and combustible liquids.					

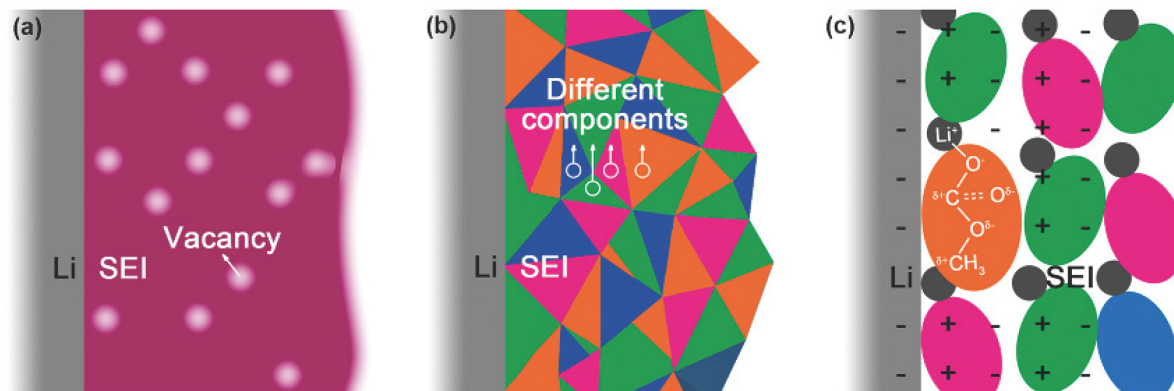


Figure 1.2.4 Three models of (a) The Peled's model (b) Mosaic model and (c) Coulombic model [56] Copyright © 2015 The Authors. Published by WILEY-VCH Verlag GmbH & Co. KGaA, Weinheim.

1.2.1.4 Anode materials

An anode provides electron and lithium ion and oxidized during discharge process as mentioned above. Thus, chemical and electrochemical properties of the anode material are important for reversible operating of LIBs. The requirement parameters of anode materials are summarized as follows.

- Low standard reduction potential: For a large operating voltage of LIBs anode material has low standard reduction potential in opposition to cathode materials.
- Structural stability: In the case of a considerable structure change during charge/discharge process, the internal strain is increased, resulting in low reversibility.
- Fast diffusion velocity: The fast diffusion velocity of lithium ion in the anode is impotent to realize the high performance of LIBs.

Since the commercialization of lithium batteries by Sony corp. in 1997, carbon materials were used as anode material, in particular, graphite anode has been widely used owing to its low cost,

abundance in nature, and stable reaction with Li at low potential (~ 0.1 V vs. Li/Li^+) [31-34]. In charge/discharge process, graphite anode is operating as following chemical reaction equation 1.1.1.



As can see in equation 1.1.1, six carbon atoms react with only one lithium ion, resulting in a formation of LiC_6 which has a theoretical capacity of 372 mA h g^{-1} . Figure 1.2.5 shows the two kinds model of lithium lithiation into graphite. For high-energy lithium batteries, improvement of capacity from cathode and anode materials is needed. Therefore, graphite-based anode materials reach the limitations of high-energy LIBs. In this section, the three kinds of anode materials are discussed depending on lithiation/de-lithiation mechanism: 1) Insertion/de-insertion materials 2) Conversion materials 3) Alloy/de-alloy materials as listed in Table 1.2.3 [35-41].

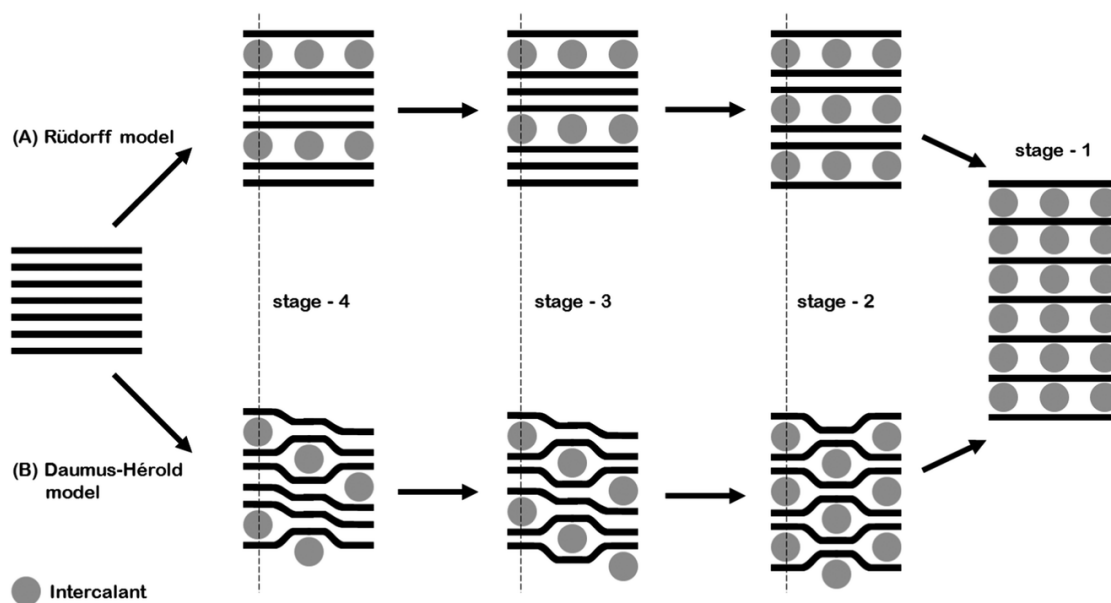


Figure 1.2.5 Schematic of lithium intercalation into graphite anode depending on Rudorff model and Daumus-Herold model [57] Copyright © The Royal Society of Chemistry 2014.

Table 1.2.3 Various kinds of anode materials and their properties [50] Copyright 2013 The Authors. Published by Elsevier B.V.

Active anode material	Theoretical capacity (mA h g ⁻¹)	Advantages	Common issues
Insertion/de-insertion materials			
A. Carbonaceous	200-600		
a. Hard carbon	1116	➤ Good working potential	➤ Low coulombic efficiency
b. CNTs	780/1116	➤ Low cost	➤ High voltage hysteresis
c. Graphene		➤ Good safety	➤ High irreversible capacity
B. Titanium oxides			
a. LiTi4O5	175	➤ Extreme safety	➤ Very low capacity
b. TiO2	330	➤ Good cycle life	➤ Low energy density
		➤ Low cost	
		➤ High power capability	
Alloy/de-alloy materials	4212	➤ Higher specific capacities	➤ Large irreversible capacity
a. Silicon	1624	➤ High energy density	➤ Huge capacity fading
b. Germanium	993	➤ Good safety	➤ Poor cycling
c. Tin	660		
d. Antimony	790		
e. Tin oxide	1600		
f. SiO			
Conversion material			
a. Metal oxides (Fe2O3, Fe3O4, CoO, Co3O4, etc)	500-1200	➤ High capacity	➤ Low coulombic efficiency
		➤ High energy	➤ Unstable SEI formation
		➤ Low cost	➤ Large potential hysteresis
		➤ Environmentally compatibility	➤ Poor cycle life
b. Metal phosphides/sulfides/nitrides (Mxy; M=Fe, Mn, Ni, Cu and X=P, S, N)	500-1800	➤ High specific capacity	➤ Poor capacity retention
		➤ Low operation potential and low polarization than counter oxides	➤ Short cycle life
			➤ High cost of production

1.3 Anode materials for lithium ion batteries

1.3.1 Insertion/de-insertion materials

Representatively, carbonaceous materials such as hard carbon, carbon nanotubes, and graphene are usually used as insertion/de-insertion anode materials for lithium batteries. These carbonaceous materials have been employed as suitable anode materials because of its a lot of advantages such as easy availability, thermal and chemical stability, electrochemical friendly for the environment, low cost, and good reversibility of lithium intercalation and de-intercalation [42-44]. These merits are an important factor as anode materials for LIBs. For these advantages, carbonaceous materials used with other anode materials to increase electrochemical properties.

He et al. reported the $\text{Li}_4\text{Ti}_5\text{O}_{12}$ which is coated by carbon to increase the low electric conductivity of $\text{Li}_4\text{Ti}_5\text{O}_{12}$. Similarly, carbon coated Silicon and Germanium were reported as anode materials for high-performance lithium batteries as shown in Fig. 1.3.1 [45, 46].

Carbonaceous materials are classified as soft carbon and hard carbon by the crystallinity of carbon material and stacking of carbon atoms. In soft carbon, as known as graphitizable carbons, is widely used as anode materials due to its good reversible capacity of ca. $350\text{-}370 \text{ mA h g}^{-1}$, outstanding cycling life and good coulomb efficiency (over than 90%) [47]. Mesocarbon micro-bead, mesophase-pitch-based carbon fiber, and vapor grown carbon fiber are famous as soft carbon materials as an anode for lithium batteries. On the other hands, hard carbon has another advantage like the superb reversible capacity of over 500 mA h g^{-1} with a potential range from 0 to 1.5 V vs. Li/Li^+ . Figure 1.3.2 depicts the hollow carbon microspheres, hollow poly(St/AN/DVB)/ Fe_3O_4 composite microspheres prepared by seeded polymerization and a wet chemical method [48].

Kureha Corp. developed hard carbon as anode materials in 1991. However, as mentioned above, carbonaceous materials are meeting the limitation for high energy lithium batteries for Electric Vehicle which need high power and energy properties of lithium batteries.

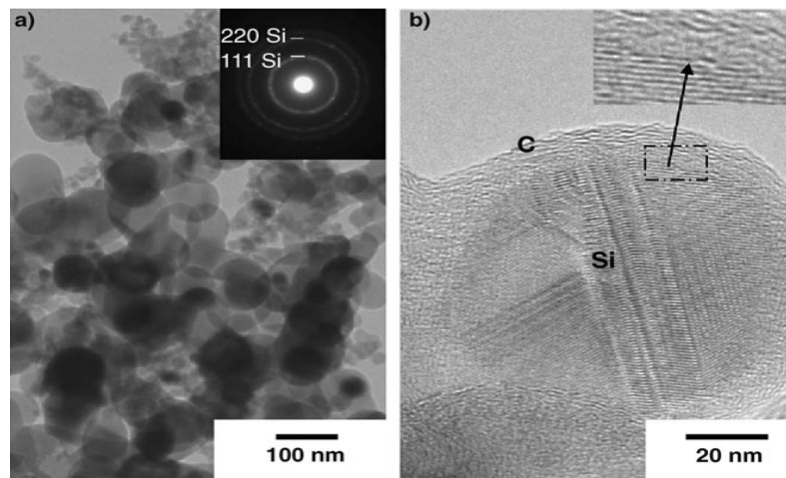


Figure 1.3.1 TEM images of (a) silicon anode coated by carbon with electron fraction and (b) its magnified images [45] Copyright 2006 Wiley-VCH Verlag GmbH & Co. KGaA, Weinheim.

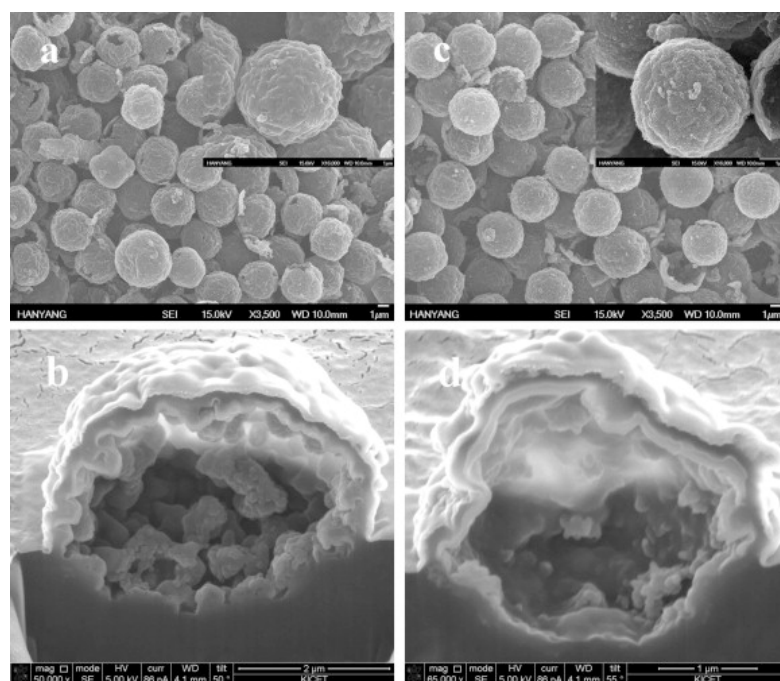
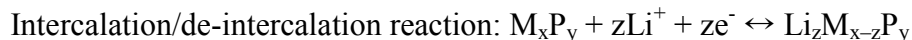
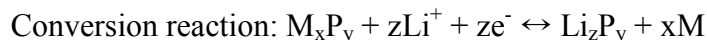


Figure 1.3.2 SEM images of (a) hollow carbon microspheres, (c) hollow poly(St/AN/DVB)/Fe₃O₄ composite microspheres and their cross-section (b), (d) [45] Copyright Copyright © 2013 Elsevier B.V. All rights reserved.

1.3.2 Conversion materials

Transition metal compounds such as iron oxide, cobalt oxide, metal phosphides, and so on, have been researched as promising anode materials for lithium batteries. Iron oxide, haematite type (α -Fe₂O₃) and magnetite type (Fe₃O₄) have a lot of merits as active material such as toxic free, abundant in nature, low cost. These materials offer a higher theoretical capacity of 926~1007 mA h g⁻¹ than conventional graphite. However, low electric conductivity and low diffusion rate of lithium ions are problems awaiting a solution to realize high energy and power lithium batteries. To overcome this de-merits, X. Zhu et al. synthesized the carbon-coated iron oxide anode using graphene. Figure 1.3.3 depicts the TEM image of graphene coated Fe₃O₄ materials with its schematic during charge/discharge process. This hybrid graphene- Fe₃O₄ anode shows outstanding capacity retention of 818 mA g⁻¹ after 50th cycle, indicating a developed performance as an anode.

Likewise, metal phosphides have been extensively researched for lithium batteries owing to their operating mechanism. When this anode reacts with lithium ions, both reactions from conversion reaction and intercalation/de-intercalation were carried out depending on electrochemical states during charge/discharge process as described as below:



In conversion reaction of metal phosphides, the reaction was carried out by breaking a bond between metal and phosphorous, forming nano-scaled metal particles and Li-phosphides. On the contrary, intercalation/de-intercalation reaction, lithium ion can react with metal phosphides without any bond breaking. M-phosphides materials, where M is a metallic material such as copper, cobalt, tin, nickel, and iron, are employed as anode material due to their good advantages such as high capacities ($500\sim 1800 \text{ mA h g}^{-1}$), and lower working potential than other oxide compounds. However, these materials have limitation like low electrical conductivity and volume change during charge/discharge. For developed metal phosphides material as an anode, a lot of attempts been deeply studied using carbon coating, size control, and so on [49, 50].

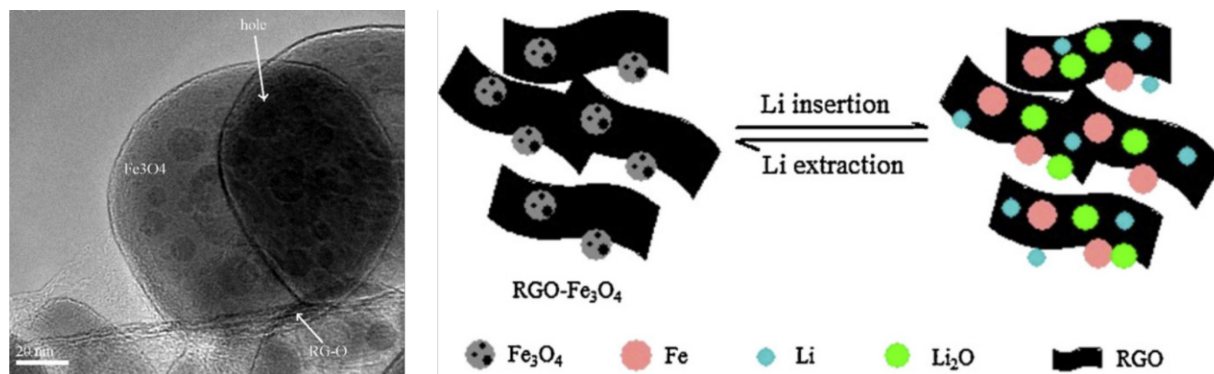


Figure 1.3.3 TEM image of Fe_3O_4 coated by graphene and its schematic for charge/discharge process [49] Copyright 2013 Elsevier Ltd. All rights reserved.

1.3.3 Alloy/de-alloy materials

As increase demands for high-energy lithium batteries, alloy/de-alloy materials such as silicon, tin, germanium, and antimony have been focused to replace conventional graphite anode because its higher theoretical capacity from 372 mA h g^{-1} (of graphite) up to 783 mA h g^{-1} (of tin oxide) or 4200 mA h g^{-1} (of silicon). Figure 1.3.4 shows the comparison of the various anode materials with its theoretical capacity. From this figure, it was confirmed that alloy/de-alloy materials such as silicon and tin have high theoretical capacity with low working potential. Despite higher theoretical capacity, these materials suffer from volume change during charge/discharge process, causing capacity fading and poor cycle ability. The mechanism of volume change in case of silicon anode during charge/discharge process is presented in Fig. 1.3.5.

As can see in Fig. 1.3.5, SEI is formed on silicon anode surface by decomposed of an electrolyte. After the SEI formation, a volume of silicon anode is changed during charge/discharge process, resulting in additional lithium ion loss and a crack of silicon anode structure. After repeating several times, isolated silicon particles which cannot react with lithium ions are generated during charge/discharge process. This volume change of silicon anode leads to not only a physical change but also electrochemical changes such as capacity fading and poor cycle ability.

To overcome these issues, numerous approaches and attempts have been pursuing such as carbon encapsulation, synthesis of nano-scale active materials, porous materials [52. 53]. Y. Ma et al. reported the N-doped carbon encapsulation of silicon materials (C/Si). These silicon materials prepared by magnesiothermic reduction from C/SiO₂ composites. From this attempt, good electrochemical properties such as a high capacity of 905 mA h g^{-1} with good coulomb efficacy of 93.1% at 100th cycle could be obtained (shown in Fig. 1.3.6). As another approach, A. Favors et al. synthesized the porous nano-silicon as anode materials for lithium ion capacitor. Figure 1.3.7 demonstrates the strategy of this research. Porous nano-silicon was prepared by highly scalable heat scavenger-assisted magnesiothermic reduction from beach sand. The obtained material achieves outstanding electrochemical performance with a discharge capacity of 1024 mA h g^{-1} after 1000th cycle.

In this regard, we attempted another approach to synthesis silicon-based composites by

electrodeposition. Detail explanation about this work will be discussed in next section.

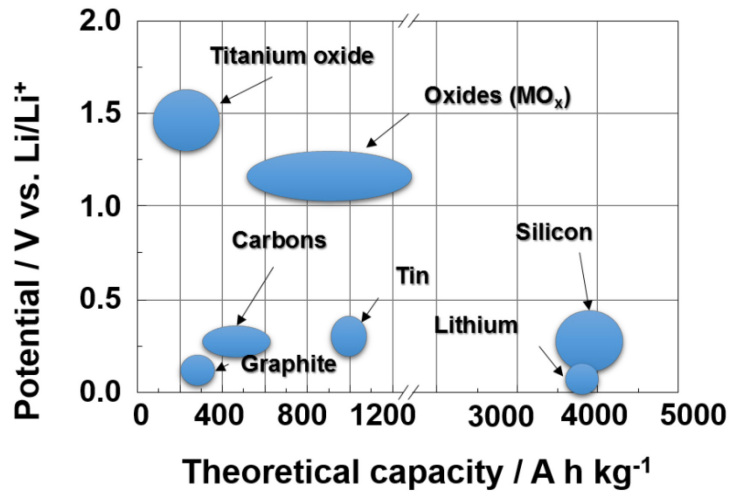


Figure 1.3.4 Various anode materials with their theoretical capacity and working potential.

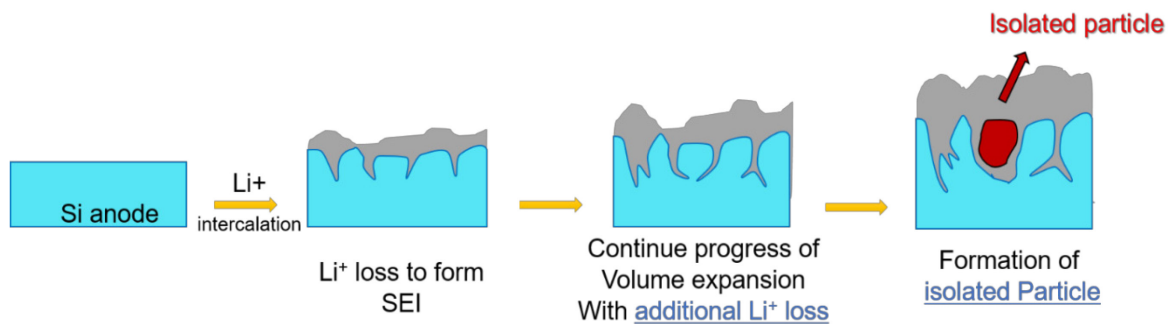


Figure 1.3.5 Schematic of volume change mechanism of silicon anode during lithiation.

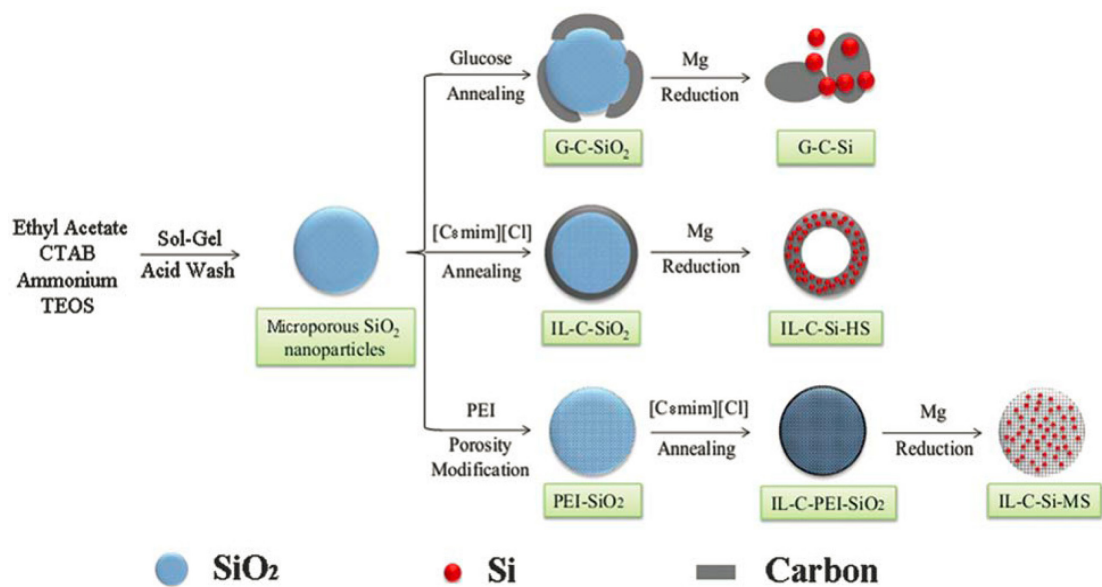


Figure 1.3.6 Schematic of carbon encapsulation with silicon anode [51] Copyright The Royal Society of Chemistry 2013.

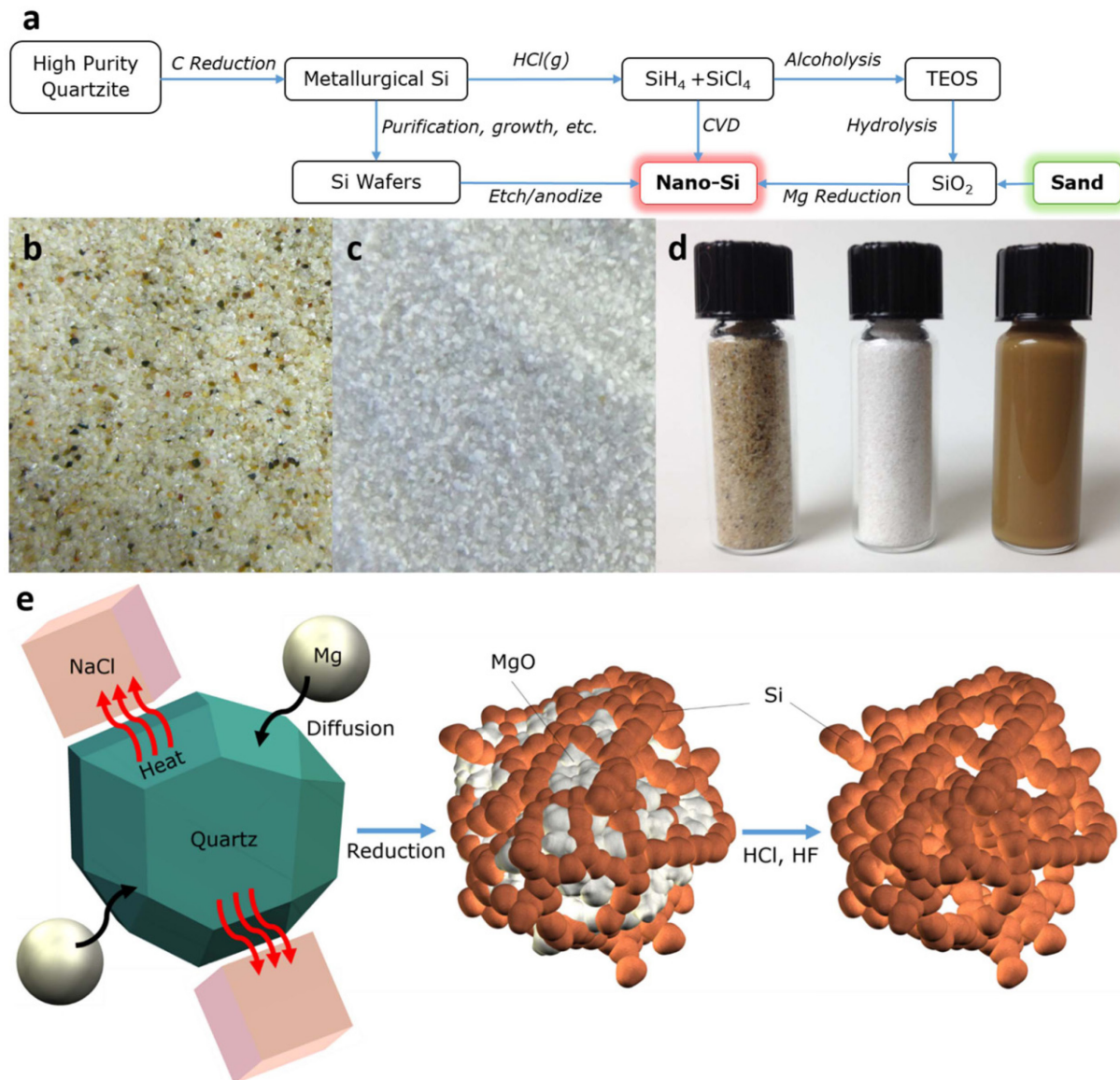


Figure 1.3.7 Synthesis of nano-scale silicon anode and its flow chart (a), beach sand (b) MgO and silicon composites and (c) nano-scale silicon material [58] Copyright © 2014, Rights Managed by Nature Publishing Group.

1.4 Si-O-C composites as anode for lithium ion batteries

1.4.1 Synthesis of Si-O-C composites and its features

We reported the novel material consist of silicon, oxygen, and carbon composites, namely Si-O-C composites, by reduction of SiCl_4 dissolved in propylene carbonate via electrodeposition method as indicated in reaction equation 1.4.1 [53].

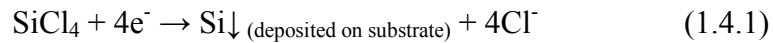


Figure 1.4.1 depicts the schematic of electrodeposition of Si-O-C composites. As can be seen this schematic, those three elements are deposited onto the copper substrate directly without any additives such as polymer binders and conductivity materials. Moreover, it can be supposed that oxygen and carbon are homogeneously dispersed in Si-O-C composites, lead to reduce internal stress during charge/discharge process. The Si-O-C composites synthesized at 2.0 coulomb cm^{-2} of passing charge has micro-nano size scale with a thickness of 0.50~0.65 μm before charge/discharge process in Fig. 1.4.2. In addition, as can see in the Fig. 1.4.2 (b), void space between Si-O-C particles was observed and this void space might be buffer space to accommodate the volume expansion during charge/discharge process. This speculation can be identified as shown in Fig. 1.4.2 (d)-(f). These SEM results depict the volume expanded Si-O-C composites after the first lithiation. The thickness of Si-O-C composites was increased from 0.50~0.65 to 2.58~4.25 μm by volume expansion after the first lithiation. Moreover, the void space between Si-O-C composites particles was disappeared after the first lithiation. This result indicates that the internal stress in Si-O-C composites from volume change can be reduced by this void spaces. To thoughtful discussion related to a volume change of Si-O-C composites, the thickness change of Si-O-C composites was measured for 100th cycles in Fig. 1.4.3. At initial cycle, the huge thickness change of Si-O-C composites was detected until 2nd cycles. However, after 5th cycle, the wide volume variation of Si-O-C composites was stable, resulting in good cycle ability until 7200th cycle with good capacity. The electrochemical characteristics of Si-O-C composites were tested and presented in Fig. 1.4.4. The charge/discharge profile of Si-O-C composites can be shown in Fig. 1.4.4 (a). At 1st cycle, huge irreversible capacity was observed

with lithiation capacity of 4731 mA h g^{-1} and de-lithiation capacity of 1403 mA h g^{-1} . This irreversible capacity is attributed to the formation of SEI on a surface of Si-O-C composites and conversation reaction of SiO_x to SiLi_y and Li_2O at ca. $0.4 \text{ V vs. Li/Li}^+$. Afterward, it was confirmed that irreversible capacity was disappeared after 2nd cycle owing to active Si-O-C composites and finish of SEI formation. In addition, the outstanding cycle ability of Si-O-C composites was observed by cycle ability in Fig. 1.4.4 (b). From this result, it was cleared that Si-O-C composites prepared by electrodeposition have bright possibility as anode materials for high energy lithium batteries.

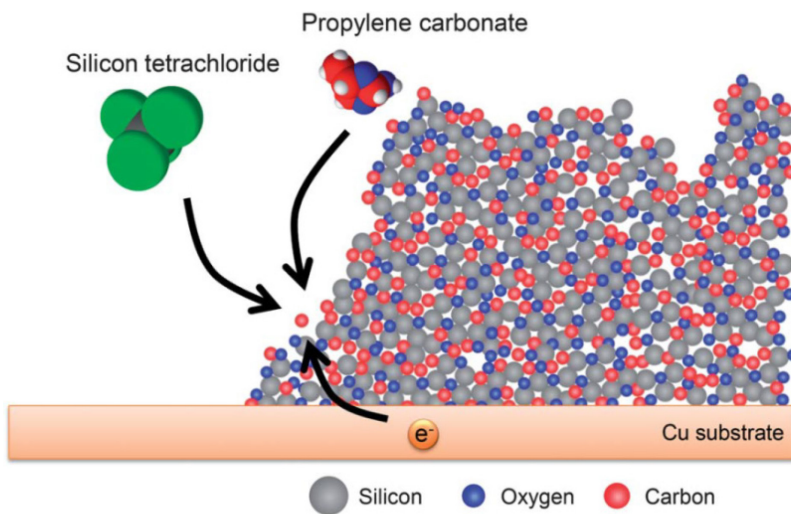


Figure 1.4.1 Schematic of Si-O-C composites with molecule structure [53] Copyright © 2012, Royal Society of Chemistry.

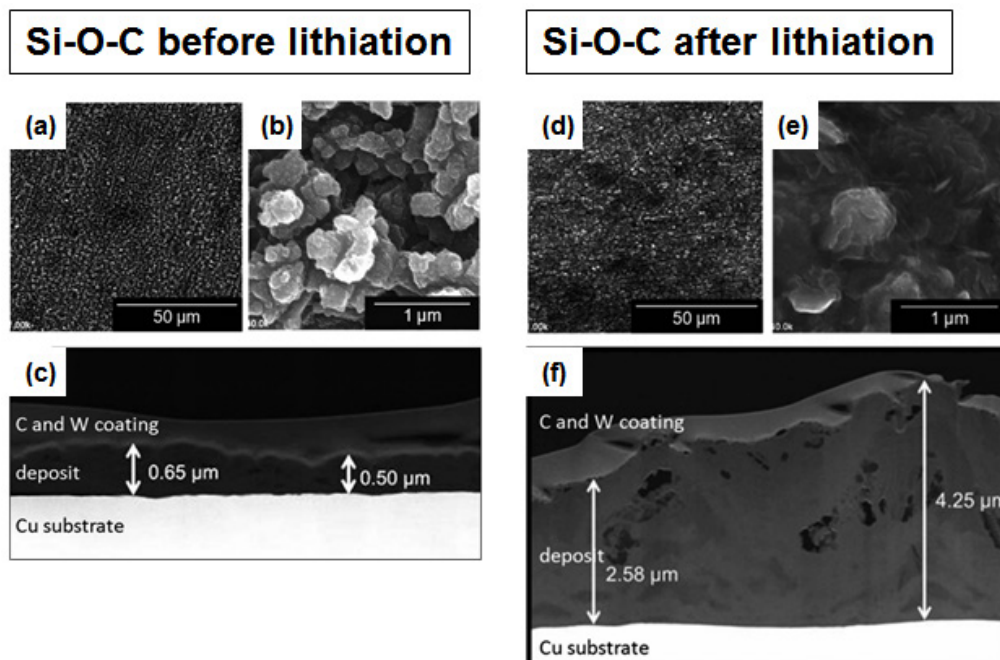


Figure 1.4.2 SEM images of (a), (b) Si-O-C before lithiation and (c) its cross-section images, (c), (d) after lithiation and (f) its cross-section [53] Copyright © 2012, Royal Society of Chemistry.

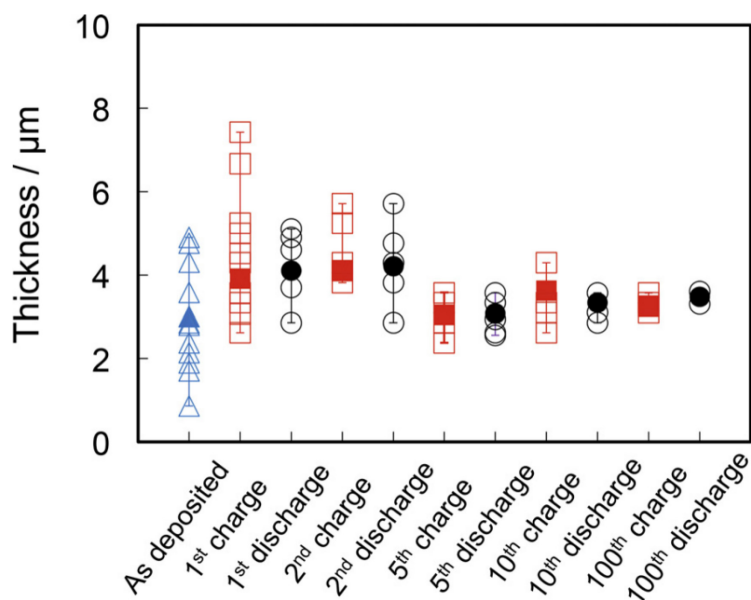


Figure 1.4.3 Thickness change of Si-O-C composites depending on charge/discharge cycle [52] Copyright © 2013 Elsevier Ltd. All rights reserved.

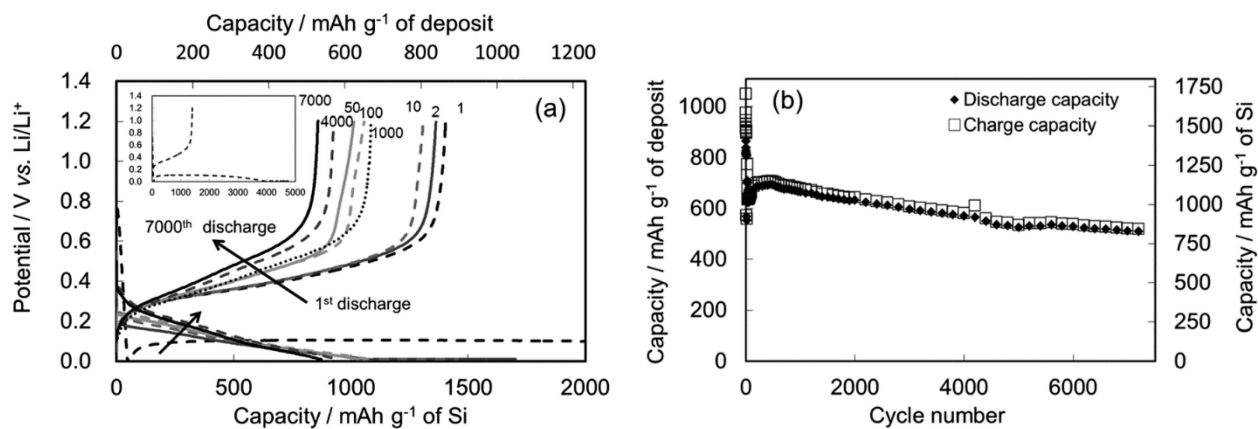


Figure 1.4.4 (a) charge/discharge profile of Si-O-C and (b) cycle ability with charge current density of 0.25 mA cm^{-2} for 7200 cycles [53] Copyright © 2012, Royal Society of Chemistry.

1.4.2 Requirement of Si-O-C composites

We could confirm that suitability of Si-O-C composites as anode material with superb cycle-ability and high discharge capacity for a 7200th cycle as discussed above. Despite the excellent performance of Si-O-C composites as anode materials, thicker Si-O-C composites are needed for matching with cathode materials which have areal capacity of over 1.0-1.5 mA h cm⁻² for high energy lithium ion batteries. However, as increasing quantity of electricity for electrodeposition, Si-O-C composites are facing physical and electrochemical challenges from poor electron conductivity and weak adhesion strength between Si-O-C composites and copper substrate, resulting in peeling off of Si-O-C composites. To overcome these issues, we reported the surface modified copper substrate by cone-shaped nickel layer (Ni-Cu substrate) as shown in Fig. 1.4.5. As a result, Si-O-C composites deposited on Ni-Cu substrate delivered a discharge capacity of 800 mA g⁻¹ after 100th cycle with outstanding capacity retention of 99.6%. Moreover, the higher discharge areal capacity could be obtained than Si-O-C composites deposited on an as-received copper substrate. However, a much amount of deposited silicon is needed for higher areal capacity over conventional graphite which has discharge areal capacity of 1.0-1.5 mA g cm⁻¹

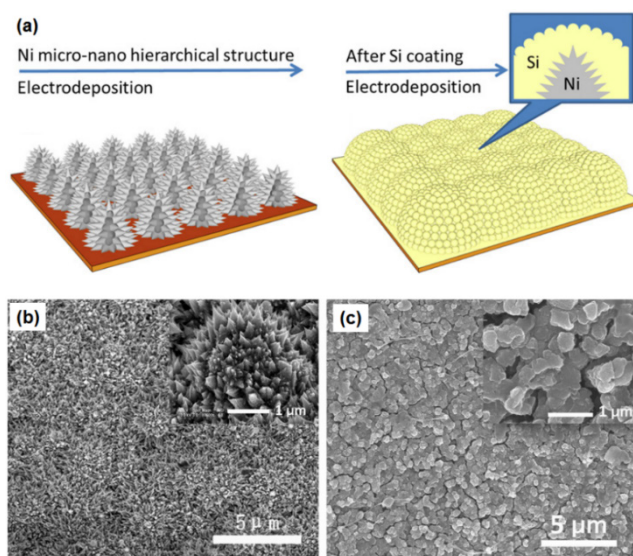


Figure 1.4.5 (a) Design of nickel cone-shaped substrate prepared on copper substrate and SEM images of (b) nickel cone-shaped substrate, (c) Si-O-C composites deposited on it [54] Copyright © 2012 Elsevier B.V. All rights reserved.

² [55].

1.5 Strategies of this dissertation

It was revealed that as-received copper substrate which has 2-dimensional (2D) structure such as smooth surface provides low adhesion strength between Si-O-C composites and copper substrate. In addition, a structural vulnerability of Si-O-C composites synthesized on an as-received copper substrate was detected during charge/discharge process. For improvement of these issues, 3-dimensional (3D) structured carbonaceous materials were used as a modification of substrate because of their advantages such as large surface area, 3D structure, and high electric conductivity of carbon.

In chapter 2, three-dimensional structured carbon paper which has millimeter-size structure was used as a substrate for Si-O-C composites. This mill scale sized structure of carbon paper offers a large space inside carbon paper. Therefore, Si-O-C composites deposited on a surface of carbon paper formed a thin layer on carbon paper with void space in the intervals. Before the use of carbon paper as the substrate, surface treatment was carried out to increase surface affinity and wettability with solvent. In addition, two kinds of organic solvents, propylene carbonate, and ethylene carbonate/diethyl carbonate are employed as an electrolyte for electrodeposition of Si-O-C composites to evaluate their suitability.

The mill scale sized structure of carbon paper was employed as a substrate for Si-O-C electrodeposition. On the contrary to chapter 2, carbon nanotubes (CNTs) which have a nano-sized carbon structure was used to compare with carbon paper. For this reason, in chapter 3, novel design surface modified copper substrate was attempted using CNTs anchor layer. The CNTs anchor layer was fabricated by electrophoretic deposition to enhance adhesion strength between Si-O-C composites and a copper substrate and structural stability of Si-O-C composites. The effect of CNTs anchor layer for Si-O-C composites is described and discussed in chapter 3.

In chapter 4, Si-O-C composites are applied as an anode for high rate lithium ion capacitor in this dissertation. For high rate performance, thin layered CNTs cathode and Si-O-C anode were synthesized by electrochemically deposition technique. The high rate performance of lithium ion capacitor consists of thin layer CNTs cathode and a Si-O-C anode is presented in this chapter.

Finally, in chapter 5, all attempts to realize enhancement of deposited silicon amounts and high performance of lithium batteries using Si-O-C anode were summarized.

1.6 References

1. E. Tsujji, T. Yamasaki, Y. Aoki, S. G. Park, K. I. Shimizu, and H. Habazaki, *Carbon*, 87 (2015) 1.
2. M. Jeong, Y. Yokoshima, H. Nara, Y. Momma, and T. Osaka, *J. Power. Sources*, 275 (2015) 525.
3. J. Y. Lim, C. S. Lee, J. M. Lee, J. Ahn, H. H. Cho, and J. H. Kim, *J. Power. Sources* 301 (2016) 18.
4. J. J. Yang, C. H. Choi, H. B. Seo, H. J. Kim, and S. G. Park, *Electrochim. Acta*, 86 (2012) 277.
5. J. J. Yang, J. H. Choi, H. J. Kim, M. Morita, and S. G. Park, *J. Ind. Eng. Chem.*, 19 (2013) 1648.
6. M. Jeong, Y. Yokoshima, H. Nara, Y. Momma, and T. Osaka, *J. Electrochem. Soc.*, 161 (2014) D3025.
7. M. Jeong, Y. Yokoshima, H. Nara, Y. Momma, and T. Osaka, *RSC Adv.*, 4 (2014) 26872.
8. M. S. Whittingham, *Science*, 192 (1976) 1126.
9. R.B. Mathur, P. H. Maheshwari, T.L. Dhamia, and R.P. Tandon, *Eelctrochim. Acta*, 52 (2007) 4809.
10. C.-H. Liu, T.-H. Ko, E.-C. Chang, H.-D. Lyu, and Y.-K. Liao, *J. Power Sources*, 180 (2008) 276.
11. Q. Si, M. Matsui, T. Horiba, O. Yamamoto, Y. Takeda, N. Seki, and N. Imanishi, *J. Power Sources*, 241 (2013) 744.
12. K. Mizushima, P.C. Jones, P.J. Wiseman, and J.B. Goodenough, *Mat. Res. Bull.*, 15 (1980) 783.
13. D. Belovv, and M. H. Yang, *J. Solid State Electrochem.*, 12 (2008) 885.
14. C. Doh, D. Kim, H. Kim, H. Shin, Y. Jeong, S. Moon, B. Jin, S. Eom, H. Kim, K. Kim, D. Oh, and A. Veluchamy, *J. Power. Sources*, 175 (2008) 881.
15. X. Zhang, H. Zheng, V. Vattaglia, and R. L. Axelbaum, *J. Power Sources*, 196 (2011) 3640.
16. A. A. Zomeren, E. M. Kelder, J. C. M. Marijnissen, and K. Schoonman, *J. Aerosol Sci.*, 25 (1

994) 1229.

17. I. Taniguchi, C. K. Lim, D. Song, and M. Wakihara, *Solid State Ionics*, 146 (2002) 239.
18. W. Liu, P. Oh, X. Liu, M. Lee, W. Cho, S. Chae, Y. Kim, and J. Cho, *Angew. Chem. Int. Ed.*, 54 (2015) 4440.
19. S. H. Choi, and Y. C. Nho, *Kor. Polym. J.*, 6 (1998) 287.
20. R. T. Giovannoni, and H. Vaidyanthan, *Braz. Pat. BR* (1989) 8804397.
21. B. D. Gupta, and A. Chapiro, *Eur. Polym. J.*, 25 (1989) 1033.
22. V. Haddadai-Asl, R. P. Burford, and J. L. Garnett, *Radiat. Phys. Chem.*, 45 (1995) 191.
23. E. Peled, *J. Electrochem. Soc.*, 126 (1979) 12.
24. N. Choi, K. Yew, K. Lee, M. Sung, H. Kim, and S. Kim, *J. Power. Sources*, 161 (2006) 1254.
25. L. Chen, K. Wang, X. Xie, and J. Xie, *J. Power. Sources*, 174 (2007) 538.
26. X. Cheng, R. Zhang, C. Zhao, F. Wei, J. Zhang, and Q. Zhang, *Adv. Sci.*, 3 (2016) 1500213.
27. E. Oeled, D. Golodnitsky, and G. Ardel, *J. Electrochem. Soc.*, 144 (1997) 8.
28. Y. E. Eli, *Electrochem. Solid-State Lett.*, 2 (1999) 212.
29. J. Kalhoff, G. G. Eshetu, D. Bresser, and S. Passerini, *ChemSusChem*, 8 (2015) 2154.
30. B. Lestriez, *Comptes Rendus Chim.*, 13 (2010) 1341.
31. S. Chou, Y. Pan, J. Wang, H. Liu, and S. Dou, *Phys. Chem. Chem. Phys.*, 16 (2014) 20347.
32. Z. Zhang, T. Zeng, Y. Lai, M. Jia, and J. Li, *J. Power Sources*, 247 (2014) 1.
33. G. Liu, H. Zheng, X. Song, and V.S. Battaglia, *J. Electrochem. Soc.*, 159 (2012) A214.
34. H. Fujimoto, K. Tokumitsu, A. Mabuchi, N. Chinnasamy, and T. Kasuh, *J. Power Sources* 19 5 (2010) 7452.
35. J. Yang, X.-y. Zhou, J. Li, Y.-l. Zou, and J.-j. Tang, *Mater. Chem. Phys.*, 135 (2012) 445.
36. C.A. Bridges, X.-G. Sun, J. Zhao, M.P. Paranthaman, and S. Dai, *J. Phys. Chem.*, C 116 (2012) 7701.
37. V. Meunier, J. Kephart, C. Roland, and J. Bernholc, *Phys. Rev. Lett.*, 88 (2002) 075506.
38. C.M. Schauerman, M.J. Ganter, G. Gaustad, C.W. Babbitt, R.P. Raffaele, and B.J. Landi, *J. Mater. Chem.*, 22 (2012) 12008.
39. K. Nishidate, and M. Hasegawa, *Phys. Rev. B*, 71 (2005) 245418.

40. J. Zhao, A. Buldum, J. Han, and J. Ping Lu, *Phys. Rev. Lett.*, 85 (2000) 1706.
41. R. MArom, S. F. Amalraj, N. Leifer, D. Jacob, and D. Aurbach, *J. Mater. Chem.*, 21 (2011) 9 938.
42. B. Scrosati, and J. Garche, *J. Power Sources*, 195 (2010) 2419.
43. H. Li, and H. Zhou, *Chem. Commun.*, 48 (2012) 1201.
44. G. Cui, L. Gu, L. Zhi, N. Kaskhedikar, P. A. Aken, K. Mullen, and J. Maier, *Adv. Mater.*, 20 (2008) 3079.
45. S. Ng, J. Wang, D. Wexler, K. Konstantinov, Z. Guo, and H. Liu, *Angew. Chem.*, 118 (2006) 7050.
46. H. Wang, M. Yoshio, T. Abe, and Z. Ogumi, *J. Electrochem. Soc.*, 149 (2002) A499.
47. O. Haik, S. Ganin, G. Gershinsky, E. Zinigrad, B. Markovsky, D. Aurbach, and I. Halalay, *J. Electrochem. Soc.*, 158 (2011) A913.
48. J. Hwang, H. Lim, Y. Sun, and K. Suh, *J. Power Sources*, 244 (2013) 538.
49. X. Zhu, W. Wu, Z. Liu, L. Li, J. Hu, H. Dai, L. Ding, K. Zhou, C. Wang, and X. Song, *Electrochim. Acta*, 95 (2013) 24.
50. S. Goriparti, E. Miele, F. D. Angelis, E. D. Fabrizio, R. P. Zaccaria, and C. Capiglia, *J. Power Sources*, 257 (2014) 421.
51. Y. Ma, G. Ji, B. Ding, and J. Lee, *J. Mater. Chem. A.*, 1 (2013) 13625.
52. H. Nara, T. Yokoshima, M. Otaki, T. Momma, and T. Osaka, *Electrochim. Acta*, 110 (2013) 40 3.
53. H. Nara, T. Yokoshima, T. Momma, and T. Osaka, *Energy Environ. Sci.*, 5 (2012) 6500.
54. T. Hang, H. Nara, T. Yokoshima, T. Momma and, T. Osaka, *J. Power Sources*, 222 (2013) 503.
55. S. S. Zhang, *J. Power Sources*, 164 (2007) 351.
56. X. B. Cheng, R. Zhang, C. Z. Zhao, F. Wei, J. G. Zjang, and Q. Zhang, *Adv. Sci.*, 3 (2016) 1500213.
57. C. Sole, N. E. Drewett, and L. J. Hardwick, *Faraday Discuss*, 172 (2014) 223.
58. Z. Favors, W. Wang, H. H. Bay, Z. Mutlu, K. Ahmed, C. Liu, M. Ozkan, and C. S. Ozkan,

Sci. Rep., 4 (2014) 5623.

59. A. Volta, *Phil. Trans. R. Soc. Lond.*, 90 (1800) 403.

60. R. J. Gummow, D. C Lies, and M. M Thackeray, *Mat. Res. Bull.*, 28 (1993) 235.

61. H. Lee, M. Yanilmaz, O. Toprakci, K. Fu, and X. Zhang, *Energy Environ. Sci.*, 7 (2014) 3857.

62. J. Barker, F. Gao, *U.S. Patent*, (1998) 5712059.

63. M. Fujimoto, Y. Shouji, T. Nohma, K. Nishio, *Denki Kagaku*, 65 (1997) 949.

Chapter 2

Synthesis of Si-O-C composites using 3D structured carbon paper substrate for high areal capacity lithium secondary battery

2.1 Introduction

There has been increasing demand for higher energy density LIBs for long term operating of electric vehicles, mobile electronics, home appliances, and so on. For these reasons, numerous issues related to high loading amounts of active materials for high areal capacity of LIBs have been extensively researched in recent years. As mentioned in general introduction part, it is not easy to increase the deposited silicon amounts of Si-O-C composites because of weak adhesion strength between Si-O-C composites and as-received copper substrate which has smooth flat surface properties [1-6]. To overcome the demerit of 2D structured as-received copper substrate, carbon paper which has 3D structure properties such as high surface area, and high porosity, was considered as an alternative substrate for electrodeposition of Si-O-C composites.

Carbon paper is widely using as current collector and electrode for energy conversion and storage devices due to its outstanding advantages such as high electrical conductivity ($12.50 \mu\text{S cm}^{-1}$), low cost than other metal current collector, extremely low density (0.2 g cm^{-3}), and specially three 3D structured properties, indicating high contact area with solvent. Despite the many advantages, it is known well than carbon materials have a low surface affinity with organic and inorganic solvents. For this reason, carbon paper was employed as a not substrate for slurry but active material.

To apply carbon paper as substrate for Si-O-C electrodeposition, it is needed to increase the surface affinity [7-12]. To enhance the surface affinity, many studies have been reported via surface treatment and modify using a various method. O. Abdel Gawad et al. increased the surface affinity of carbon fiber by electrodeposition of chromium. The Cr-coated carbon fibers obtained higher coated amounts of aluminum of 13.1 mg, whereas, as-received carbon fibers show little differentiation in coated aluminum amounts [13]. In addition, H. Zhou et al. could obtain surface modified carbon which has strong affinity and wettability with organic solvent by fluorine doping method. The fluorine-doped carbon delivered a higher discharge capacitance of 168 F g^{-1} than as-received carbon [14]. Therefore, to increase the surface affinity, sulfuric acid-hydrogen peroxide mixture (SPM) solution, called also piranha solution, was used for surface treatment of carbon paper to generate oxygen-containing functional groups.

Afterward, two kinds of solvent, propylene carbonate (PC) or ethylene carbonate/diethyl carbonate (EC/DEC), were used as electrolyte for electrodeposition of Si-O-C composites to

evaluate suitability for Si-O-C electrodeposition. Because it is reported well that PC molecule is decomposed and co-intercalated with lithium ion into carbon layer during charge/discharge process, resulting in exfoliation of graphite layer. For this reason, EC/DEC solvent is also employed in this research and compared with PC solvent.

2.2 Experimental

2.2.1 SPM treatment of carbon paper

The 3D structured carbon paper (TORAY, TGP H-060) was employed as a substrate for electrodeposition of Si-O-C composites. For SPM treatment, carbon paper was sonicated for 30min in distilled water and ethanol for 30min, respectively. Subsequently, washed carbon paper by water and ethanol soaked in SPM solution (H₂O₂: H₂SO₄, 1:4 v/v) and sonicated again for 15 min. During this process, removal of impurities and generation of oxygen-containing functional groups on carbon paper surface were carried out. After SPM treatment, the carbon paper was rinsed by distilled water and dried in a dry room for overnight.

2.2.2 Electrodeposition of Si-O-C composites on carbon paper

All procedure of electrodeposition was carried in Ar-filled globe box which has a low dew point of around -80 °C. The carbon paper without or with SPM treatment, platinum wire, and lithium piece were used as working, counter, and a reference electrode. In this chapter, two kinds of solvent, i.e., propylene carbonate (PC, Kishida) and ethylene carbonate/diethyl carbonate (EC/DEC, 1:1 v/v, Kishida), were used as an electrolyte for electrodeposition of Si-O-C composites. The reason of using two kinds of solvents as an electrolyte for electrodeposition is to evaluate the suitability for electrodeposition of Si-O-C composites. A constant current of -1.0 mA cm⁻² was applied to pass a charge of various coulomb cm⁻² from 2 to 50. Figure 2.2.1 shows the schematic of electrodeposition of Si-O-C composites using three electrode cell system.

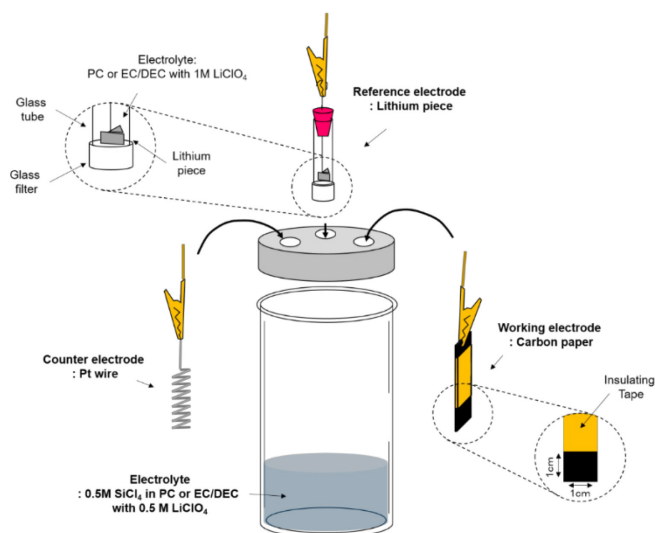


Figure 2.2.1 Schematic diagram of electrodeposition of Si-O-C composites using three electrode cell system.

2.2.3 Material measurement of Si-O-C composites

The existence of oxygen-containing functional groups on as received and SPM treated carbon paper were investigated by Fourier transform infrared spectroscopy (FT-IR, JASCO, 4200 Spectrometer). The SEM and elemental mapping measurement of Si-O-C composites were observed by field emission scanning electron microscopy (FE-SEM, Hitachi, S-4800) with energy dispersive X-ray spectroscopy (SEM-EDX, Hitachi, TM-3000). The deposited silicon amounts of Si-O-C composites were measured by inductively coupled plasma (ICP, Thermo Scientific, iCAP6500 Duo). Defect degree of a graphic layer in carbon paper of Si-O-C composites prepared by PC or EC/DEC solvents was measured by Raman spectroscopy before and after charge /discharge cycle with a laser wavelength of 532 nm, a power of 20 mV, and accumulation time of 20 seconds (Renishaw, inVia Raman Microscope).

2.2.4 Electrochemical measurement of Si-O-C composites

For measurement of electrochemical characteristics of Si-O-C composites, Coin typed half-cell (2032 type) was assembled with EC/DEC (1:1 v/v) electrolyte (Kishida) containing 1.0 mol dm⁻³ lithium hexafluorophosphate (LiPF₆) in an argon-filled glove box with a dew point lower -110 °C. The charge/discharge test of Si-O-C composites was carried out by a constant current in the potential range between 0.01-1.20 V vs. Li/Li⁺.

2.3 Results and discussions

2.3.1 Effect of SPM treatment for electrodeposition of Si-O-C composites

To modify the surface of carbon materials for enhanced surface affinity, many kinds of strong acid solutions such as nitric acid, phosphoric acid, and sulfuric acid, are widely employed for generating functional groups on a surface of carbon materials and shorting the length of linear carbon materials [15, 16]. In this study, the SPM solution was used as oxidization reagent to enhance surface affinity and wettability of carbon paper with solvent.

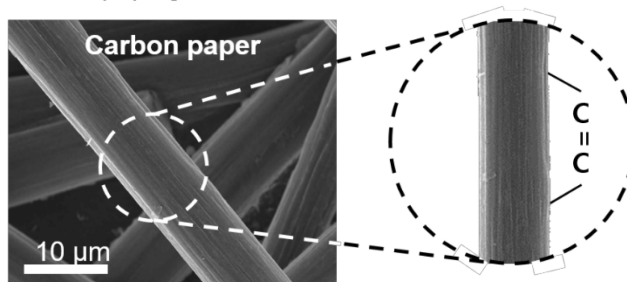
It is known well that surface treatment of carbon paper by SPM treatment is an easy way to generate oxygen-containing functional groups on a surface of carbon paper due to a synthesis of peroxymonosulfuric acid as known as Caro's acid [17]. The Caro's acid is synthesized by dehydration reaction by sulfuric acid in SPM solution. The relevant chemical reaction is indicated below.

- $\text{H}_2\text{SO}_4 + \text{H}_2\text{O}_2 \rightarrow \text{H}_2\text{SO}_5$ (Caro's acid) + H_2O
- $\text{H}_2\text{SO}_4 + \text{H}_2\text{O}_2 \rightarrow \text{H}_3\text{O}^+ + \text{HSO}_4^- + \text{O}$
- $\text{H}_2\text{SO}_5 + \text{H}_2\text{SO}_4 \rightarrow \text{H}_2\text{S}_2\text{O}_8 + \text{H}_2\text{O}$

This strong reagent attacks to C=C double bond on the surface of carbon paper, resulting in a generation of a carbonyl group (-C=O). Continually, a double bond between C and O in carbonyl group was destructed and formed the other oxygen-containing functional groups such

as hydroxyl group and carboxylic acid. Figure 2.3.1 demonstrates the procedure of generation of oxygen-containing functional groups on a surface of carbon paper by SPM treatment.

[SEM images of carbon paper]



[Mechanism of generation of oxygen containing groups]

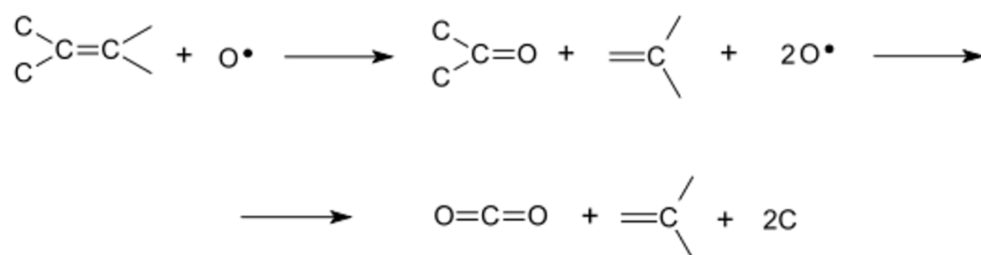


Figure 2.3.1 FT-IR spectra of the surface of carbon paper with and without SPM treatment.

Figure 2.3.2 shows the FT-IR spectra of as-received carbon paper and SPM treated carbon paper. It reveals that as-received carbon paper has no peaks related to an oxygen-containing functional groups. However, in a case of SPM treated carbon paper, some peaks appeared at 1006, 1781.9, and 3345.9 cm^{-1} , corresponding to a peak of epoxy group (C-O), carbonyl group (C=O), and a carboxyl group (-COOH) which are known as typical oxygen-containing functional group, respectively. In addition, a peak of water and hydroxyl groups can be detected at 3442, and 1365 cm^{-1} , representing O-H stretching vibration. It is surmisable that these oxygen-containing functional groups effect on a surface affinity between carbon paper and electrolyte during electrodeposition of Si-O-C composites [18, 19].

In addition, peak of aliphatic sp^3 C-H band was detected after SPM treatment at ca. 2877.3 cm^{-1} . It was reported that chemical oxidation including sulfuric acid occurs exfoliation of carbon paper because of sulfuric acid intercalates into graphitic layer in carbon paper, leading to exfoliation of hexagonal carbon layer. Therefore, it is widely used to synthesis graphene from graphitic carbon paper or graphite [27, 28].

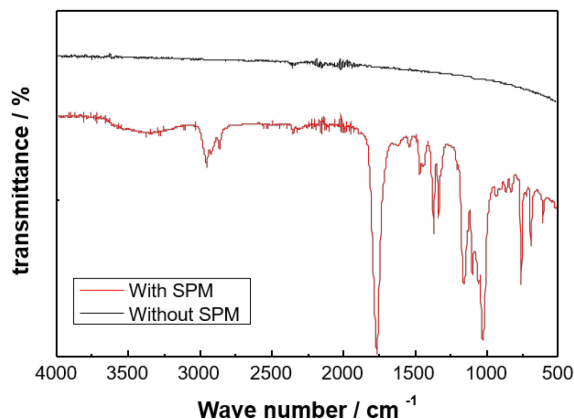


Figure 2.3.2 FT-IR spectra of the surface of carbon paper with and without SPM treatment [26] Copyright © 2017 The Electrochemical Society.

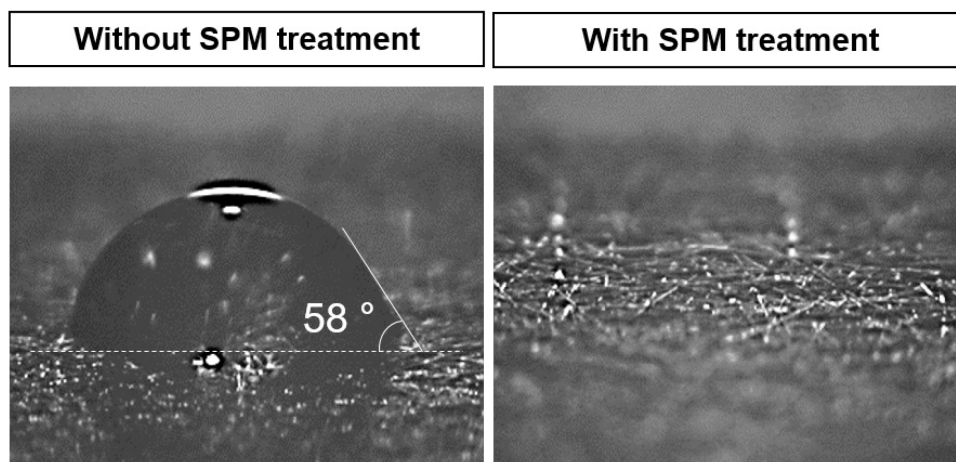


Figure 2.3.3 The behavior of a PC solvent droplet on the carbon paper surface with and without SPM treatment respectively [26] Copyright © 2017 The Electrochemical Society.

To verify the effect of oxygen-containing functional groups on surface affinity, a contact angle between each carbon paper and PC solvent was measured and presented in Fig. 2.3.3. In the case of using as-received carbon paper, the contact angle between carbon paper and PC drop is 58 ° because of its low wettability, resulting in high surface tension. It is expectable that as-received carbon paper offers low reactivity with PC solvent during electrodeposition of Si-O-C composites. On the other hand, after SPM treatment, PC drop permeated into carbon paper rapidly. It demonstrates that oxygen-containing functional groups of a surface of carbon paper improve the surface affinity and wettability with the solvent with carbon paper. From these results, enhanced reactivity can be expected during electrodeposition of Si-O-C composites.

Electrodeposition of Si-O-C composites was carried out on as-received and SPM treated carbon paper, namely Si-O-C/CP-as and Si-O-C/CP-SPM, to compare the deposited silicon amounts and areal capacity of each sample. Figure 2.3.4 depicts surface morphological properties of Si-O-C composites prepared by electrodeposition at 2 coulomb cm⁻² of passing charge by SEM-EDX measurement. From the plan views of both samples, it is confirmed that both of carbon papers were completely covered by Si-O-C composites. It indicates that the deposition of Si-O-C composites is irrelevant to the SPM treatment and carbon paper has possibility as substrate for Si-O-C composites. In addition, elemental mapping of Si-O-C/CP-as and Si-O-C/CP-SPM depicts the existence of silicon, oxygen, and carbon presented by purple, blue-green, and yellow color in Fig. 2.3.4. The results of elemental mapping indicate that all elements are deposited not only silicon but also oxygen and carbon and distributed homogeneously. Table 2.3.1 shows the weight percentages of each element from Si-O-C/CP-as and Si-O-C/CP-SPM prepared by electrodeposition at 2 coulomb cm⁻² of passing charge. The Si-O-C/CP-as has low silicon weight percentages of 11.54 wt %, whereas, Si-O-C/CP-SPM shows higher silicon weight percentages of 22.65 wt %. The main reason of increased Si amounts using SPM treated carbon paper is improvement of reactivity by enhanced surface affinity and wettability of carbon paper with solvent. This behavior is in good agreement with the results of contact angle between both carbon papers and PC solvent.

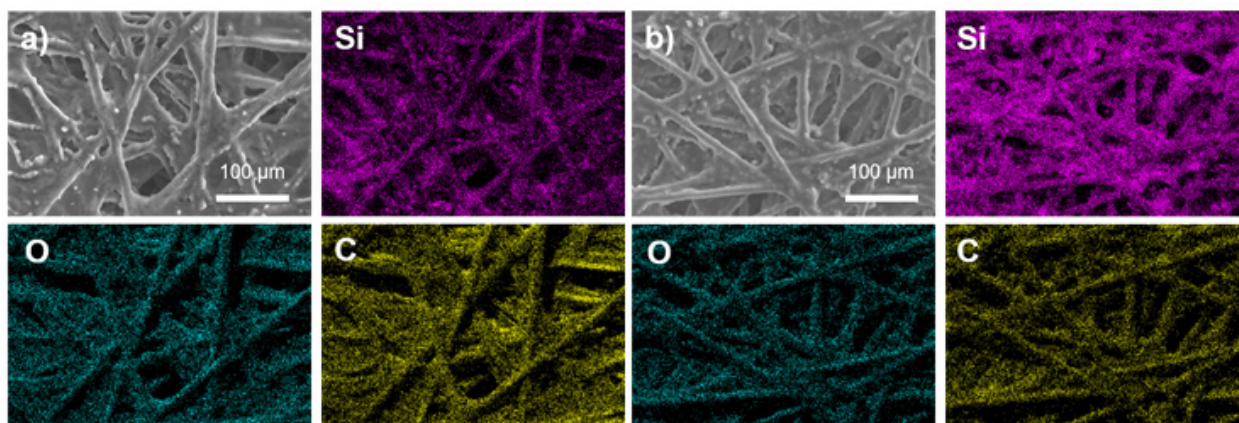


Figure 2.3.4 The SEM image and the corresponding element mapping of Si, O and C of Si-O-C/CP-as and Si-O-C/CP-SPM electrode [26] Copyright © 2017 The Electrochemical Society.

Table 2.3.1 Weight percentage of Si, O, and C from Si-O-C/CP-as and Si-O-C/CP-SOM by EDX measurement [26] Copyright © 2017 The Electrochemical Society.

Elemental	as-received carbon paper / wt %	SPM treated carbon paper / wt%
Silicon	11.54	22.65
Oxygen	28.45	28.89
Carbon	60.01	48.46

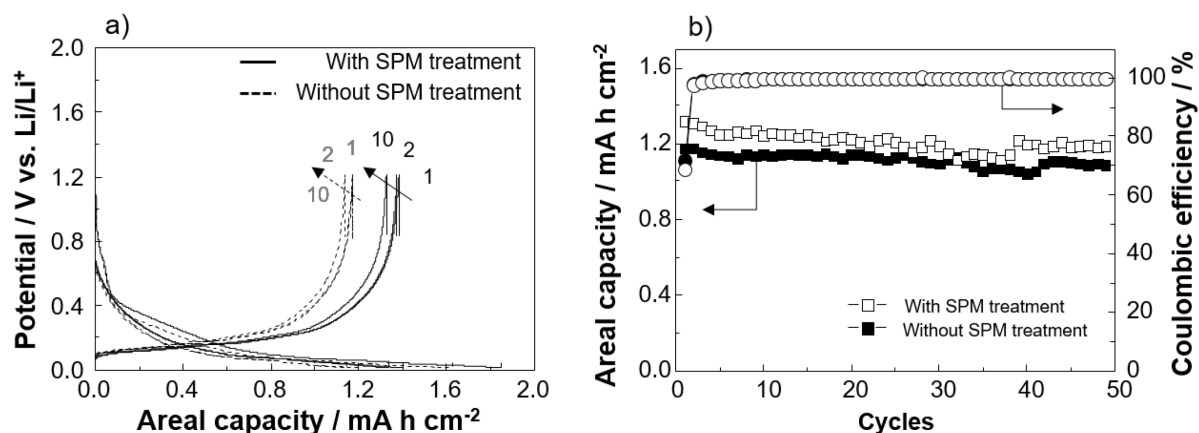


Figure 2.3.5 (a) The charge/discharge curve of of Si-O-C composites deposited on as-received carbon paper and SPM treated carbon paper at 2 coulomb cm⁻² of passing charge at 1st, 2nd, and 10th cycle with charge current density of 0.1 mA cm⁻², (b) The cycle ability of Si-O-C/CP-as and Si-O-C/CP-SPM with charge current of 0.5 mA h cm⁻² for 50 cycles [26] Copyright © 2017 The Electrochemical Society.

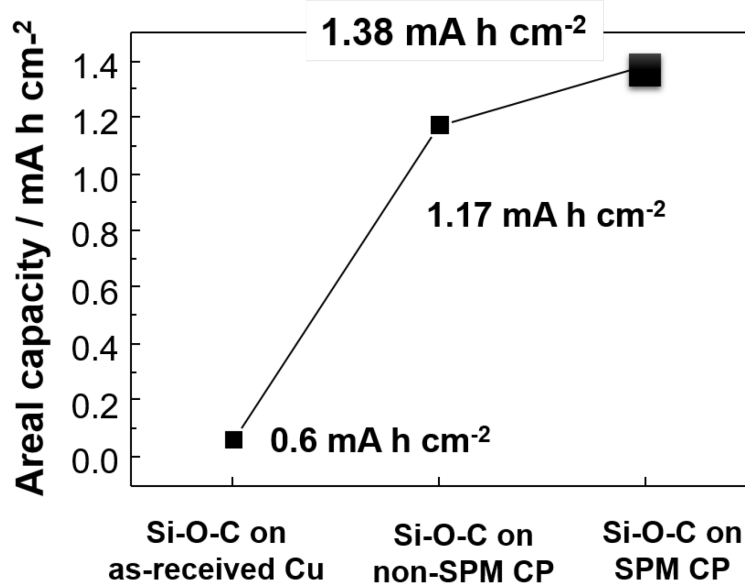
The electrochemical properties of Si-O-C composites deposited on as-received carbon paper and SPM treated carbon paper at 2 coulomb cm⁻² of passing charge were tested by charge/discharge test by constant current charge (lithiation) and discharge (delithiation) measurement. Figure 2.3.5 (a) shows the charge/discharge curve of both samples at 1st, 2nd, and 10th cycle. At the 1st cycle, there is irreversible capacity from Si-O-C/CP-as and Si-O-C/CP-SPM because of conversion reaction of SiO_x to Si_yLi_z and Li₂O and formation of SEI on a surface of Si-O-C composites, which is located at ca. 0.8 V vs. Li/Li⁺ [20]. These results are a good agreement with our previous reports [21]. After the 1st cycle, the irreversible capacity of both samples was decreased, indicating reactions related to the formation of SEI and conversion reaction are almost finished. In addition, Si-O-C/CP-SPM delivered a higher discharge areal capacity of 1.32, 1.31, and 1.24 mA h cm⁻² than Si-O-C/CP-as, which has discharge areal

capacity of 1.17, 1.17, and 1.14 mA h cm⁻² at 1st, 2nd, and 10th cycle, respectively.

Figure 2.3.5 (b) shows the cycling ability of Si-O-C/CP-as and Si-O-C/CP-SPM with a charge current of 0.5 mA h cm⁻² for 50 cycles. It demonstrates that both samples have good cycle ability, which is indicating that carbon paper is appropriate as a substrate for Si-O-C composites. Likewise, the irreversible capacity at the 1st cycle of both sample was observed because of conversation reaction of SiO_x and formation of SEI and it is corresponding to charge/discharge curve. Following charge/discharge cycling, the irreversible capacity of Si-O-C/CP-as and Si-O-C/CP-SPM was reduced from 72.0 and 68.9 % to 99.8 and 99.9 % at 1st and 50th cycle.

The comparison of areal capacity depending on kinds of substrate, i.e. as-received copper substrate, as-received carbon paper substrate, and SPM treated carbon paper substrate is shown in Fig. 2.3.6. The Si-O-C composites deposited of Si-O-C/CP-as and Si-O-C/CP-SPM have higher areal capacity of 1.17 and 1.38 mA h cm⁻² than case of as-received copper substrate, which has areal capacity of 0.6 mA h cm⁻² due to 3D structured properties, which has higher reaction areal during electrodeposition of Si-O-C composites, resulting in high deposited amounts of silicon. As the above results, using carbon paper as a substrate for Si-O-C composites is a good attempt for a higher areal capacity of lithium secondary battery.

Figure 2.3.6 The comparison of areal capacity depending on substrate, as-received copper substrate, as-received carbon paper substrate, and SPM treated carbon paper substrate [26] Copyright © 2017 The Electrochemical Society.



2.3.2 Evaluation of suitability of PC or EC/DEC as electrolyte

In this chapter, carbon paper was used as a substrate for Si-O-C composites. However, it is widely known that PC is decomposed around 1.0 V vs. Li/Li⁺ and co-intercalate with lithium ion during charge/discharge, resulting in exfoliation of graphite layer. For this research, exfoliation of graphite layer might be the main reason of capacity fading because of detachment of Si-O-C composites from carbon paper, indicating loss of active material, whereas, usage of EC/DEC as electrolyte forms stable SEI on anode carbon paper surface [22]. In this chapter, PC was used as electrolyte only Si-O-C electrodeposition. However, after electrodeposition, a small amount of PC remains in Si-O-C composites, and this Si-O-C composites assembled with lithium metal as half-cell. Thus, there is a possible to occur decomposition and co-intercalation of PC molecule and lithium ion into graphite layer in carbon paper. To investigate the effect of exfoliation for Si-O-C composites deposited on carbon paper depending on solvent, PC or EC/DEC were used and evaluated the suitability for electrodeposition of Si-O-C composites. Figure 2.3.7 demonstrated the mechanism of exfoliation of graphite layer and formation of SEI depending on the solvent, PC or EC/DEC as an electrolyte.



Figure 2.3.7 Schematic diagram of the mechanism of exfoliation of graphite layer and formation of SEI depending on solvent of PC and EC/DEC as electrolyte.

The deposited amounts of silicon prepared by PC or EC/DEC were compared and presented in Fig. 2.3.8. The Si-O-C composites deposited on SPM treated carbon paper using PC or EC/DEC, namely Si-O-C/CP-PC and Si-O-C/CP-ECDEC, have similar amounts of silicon of 0.17 and 0.16 mg cm⁻² at 8coulomb cm⁻² of passing charge. This result means that EC/DEC is also can be used as the electrolyte for electrodeposition of Si-O-C composites. However, the detailed mechanism of Si-O-C electrodeposition in EC/DEC is not revealed yet. Despite EC/DEC shows similarly deposited silicon amounts with PC, it is not easy to use EC/DEC as an electrolyte for electrodeposition of Si-O-C composites. Because EC/DEC is a solid state at room temperature due to high melting point of EC (33~35°C). For this reason, EC/DEC must be melted before using for electrodeposition of Si-O-C composites. Despite these demerits, both samples show large amounts compare to Si-O-C composites deposited on an as-received copper substrate. It reveals that carbon paper offers larger deposited silicon amounts without reference to a type of electrolyte, PC or EC/DEC.

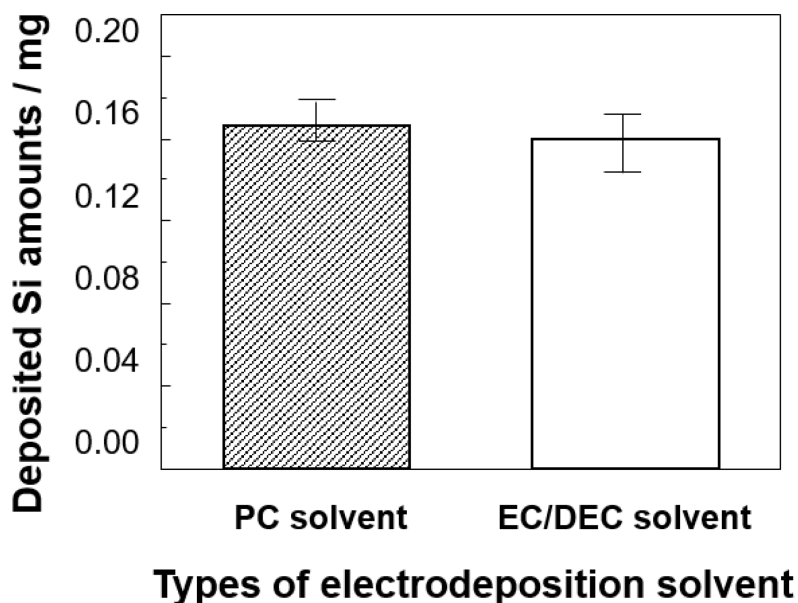


Figure 2.3.8 Comparison of the deposited amounts of silicon prepared by PC or EC/DEC solvent [26] Copyright © 2017 The Electrochemical Society.

To investigate the electrochemical properties of Si-O-C composites as anode depending on different solvent types, charge/discharge test was carried out with a high current density of 1.0 mA h cm^{-2} . The reason of using a higher current density of 1.0 mA h cm^{-2} instead of 0.5 mA h cm^{-2} is to maximize the exfoliation of graphite layer from carbon paper during charge/discharge process. Figure 2.3.9 shows the cycle ability of Si-O-C/CP-PC and Si-O-C/CP-ECDEC for 100 cycles with their coulomb efficiency. The Si-O-C/CP-PC and Si-O-C/CP-ECDEC delivered a discharge areal capacity of 0.96, 0.50, and 0.43 mA h cm^{-2} and 0.71, 0.50, and 0.474 mA h cm^{-2} , respectively, at 1st, 50th, and 100th cycle. Until 34th cycle, Si-O-C/CP-PC shows higher discharge areal capacity than Si-O-C/CP-ECDEC due to higher deposited amounts of silicon. However, it can be observed that Si-O-C/CP-PC shows a rapid capacity fading from ca. 20th cycle, whereas, Si-O-C/CP-ECDEC has relatively stable cycle ability for 100 cycles. For a thorough investigation of above results, discharge areal capacity retention ratio was calculated from Figure 2.3.9 (a) and shown in Fig. 2.3.9 (b). From this converted result, it was confirmed that Si-O-C/CP-PC shows low capacity retention ratio 45.4 % at 100th cycle. On the other hand, Si-O-

C/CP-ECDEC has higher capacity retention ratio of 66.4 % at 100th cycle. It can be considered that loss of Si-O-C composites was occurred by exfoliation of graphite layer of carbon paper due to remain PC in Si-O-C composites.

Figure 2.3.9 (c) and (d) demonstrates charge/discharge curve of Si-O-C/CP-PC and Si-O-C/CP-ECDEC at 1st, 2nd, 10th, and 50th cycle. As mentioned in Fig. 2.3.5, the irreversible capacity was observed from both samples owing to conversion reaction of SiO_x and SEI formation at 1st cycle. This behavior is corresponding to our previous report [2, 5, 6]. In addition, it can be checked that rapid capacity fading of Si-O-C composites prepared by PC was occurred from 10th to 50th cycle, in comparison to Si-O-C/ECDEC. From charge/discharge test, it was confirmed that PC is not appropriate as an electrolyte for electrodeposition of Si-O-C composites because it leads to exfoliation of graphite layer from carbon paper, resulting in rapid capacity fading during charge/discharge cycles.

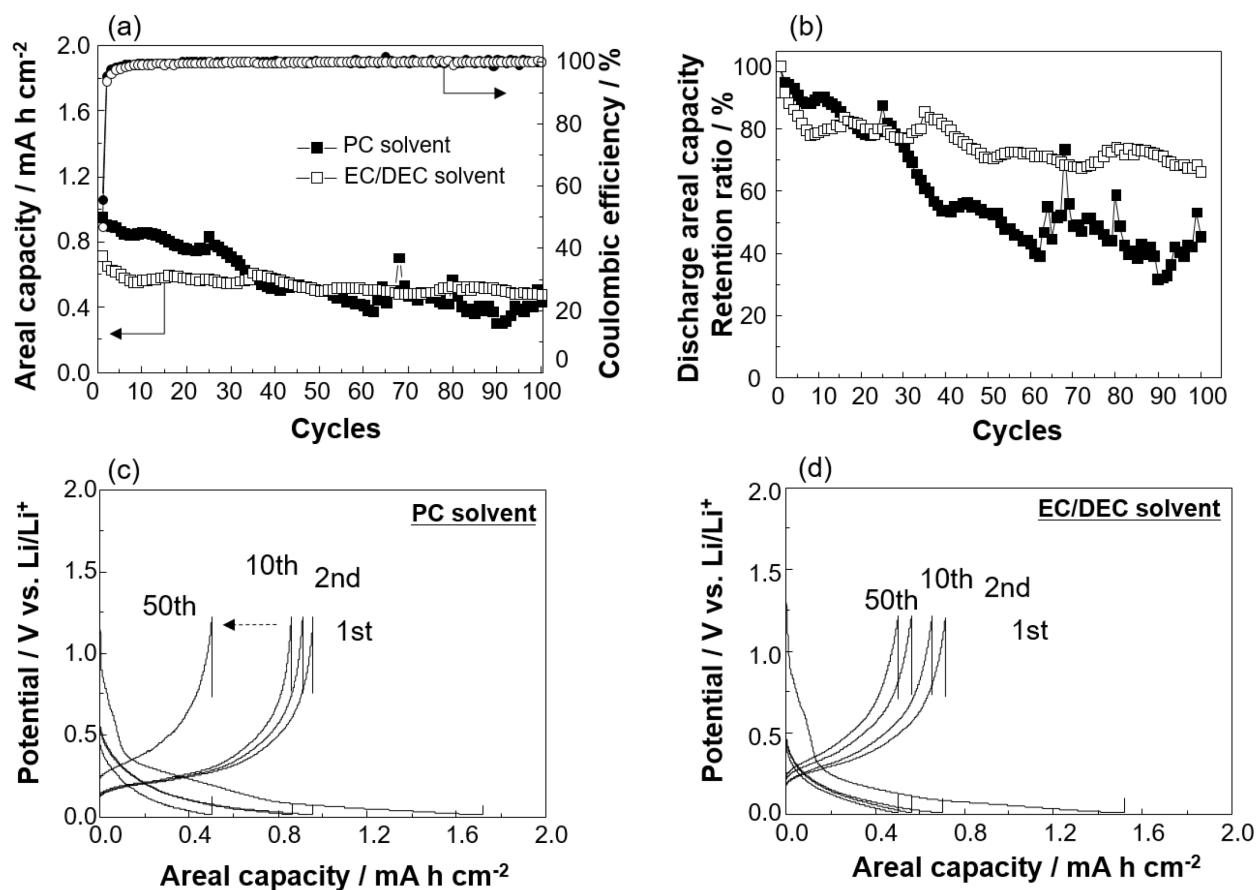


Figure 2.3.9 (a) The cycle ability of Si-O-C/CP-PC and Si-O-C/CP-ECDEC for 100 cycles with their Coulombic efficiency. (b) The discharge area capacity retention ratio of different cycles of Si-O-C/CP-PC and Si-O-C/CP-ECDEC. The charge/discharge curve of (c) Si-O-C/CP-PC and (d) Si-O-C/CP-ECDEC at 1st, 2nd, 10th, and 50th cycle [26] Copyright © 2017 The Electrochemical Society.

For further investigation about exfoliation of graphite layer in carbon paper, Raman measurement of Si-O-C/CP-PC and Si-O-C/CP-ECDEC was carried out and shown in Fig. 2.3.10. Raman measurement is widely used to examine the degree of structural defects in carbon material such as carbon nanotubes, carbon fibers, and carbon paper. The results of Raman measurement consist of line width and intensity indicates the structural transitions and crystalline qualities in carbon structure. In results of Raman measurement in Fig. 2.3.10 (a), two peaks were located at $\sim 1350\text{ cm}^{-1}$ and $\sim 1580\text{ cm}^{-1}$ called by D-band and G-band, respectively, which is known well as typical graphitic carbon. D-band reveals that the degree of structural defect levels in carbon paper with a disorder, deformation, and defoliation levels in graphite layer [23-25]. Unlike this, G-band indicates the crystalline characteristics of carbon paper. Before charge/discharge process, both samples shows typical D-band and G-band peaks of carbon paper located at $\sim 1350\text{ cm}^{-1}$ and $\sim 1580\text{ cm}^{-1}$, respectively, which is meaning that the carbon paper used as a substrate for Si-O-C composites is graphitic carbon material and there was no change of the degree of structural defects in carbon paper. However, after 20th cycle, D-band of Si-O-C/CP-PC was increased, whereas, Si-O-C/CP-ECDEC shows a similar increasing level of D-band. For easy understanding of results of Raman measurement, D/G band intensity ratio was calculated and presented in Fig. 2.3.10 (b). As can be seen in Fig. 2.3.10 (b), Si-O-C/CP-PC demonstrates comparatively increased D/G band intensity ratio from 0.483 to 1.105, whereas, Si-O-C/CP-ECDEC has lower increased intensity values of 0.301 to 0.606 before and after 20th cycle, respectively. From results of Raman measurement, it was clear that PC solvent remained on the surface of Si-O-C composites were decomposed and co-intercalate into graphitic layer from carbon paper during charge/discharge cycle, resulting in rapid capacity fading at high current density during charge/discharge process.

Despite the low stability of Si-O-C composites prepared by PC solvent, Si-O-C composites deposited on 3D structured carbon paper using PC or EC/DEC shows higher discharge areal capacity of 1.8 and 2.7 mA h cm⁻² (Figure 2.3.11), in comparison to Si-O-C composites deposited on copper-based substrate, which has areal capacity of 0.7 mA h cm⁻² at 50 coulomb cm⁻² of passing charge. It was clear that using of carbon paper which has 3D structural characteristics is one of the attempts to obtain higher deposited amounts of silicon and discharge areal capacity for high energy lithium secondary battery.

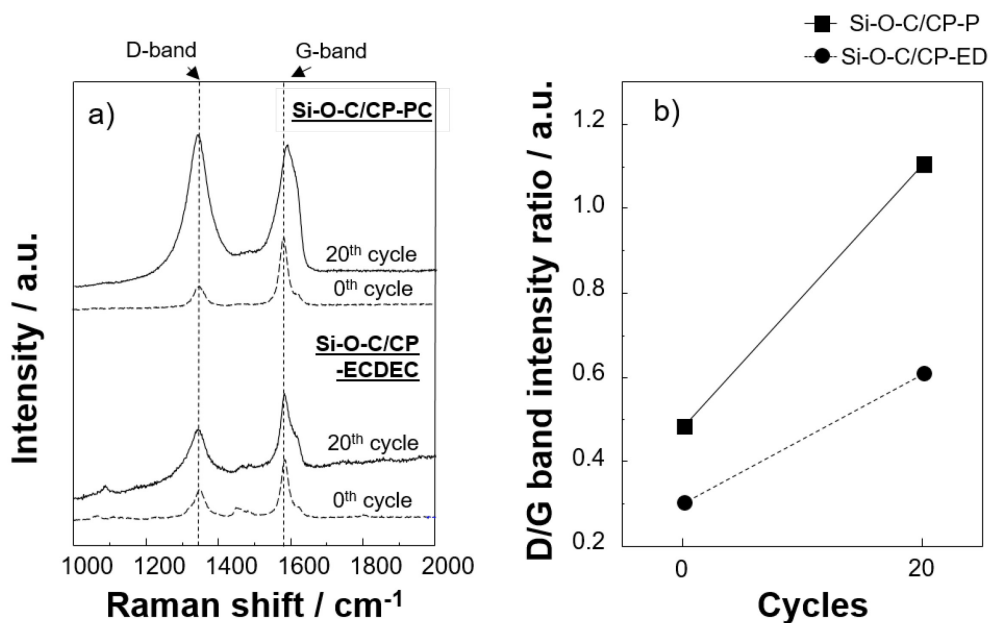


Figure 2.3.10 (a) Raman spectra obtained from Si-O-C/CP-PC and Si-O-C/CP-ECDEC. (b) The peak intensity ratio of D/G band with different cycles [26] Copyright © 2017 The Electrochemical Society.

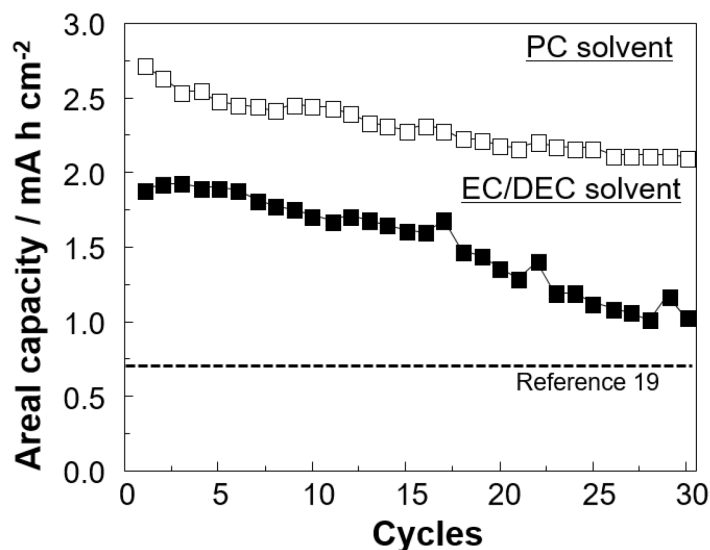


Figure 2.3.11 The areal capacity of Si-O-C composites deposited on 3D structured carbon paper using PC or EC/DEC for 30 cycles [26] Copyright © 2017 The Electrochemical Society.

2.4 Summary

In summary, I tried to use carbon paper as a substrate for Si-O-C composites because of its good advantages such as a large surface area with good electric conductivity. It was clear that surface affinity and wettability between carbon paper and PC solvent was developed by SPM treatment because of generated oxygen-containing functional groups on a surface of carbon paper. SPM treated carbon paper shows the contact angle of 0 °, in comparison to, as-received carbon paper has 58 ° between PC drop and carbon paper because of a low surface affinity of carbon paper.

In addition, PC and EC/DEC solvents were used and compared as an electrolyte for electrodeposition of Si-O-C composites. As a result, it was clear that PC solvent leads to exfoliation of graphite layer from carbon paper, resulting in peeling off of Si-O-C composites from a surface of carbon paper and rapid capacity fading at high charge/discharge current density of 1.0 mA cm⁻². Moreover, it was confirmed that using carbon paper as a substrate for Si-O-C composites is a promising way to increase the deposited amounts of silicon and discharge are capacity.

2.5 References

1. J.-J. Yang, C.-H. Choi, H.-B. Seo, H.-J. Kim, and S.-G. Park, *Electrochim. Acta*, 86 (2012) 277.
2. M. Jeong, T. Yokoshima, H. Nara, T. Momma, and T. Osaka, *RSC Adv.*, 4 (2014) 26872.
3. S.-K. Ahn, J.-J. Yang, H.-I. Kim, H. Habazaki, and S.-G. Park, *Chem. Lett.*, 43 (2014) 898.
4. E. Tsuji, T. Yamasaki, Y. Aoki, S.-G. Park, K-I Shimizu, and H. Habazaki, *Carbon*, 87 (2015) 1.
5. H. Nara, T. Yokoshima, T. Momma, and T. Osaka, *Energy Environ. Sci.*, 5 (2012) 6500.
6. T. Hang, H. Nara, T. Yokoshima, T. Momma, and T. Osaka, *J. Power Sources*, 222 (2013) 503.
7. J. Yan, X. Liu, H. Qi, W. Li, Y. Zhou, M. Yao, and B. Li, *Chem. Mater.*, 27 (2015) 6394.
8. R.B. Mathur, P. H. Maheshwari, T.L. Dhamia, and R.P. Tandon, *Electrochim. Acta*, 52 (2007) 4809.
9. C.-H. Liu, T.-H. Ko, E.-C. Chang, H.-D. Lyu, and Y.-K. Liao, *J. Power Sources*, 180 (2008) 276.
10. Q. Si, M. Matsui, T. Horiba, O. Yamamoto, Y. Takeda, N. Seki, and N. Imanishi, *J. Power Sources*, 241 (2013) 744.
11. Q. Si, M. Kawakubo, M. Matsui, T. Horiba, O. Yamamoto, Y. Takeda, N. Seki, and N. Imanishi, *J. Power Sources*, 248 (2014) 1275.
12. X. Zhang, and Z. Shen, *Fuel*, 81 (2002) 2199.
13. O. A. Gawad, M.H. A. Tabl, Z. A. Hamid, and S.F. Mostafa, *Surf. Coat. Tech.*, 201 (2006) 1357.
14. H. Zhou, Y. Peng, H. B. Wu, F. Sun, and H. Yu, *Nano Energy*, 21 (2016) 80.
15. K. J. Ziegler, Z. Gu, H. Peng, E. L. Flor, R. H. Hauge, and R. E. Smalley, *J. Am. Chem. Soc.*, 127 (2005) 1541.
16. V. Datsyuk, M. Kalyva, K. Papagelis, J. Parthenios, D. Tasis, A. Siokou, I. Kallitsis, and C. Galiotis, *Carbon*, 46 (2008) 833.
17. H. Caro, *Z. Angew. Chem.*, (1898) 845.

18. J. Li, M. J. Vergne, E. D. Mowles, W.-H. Zhong, D. M. Hercules, and C. M. Lukehart, *Carbon*, 43 (2005). 2883.
19. K. A. Wepasnick, B. A. Smith, J. L. Bitter, and D. H. Fairbrother, *Anal. Bioanal. Chem.*, 396 (2010) 1003.
20. C. Wang, I. Kakwan, A. J. Appleby, and F. E. Little, *J. Electroanal. Chem.*, 489 (2000) 55.
21. S. Ahn, M. Jeong, T. Yokoshima, H. Nara, T. Momma, and T. Osaka, *J. Power Sources*, 336 (2016) 203.
22. S.-K. Jeong, M. Inaba, R. Mogi, Y. Iriyama, T. Abe, and Z. Ogumi, *Langmuir*, 17 (2001) 8281.
23. Z. Luo, T. Yu, Z. Ni, S. Lim, H. Hu, J. Shang, L. Liu, Z. Shen, and J. Lin, *J. Phys. Chem. C*, 115 (2011) 1422.
24. A. K. Gupta, Y. Tang, V. H. Crespi, and P. C. Eklund, *Phys. Rev. B*, 82 (2010) 241406(R).
25. F. Tuinstra, and J. L. Koenig, *J. Chem. Phys.*, 53 (1970) 1126.
26. S. Ahn, M. Jeong, K. Miyamoto, T. Yokoshima, H. Nara, T. Momma, and T. Osaka, *J. Electrochem. Soc.*, 164, 2 (2017) A355.
27. N. D. K. Tu, J. Choi, C. R. Park, and H. kim, *Chem. Mater.*, 27 (2015) 7362.
28. V. Singh, D. Joung, L. Zhai, S. Das, S. I. Khondaker, and S. Seal, *Progress in Materials Science*, 56 (2011) 1178.

Chapter 3

Preparation of carbon nanotube anchor layer to improve areal capacity of Si-O-C composite anode for lithium ion batteries

3.1 Introduction

For high areal capacity and large deposited amounts of silicon, usage of carbon paper as a substrate for Si-O-C composites was discussed in chapter 2. From this attempt, it is revealed that SPM treatment enhances the surface affinity and wettability between carbon paper and solvents such as PC and EC/DEC, resulting in improved reactivity of electrodeposition of Si-O-C composites. In addition, higher areal capacity was obtained than in the case of using an as-received copper substrate (Si-O-C/CP-as: $1.17 \text{ mA h cm}^{-2}$, Si-O-C/CP-SPM: $1.38 \text{ mA h cm}^{-2}$, Si-O-C/as-received copper: 0.6 mA h cm^{-2} at $2 \text{ coulomb cm}^{-2}$ of passing charge). Besides, it was discovered that Si-O-C composites prepared by EC/DEC show higher stability for 100th cycle than that of PC owing to exfoliation of graphite layer from carbon paper by co-intercalation of PC molecule and lithium ion.

However, complex process for experiment, i.e. SPM treatment and melting of EC/DEC, is needed for usage of carbon paper as the substrate. Moreover, on the other side, usage of different carbonaceous material which has infinitesimal structure characteristics is considerable to compare with carbon paper which has millimeter scale structure. In the case of carbon paper, Si-O-C composites are deposited on a surface of carbon paper and there is void space in between Si-O-C/carbon paper which can play a role as buffer space to accommodate volume change of silicon. By contrast, in the case of CNTs, Si-O-C composites might be densely deposited inside CNTs layer without void space, resulting in less volumetric properties. For these reasons, in this chapter, CNTs were used to modify the as-received copper substrate. Furthermore, CNTs layer might play a role as an adhered layer and a reinforcing agent for enhancement of adhesion strength and stable structure.

CNTs are used for chemical, biological, and mechanical fields due to its various advantages such as high electric conductivity ($5 \times 10^5 \text{ S m}^{-1}$), lightweight, flexibility, high tensile strength (over 100 times stronger than steel per unit of weight), and so on. Thus, CNTs are also used widely as active materials for electrode, coating materials, and sports goods [1-6].

For modification of the as-received copper substrate, CNTs layer was prepared by high voltage electrophoretic deposition, namely CNTs anchor layer. Electrophoretic deposition is a good way to form this layer on a surface of a substrate without any additives [7]. To increase the stronger attachment of CNTs, a lot of researchers reported the using of metal additive as electric

charge transfer agent on a surface of CNTs [8-12]. Figure 3.1.1 shows the mechanism of electrophoretic deposition using CNTs and metal additives. During electrophoretic deposition, metal additive is decomposed and forms the double electron layer with CNTs which have negatively charge on their surface. Afterward, this metal additive-CNTs migrate toward oppositely charged electrode by electrostatic repulsion force and deposited on an electrode surface.

Using metal additive for electrophoretic deposition has some advantages which are described as following:

- a. To impart the positive charge to CNTs under an electric field.
- b. To hold the CNTs on the surface of electrode even after electrophoretic deposition.
- c. To improve the adhesion strength between CNTs and electrode.
- d. To increase the deposition rate during electrophoretic deposition.

The obtained CNTs anchor layer might play a role as an adhesive layer to hold the Si-O-C composites with a copper substrate and high electron pathway, expecting enhanced adhesion strength between Si-O-C composites and a copper substrate and reduced internal stress. The material characteristics of CNTs anchor layer and Si-O-C composites were measured and discussed in this chapter using various examine methods.

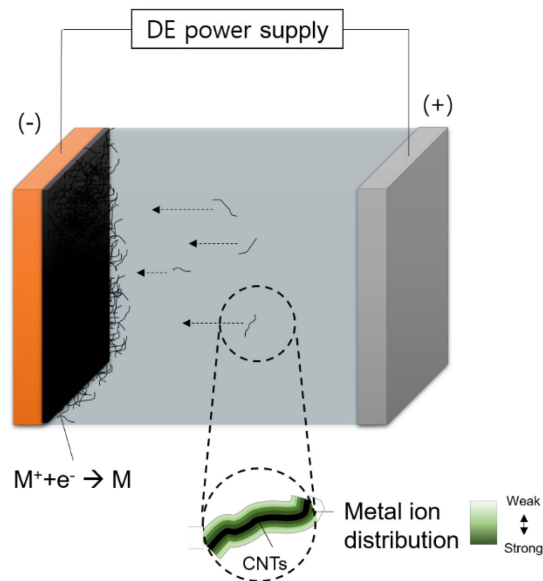


Figure 3.1.1 Schematic diagram of the mechanism of electrophoretic deposition using CNTs and metal additives.

3.2 Experimental

3.2.1 Fabrication of CNTs anchor layer

The purchased CNTs, which has carbon purity over 90% with diameter around 10nm (Nanocyl -NC7000) were employed for anchor layer. Before electrophoretic deposition, surface treatment of CNTs was carried out using concentrated H₂SO₄/HNO₃ mixed acid (3:1; v/v, purity of 96.0 % and 60.0 %, respectively) for 4 hours at 45 °C by sonication to functionalize the surface of CNTs. After that, acid-treated CNTs were washed by water until it has pH 7 and vacuumed at 80 °C for 4 hours. Subsequently, surface treated CNTs (0.05 mg ml⁻¹ of IPA) were dispersed in isopropyl alcohol (IPA) using sonication for 30 min. At the same time, cobalt dichloride (CoCl₂) is also dispersed by sonication in IPA at the same time. After dispersion of CNTs and CoCl₂, both solvents were mixed and sonicated together for 30 min again. The copper substrate, platinum plate with exposed area of 1x1 and 2x2 cm, respectively, were used as working and counter electrode for electrophoretic deposition. The two electrodes were soaked CNTs and CoCl₂ dispersed IPA solution with a gap of 1 cm between both electrode. A direct current power supply was used as power source and a constant voltage of -120 V was applied. The time of electrophoretic deposition and amounts of CoCl₂ were controlled to evaluate appropriate values for CNTs anchor layer. After electrophoretic deposition, the CNTs anchor layer was deposited on a copper substrate and the obtained CNTs/Cu substrate was washed by distilled water and ethanol to remove aggregated CNTs particles and impurities of their surface. After washing process, the CNTs/Cu substrate was dried in a dry room for overnight. Figure 3.2.1 depicts the experiment equipment for electrophoretic deposition.

3.2.2 Electrodeposition of Si-O-C composites on carbon paper

All procedures of electrodeposition of Si-O-C composites are similar to chapter 2. A 0.5 mol dm⁻³ of SiCl₄ (Sigma-aldrich) was employed as a silicon source and same amounts of tetrabutylammonium perchlorate (Kanto Chemical) was used as supporting electrolyte and dissolve in propylene carbonate solvent (Kishida). Electrodeposition was carried using as-received or CNTs/Cu substrate, platinum wire, and lithium metal as a working, a counter, and a

reference electrode in glove box which is filled by argon gas with a dew point lower than $-90\text{ }^{\circ}\text{C}$. A constant cathodic current of -1.0 mA cm^{-2} and various quantity of electricity for electrodeposition from 2 to 15 coulomb cm^{-2} was applied for electrodeposition of Si-O-C composites.

3.2.3 Material characteristics of CNTs anchor layer and Si-O-C composites

Morphological properties of CNTs anchor layer and Si-O-C composites were examined by field emission scanning electron microscopy (FE-SEM, Hitachi, S-4800) with energy dispersive X-ray spectroscopy (SEM, Hitachi TM-3000). X-ray photoelectron spectroscopy (XPS, JEOL, JPS-9010TR) was used to measure the surface characteristics of Si-O-C composites depending on charge/discharge cycling number. Deposited amounts of silicon were analyzed by inductively coupled plasma (ICP, Thermo Scientific, iCAP6500 Duo) analysis and these values were used to calculate the charge/discharge current density.

3.2.4 Electrochemical characteristics of Si-O-C composites

For the electrochemical measurement, coin typed cell (2032 type) was used with Si-O-C and Li metal as working and counter electrode, respectively. A 1.0 mol dm^{-3} lithium perchlorate (LiClO_4) in propylene carbonate-ethylene carbonate (PC/EC = 1:1, v/v, Kishida) was used as electrolyte for Electrochemical cell test. The coin typed cell was assembled in argon filled glove box with a dew point of $-100\text{ }^{\circ}\text{C}$. To compare the surface area between as-received copper substrate and CNTs/Cu substrate, cyclic voltammogram (CV) was used in the potential range of 0.01-1.20 V vs. Li/Li^+ at a scan rate of 0.1 mV s^{-1} (Hokuto Denko, HZ-5000). In addition, CV measurement was used to identify the electrochemical characteristics of Si-O-C composites with above condition. The charge/discharge test of Si-O-C composites depending on type of substrate, the as-received copper substrate or CNTs/Cu substrate, was investigated by a constant current (CC) charge/discharge measurement with 0.1 C-rate in the potential range between 0.01-1.20 V vs. Li/Li^+ , and the C-rate value was calculated depending on deposited amounts of silicon as mentioned above.

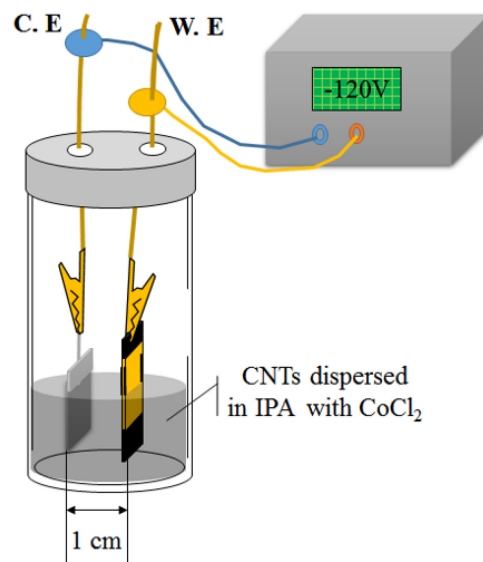


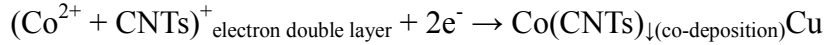
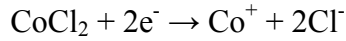
Figure 3.2.1 The experiment equipment for electrophoretic deposition.

3.3 Results and discussions

3.3.1 Evaluation of CNTs/Cu substrate for Si-O-C composites

Figure 3.3.1 depicts the surface morphological properties of a copper substrate after electrophoretic deposition depending on amounts of CoCl_2 and time for electrophoretic deposition. It was revealed that in the case of 0.00 mg ml^{-1} of CoCl_2 shows raw state copper surface without any CNTs anchor layer due to absence of metal additives. The reason of non-deposited copper substrate after electrophoretic deposition is that Co^{2+} can play a role as an important factor for the formation of stable CNTs layer. Co^{2+} imparts a positive charge on CNTs surface which is dispersed well in IPA, forming electron double layer in an electric field. Afterward, when the Van Der Waals force overcomes repulsive forces between $(\text{CNTs/Co})^+$, it transfers toward negative electrode and co-deposited on its surface. The reaction mechanism of

electrophoretic deposition of CNTs with cobalt is as below.



Thus, concentration of metal additives is important. On the other hand, in a case of 0.15 and 0.50 mg m⁻¹ of CoCl₂ demonstrate copper substrate are covered by CNTs and it became dark as increase the amounts of CoCl₂ and time of electrophoretic deposition. From there results, it was observed that control of amounts of CoCl₂ and time of electrophoretic deposition is a key factor to the fabrication of CNTs anchor layer on a copper substrate. The surface area of each sample was measured by razor microscope measurement and presented in Fig. 3.3.1. As a result, it could be obtained that the highest surface area of 2.5, 3.1, and 3.2 cm⁻² from each sample and these samples were selected as substrate for electrodeposition of Si-O-C composites. The charge/discharge cycle test of these three samples was measured to identify the suitability as a substrate for Si-O-C composites in Fig. 3.3.2.

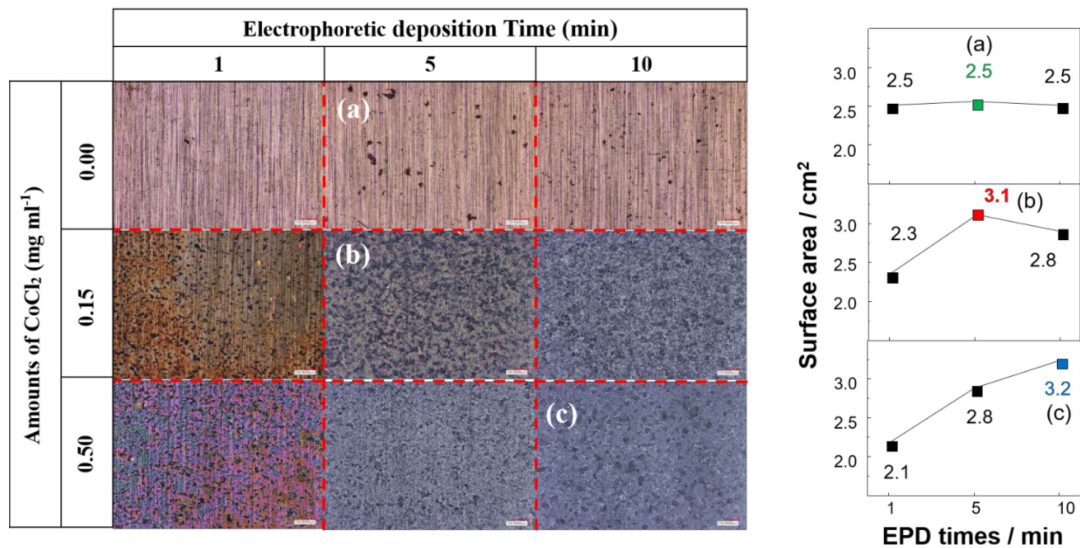


Figure 3.3.1 SEM image of the copper substrate after electrophoretic deposition depending on different amounts of CoCl₂ and time of electrophoretic deposition.

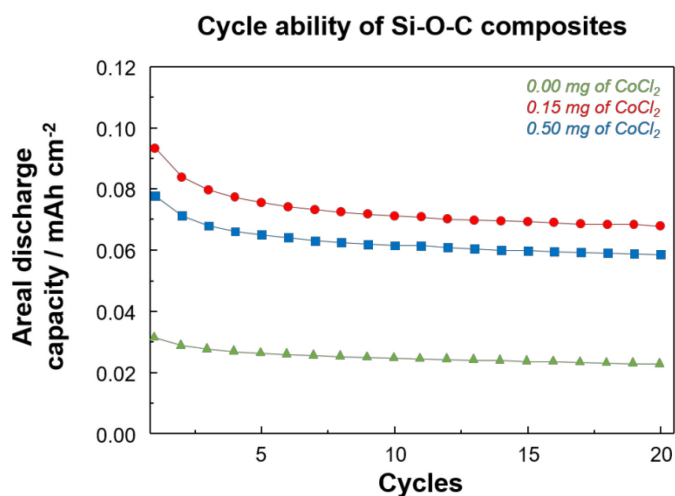


Figure 3.3.2 Cycle ability Si-O-C composites deposited on CNTs/Cu fabricated depending on different amounts of CoCl₂.

As seen in Fig. 3.3.2, the Si-O-C composites deposited on CNTs/Cu substrate (Si-O-C/CNTs/Cu), which was prepared by 0.15 mg ml⁻¹ of CoCl₂ shows highest areal capacity of 0.092 and 0.071 mA h cm⁻² at 1st and 20th cycle, whereas, Si-O-C/CNTs/Cu prepared by 0.00 mg ml⁻¹ of CoCl₂ shows lowest areal capacity of 0.078 and 0.061 mA h cm⁻² at 1st and 20th cycle. It is assumed that higher surface area of CNTs/Cu effect on deposited amounts of silicon during electrodeposition, resulting in higher areal capacity. In addition, Si-O-C/CNTs/Cu fabricated by 0.50 mg ml⁻¹ of CoCl₂ demonstrates lower areal capacity in comparison to Si-O-C/CNTs/Cu by 0.15 mg ml⁻¹ of CoCl₂ even it has CNTs anchor layer and higher surface area. To figure out the reason for this result, XPS measurement was carried (in Fig. 3.3.3).

In XPS result of above three CNTs/Cu substrates, it is clear that cobalt oxide compounds peaks located at 786 and 781 eV was increased and it might play a role as resistance materials to decrease cell performance, resulting in lower areal capacity of Si-O-C/CNTs/Cu (with CoCl₂ amounts of 0.50 mg ml⁻¹ of CoCl₂) during electrophoretic deposition. From those results, appropriate amounts of CoCl₂ and electrophoretic deposition time were decided as a substrate for Si-O-C composites.

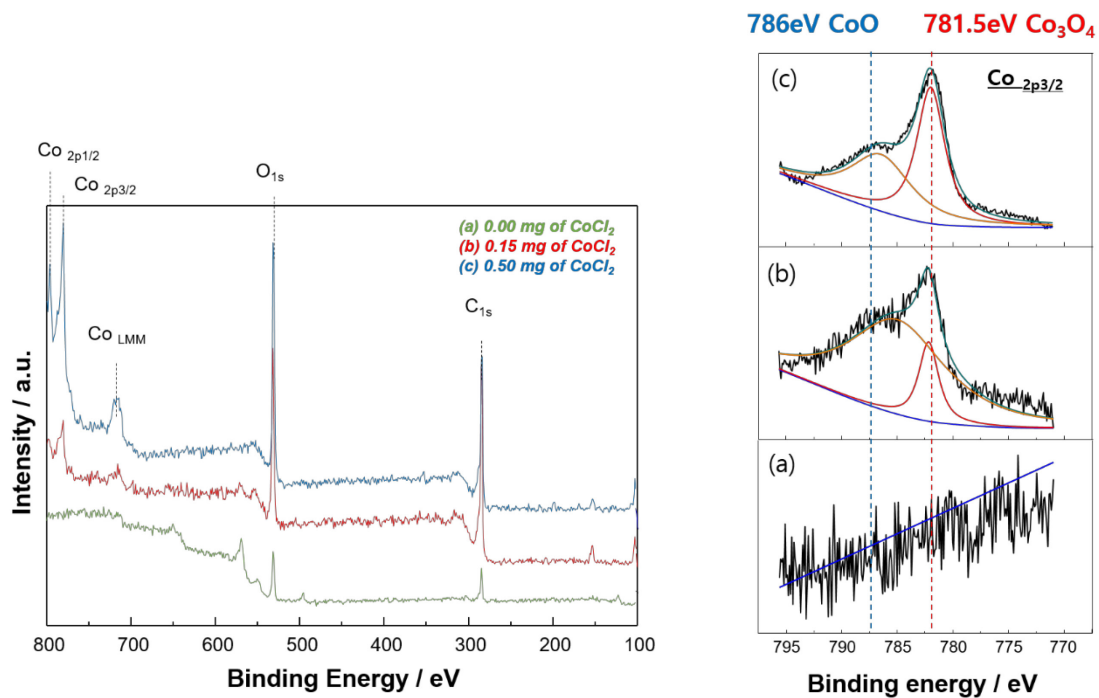


Figure 3.3.3 XPS analysis of Si-O-C/CNTs/Cu fabricated with different amounts of CoCl_2 .

3.3.2 Effect of CNTs anchor layer for Si-O-C composites

Si-O-C composites were deposited on as-received copper substrate (Si-O-C/Cu) and CNTs/Cu substrate at 2 coulomb cm^{-2} of passing charge. The surface plane view of both substrates measured by FE-SEM in Fig. 3.3.4 (a) and (b). It reveals that as-received copper substrate shows smooth and flat surface property. It might offer low adhesion strength between Si-O-C composites and substrate. On another hand, a copper substrate which is covered by CNTs anchor layer depicts opposite surface characteristics such as rough, 3D structure, large surface area, implying enhanced adhesion strength by CNTs anchor layer. Figure 3.3.4 (c) and (d) demonstrate the Si-O-C composites deposited on an as-received copper substrate and CNTs/Cu substrate, respectively. As can see in Fig. 3.3.4 (c), cracked surface of Si-O-C composites was observed. Meanwhile, there is no cracked surface on Si-O-C/CNTs/Cu because CNTs anchor layer holds each Si-O-C composites to prevent structural collapse. From this result, improvement of electrochemical performance of Si-O-C/CNTs/Cu is expected than Si-O-C/Cu composites.

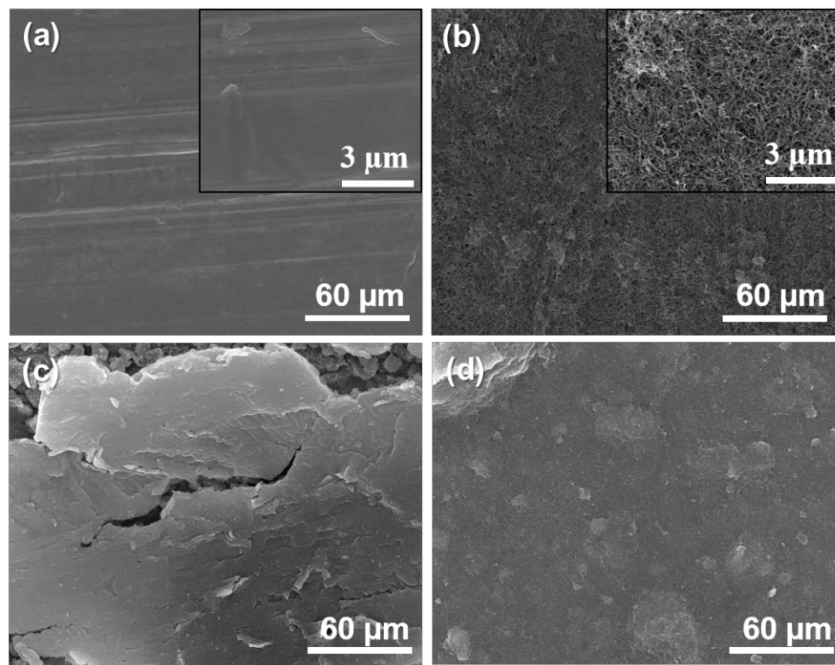


Figure 3.3.4 SEM images of (a) as-received copper substrate (b) CNTs/Cu substrate, (c) Si-O-C/Cu, and (d) Si-O-C/CNTs/Cu at 2 coulomb cm^{-2} of passing charge amount [21]
Copyright © 2016 Elsevier B.V. All rights reserved.

To compare the effect of surface area from an as-received copper substrate and CNTs/Cu substrate, cyclic voltammogram (CV) was carried out in the potential range of 0.01-1.20 V vs. Li/Li⁺ at a scan rate of 0.1 mV s⁻¹. Figure 3.3.5 shows the CV curve of Si-O-C/Cu and Si-O-C/CNTs/Cu. The Si-O-C/CNTs/Cu has a higher capacitance of 7.54 mF cm⁻² than Si-O-C/Cu which has a capacitance of 0.57 mF cm⁻².

The capacitance of both samples calculated by following equation (1). The C is capacitance (F), Q is amounts of charge (A), and V is voltage range (V). However, this equation can be converted using a factor of a surface of the electrode as following equation (2).

$$C(\text{Capacitance, F}) = \frac{Q(\text{Charge})}{V(\text{Voltage})} \quad (1)$$

$$C = \varepsilon \frac{A(\text{Area of eletrode})}{d(\text{Distance between electrode})} \quad (2)$$

The higher capacitance indicates not only the ability to store charge in the electric double layer but also parameter to compare the surface area of the electrode. Thus, higher capacitance means the larger ions can contact with the electrode, in other words, much more ions can react with the surface of the electrode. This hypothesis also relates to higher reactivity between the substrate and silicon ion during electrodeposition.

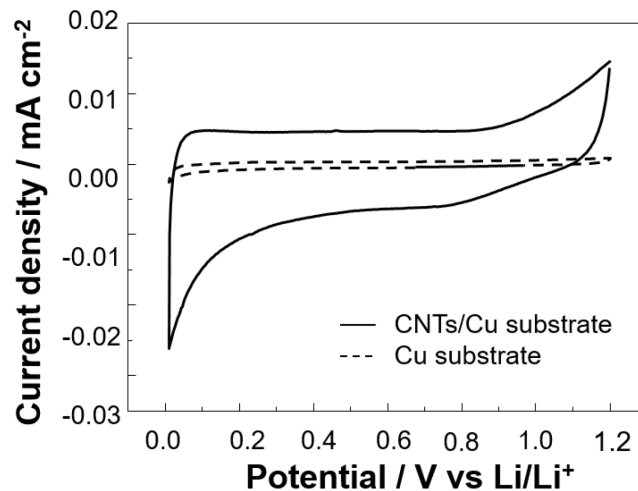


Figure 3.3.5 The CV curve of Si-O-C/Cu and Si-O-C/CNTs/Cu [21] Copyright © 2016 Elsevier B.V. All rights reserved.

Deposited silicon amounts of Si-O-C/Cu and Si-O-C/CNTs/Cu were examined and presented in Fig. 3.3.6. As supposed in CV result, Si-O-C/CNTs/Cu show higher deposited silicon amounts 0.056 mg cm^{-2} , whereas, Si-O-C/Cu have 0.048 mg cm^{-2} . The improved reactivity between silicon ion and substrate was speculated because of increased surface area by CNTs anchor layer. However, it is not enough as answer for improvement of deposited silicon amounts. Therefore, another presumption can be considered for enhanced reactivity of electrodeposition. It is known well that CNTs has lower electric resistance than silicon (CNTs: $1 \times 10^{-6} \Omega \text{ m}$, Silicon: $2.3 \times 10^3 \Omega \text{ m}$), and this difference has large influence in chemical and electrochemical reaction such as oxidation, reduction, and diffusion of electron. To verify these hypotheses, efficiency of Si-O-C electrodeposition was calculated depending on Si-O-C/Cu and Si-O-C/CNTs/Cu and the values are as below.

■ Electrodeposition efficiency

- as-received copper substrate: 68.8%

- CNTs/Cu substrate: 84.4%

From these two parameters, i.e. large surface area and low electric resistance, it reveals the large deposited silicon amounts of Si-O-C/CNTs/Cu as same quantity of electricity for electrodeposition. To clearly summarize the relationship among above parameters, the detailed investigation about internal resistance should be focus in future work.

In addition, the reproducibility of Si-O-C electrodeposition was tested and listed in Table 3.3.1. These samples have similar deposited amounts of silicon through repetition of electrodeposition at same condition for three times regardless of as-received copper and CNTs/Cu substrate. From this investigation, it is known that electrodeposition of Si-O-C composites on CNTs/Cu substrate has reversible reaction during electrodeposition, meaning CNTs/Cu substrate can be reacted well like as as-received copper substrate.

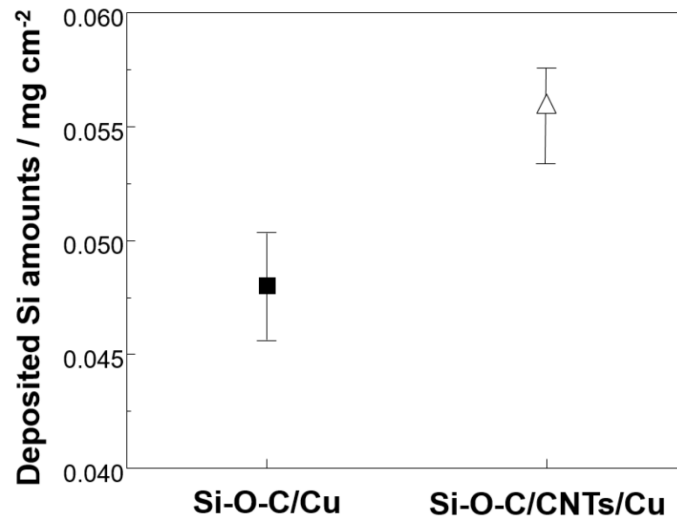


Figure 3.3.6 Deposited amounts of silicon from Si-O-C/Cu and Si-O-C/CNTs/Cu prepared at 2 coulomb cm⁻² of passing charge [21] Copyright © 2016 Elsevier B.V. All rights reserved.

Table 3.3.1 Deposited silicon amounts of Si-O-C/Cu and Si-O-C/CNTs/Cu prepared by electrodeposition at 2 coulomb cm⁻² of passing charge with average values.

	Sample number	Deposited silicon / mg cm ⁻²
Si-O-C/Cu	1	0.050
	2	0.046
	3	0.047
Si-O-C/CNTs/Cu	1	0.056
	2	0.057
	3	0.055

The plane view of Si-O-C/CNTs/Cu substrate was measured by SEM with elemental mapping of silicon, oxygen, carbon, and cobalt (Fig. 3.3.7). The three elements of silicon, oxygen, and carbon were observed on all surface of Si-O-C composites. It was clear that these three elements are deposited on surface of CNTs/Cu substrate homogeneously. And this behavior is corresponding to previous results in Fig. 2.3.4. It means that electrodeposition of Si-O-C composites have less of an effect on type of substrate such as as-received copper and carbonaceous substrate. On the other hands, cobalt was not detected on surface of Si-O-C composites. Because as less amount of cobalt dichloride as possible was introduced to form holding layer between CNTs and copper substrate. As described before, it is important to control the appropriate amounts of cobalt dichloride additive during electrophoretic deposition. If exceed amount of metal additive are used, the cobalt ion deposited on substrate and surface of CNTs, forming cobalt oxide compound. This adduct play a role as resistance and deteriorate performance of LIBs. By contrast, in the case of using the less amount of cobalt dichloride additive, the cobalt ion cannot form holding layer, causing low adhesion strength between CNTs and copper substrate.

The cobalt and its compound located in CNTs/Cu should be identified to prove the existence of holding layer formed by cobalt. For this reason, deposited cobalt amounts were also examined by ICP measurement. As can see in Table.3.3.2, Each sample have the deposited amounts of cobalt of 0.580, 0.460, and 0.535 $\mu\text{g cm}^{-2}$, respectively, and the average value is 0.525 $\mu\text{g cm}^{-2}$. By SEM-EDX analysis, it was detected that cobalt compounds are nonexistent on surface of Si-O-C/CNTs/Cu, however, existence of cobalt and its amounts was observed in Si-O-C/CNTs by ICP measurement.

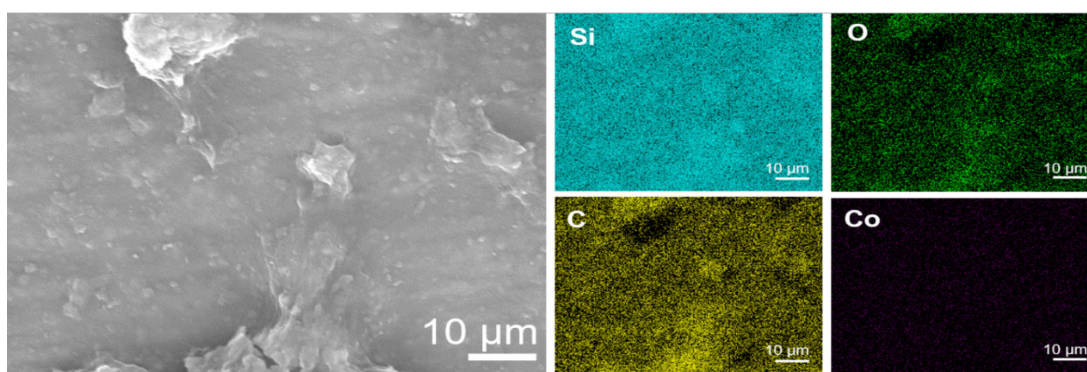


Figure 3.3.7 The plane view of Si-O-C composites deposited on CNTs/Cu substrate was measured by SEM with elemental mapping of silicon, oxygen, carbon, and cobalt [21] Copyright © 2016 Elsevier B.V. All rights reserved.

Table 3.3.2 Deposited cobalt amounts of CNTs/Cu substrate with average values.

Samples number	Deposited cobalt / $\mu\text{g cm}^{-2}$	Average amount / $\mu\text{g cm}^{-2}$
1	0.580	0.525
2	0.460	
3	0.535	

To discover the cobalt holding layer between CNTs anchor layer and copper substrate, cross-section view of Si-O-C/CNTs/Cu was observed before and after charge/discharge process with EDX elemental mapping. However, it was difficult to accurately measure about the cobalt holding layer. There is some possible reason for fail to examine the cobalt holding layer. 1) Very little amount of cobalt dichloride for electrophoretic deposition. 2) The very thin thickness of holding layer, 3) Use of inappropriate measuring equipment. For these reasons, related literature was referred to figure out the holding layer. S. Santhanagipalan et al. reported the electrophoretic deposition using CNTs to form vertically aligned forests. In that of literature, an existence of holding layer and its role are described. The holding layer is prepared by co-deposition of a metal additive, resulting in the formation of strong adhesiveness between CNTs and substrate [12]. In addition, the metal hydroxide compound provides stronger binding strength than metal alkoxides compound [22]. Through these literature surveys, it reveals that cobalt holding layer offers good adhesiveness, resulting in strong bonding between CNTs and copper substrate.

Thickness change of Si-O-C/CNTs/Cu were observed before and after charge/discharge process by electro-optical measurement of Si-O-C cross-section. Before charge/discharge test, the Si-O-C/CNTs/Cu has a thickness of 6.3 μm including CNTs anchor layer. From EDX mapping, it was confirmed that three elements are deposited on CNTs/Cu substrate homogeneously as shown in Fig. 3.3.8. After charge/discharge test, the thickness of Si-O-C/CNTs layer was increased up to 14.9 μm because of volume change of silicon. Moreover, it is observed that Si-O-C/CNTs composites show the linear shape and tangled each other due to binding properties of CNTs anchor layer. As a result, it is supposed that the CNTs anchor layer might play a role as not only an adhesiveness layer to prevent peeling off of Si-O-C composites but also binding agent during charge/discharge cycling. Furthermore, distribution of silicon,

oxygen, and carbon still remain after volume change of silicon, an indication has structural stability.

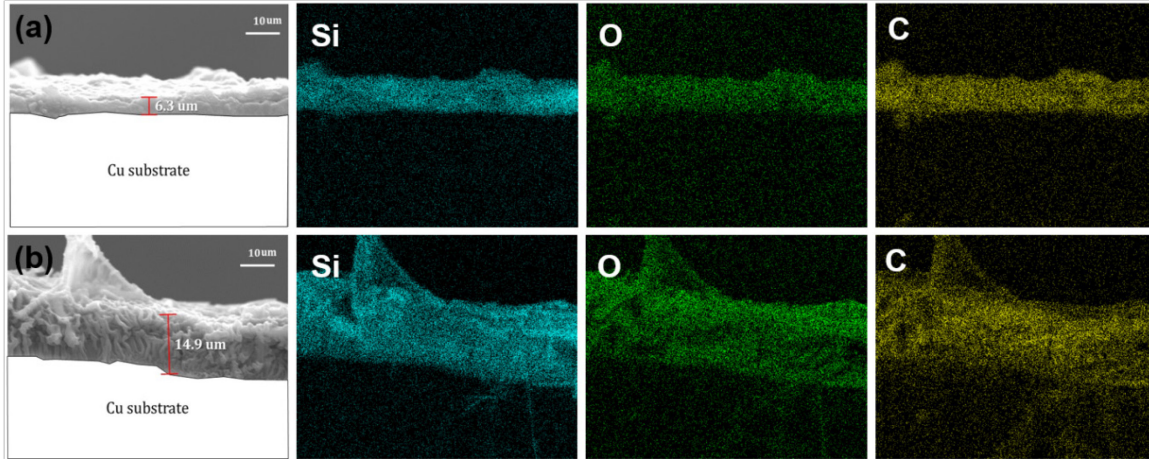
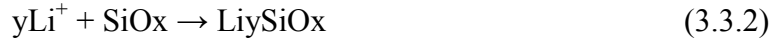


Figure 3.3.8 The SEM images of cross-section from Si-O-C/CNTs/Cu before and after charge/discharge process were examined with EDX elemental mapping of silicon, oxygen, and carbon without cobalt [21] Copyright © 2016 Elsevier B.V. All rights reserved.

Figure 3.3.9 shows the CV results of Si-O-C/CNTs/Cu in the potential range between 0.01 and 1.2 V at a scan rate of 0.1 mV s^{-1} for 5 cycles. At 1st cycle, a huge irreversible peak was appeared at ca. 0.01 V vs. Li/Li^+ because of conversion reaction of SiO_x to Li_xSi_y and Li_2O and SEI formation on a surface of Si-O-C composite. However, this huge irreversible peak was disappeared after 2nd cycle, indicating the finish of conversion reaction and SEI at 1st cycle. Thus, there was no huge cathodic peak after 2nd cycle. The mechanism of irreversible capacity is indicated in equation 3.3.1 and 3.3.2. In addition, the reaction mechanism of SEI formation on surface of Si-O-C composites described as equation 3.3.3. Those chemical reactions were carried on in charge process at 1st cycle, resulting in huge irreversible capacity of Si-O-C composites. Reaction in equation 3.3.4 is responsible for reversible capacity after 1st cycle and it is typical reaction of silicon-based materials as anode.





At 2nd cycle, new peaks located at ca. 0.2 and 0.01 V vs. Li/Li⁺ were detected. These peaks were discovered as lithiation reaction of Si by our previous report [18-20]. Moreover, delithiation peaks of Li_xSi_y forward to amorphous-Si were observed at ca. 0.37 and 0.50 V vs. Li/Li⁺. More detail analysis about conversation reaction of SiO_x to Li_xSi_y will be discussed in part of charge/discharge test. This CV result shows the typical oxidation and reduction reaction of Si-O-C composites during charge/discharge process, and it is good agreement with our previous report. From this result, it is surmisable that CNTs/Cu substrate offers reversible reaction as substrate during interface reaction between anode and electrolyte, accompanying good electron transfer capability.

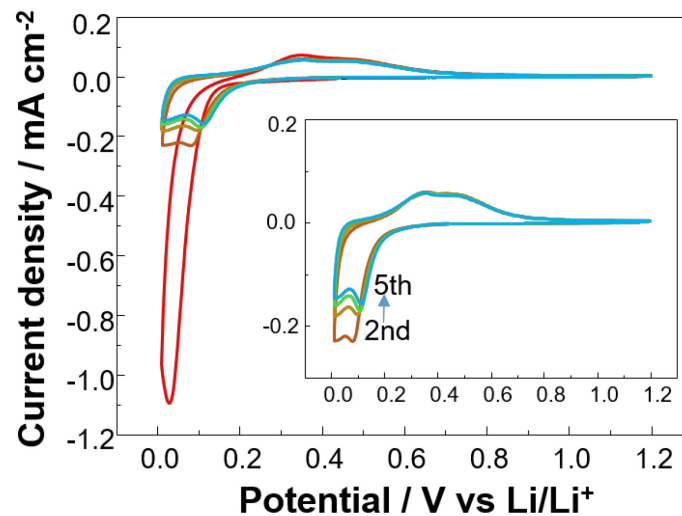


Figure 3.3.9 The CV curves of Si-O-C composites deposited on CNTs/Cu substrate in the potential range between 0.01 and 1.2 V at a scan rate of 0.1 mV s⁻¹ for 5 cycles [21]

Copyright © 2016 Elsevier B.V. All rights reserved.

The XPS Peaks of the Si-O-C/CNT/Cu before and after charge/discharge cycle for the 100th cycle are shown in Fig. 3.3.10. The peaks of Si_{2p}, C_{1s}, O_{1s}, and Li_{1s} were observed without Co_{2p3} because of fewer amounts of cobalt dichloride during electrophoretic deposition, corresponding to result of EDX elemental mapping in Fig. 3.3.7. After charge/discharge cycle for 100th cycle, the binding energies of Si_{2p} located at ca. 103.4 eV was shifted to a lower binding energy of ca. 102.5 eV, which is attributed to a lithiation reaction of Si with lithium ion to form Li_xSi_y. In the spectrum of C_{1s}, only one peak was observed before charge/discharge cycle at ca. 284.4 eV. However, after charge/discharge for the 100th cycle, the C_{1s} peak located at ca. 284.4 eV was decreased, in addition, a new peak was detected at ca. 298.4 eV, attributed to carbonate peak including Li₂CO₃ and R-CH₂OCO₂Li. Moreover, the peak located at the around 284.4 eV has a lower intensity than our previously study [18-20]. It is supposed that the concentration of carbon was changed because of enhanced electric conductivity by CNTs anchor layer during electrodeposition of Si-O-C composites. For more specific reasons, GDOES analysis was carried to measure the concentration of each element (not shown here). From this result, it was confirmed that Si-O-C/CNTs/Cu has higher carbon ratio in comparison to Si-O-C/Cu. Of course, there is possible that CNTs anchor layer contributed to increasing the carbon ratio. The peak of O_{1s} located at the ca. 532.7 eV was shifted to ca. 531.8 eV after charge/discharge for 100th cycles. This peak is attributed to the present of Li₂CO₃, LiOH, Li₂O, Li₄SiO₄, and R-CH₂OCO₂Li because of decomposition of organic electrolyte during cycling. The peak of Li_{1s} was not detected before charge/discharge. However, after charge/discharge for 100th cycles, the new peak was observed at the binding energy of ca. 55.4 eV, indicating the completion of alloy/dealloy reaction of lithium ion with silicon. These results are in good agreement with results of Si_{2p} peaks. By contrast, there were no changes in a peak of Co_{2p3}. It is clear that very small quantities of cobalt cannot influence the electrochemical reaction, and it is corresponding to results of elemental mapping in Fig. 3.3.7.

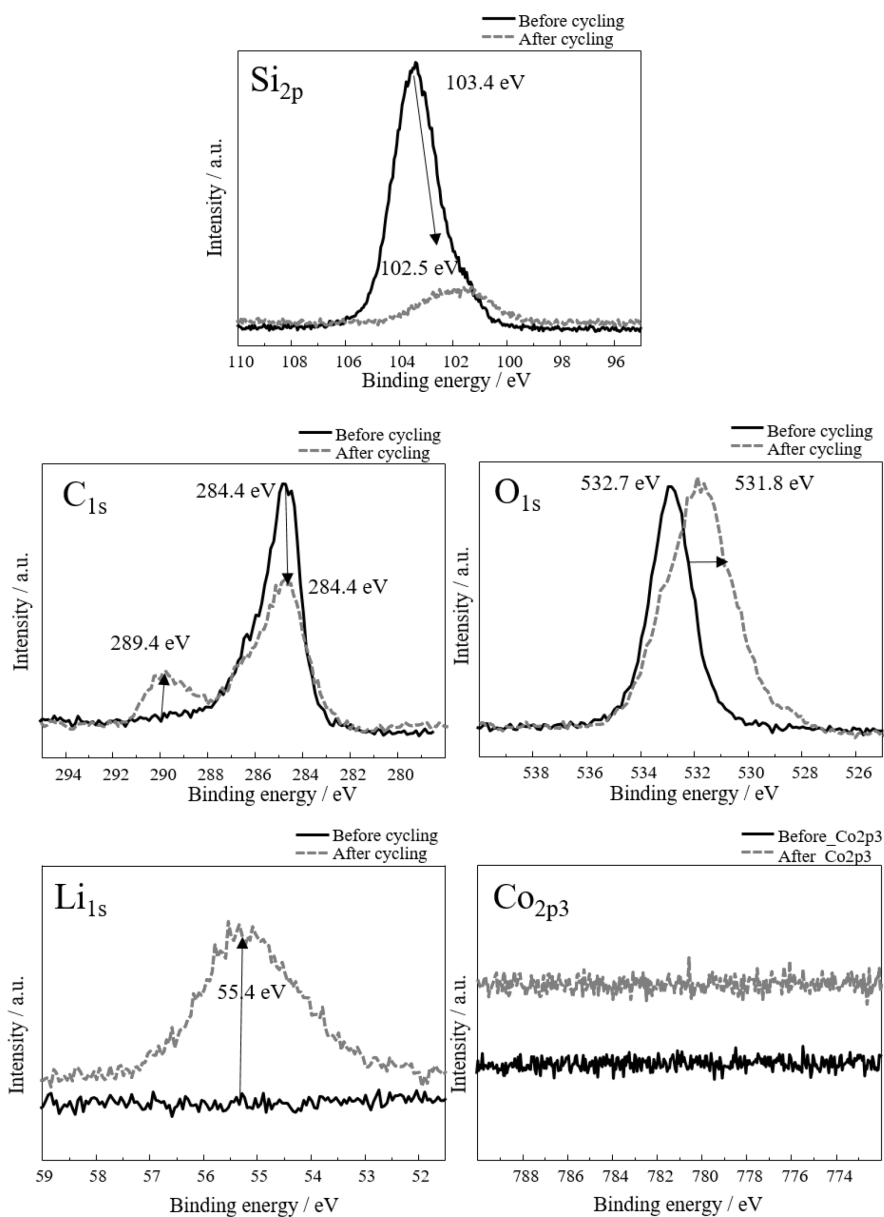


Figure 3.3.10 The XPS Peaks of Si_{2p}, C_{1s}, O_{1s}, Li_{1s} and Co_{2p3} of the Si-O-C/CNT/Cu before and charge/discharge process after 100th cycle.

Figure 3.3.11 shows the charge/discharge cycle performance of Si-O-C/CNTs/Cu and Si-O-C/Cu with their coulomb efficiency for the 100th cycle. The Si-O-C/Cu delivered a discharge specific capacity of 1173, 943, and 840 mA h (g of Si)⁻¹ at 1st, 50th, and 100th cycle, respectively. On the other hand, Si-O-C/CNTs/Cu shows a higher discharge specific capacity of 1696, 1268, and 1078 mA h (g of Si)⁻¹ at 1st, 50th, and 100th cycle, respectively. From this comparison result, it is supposed that CNTs anchor layer influences on electrochemical properties. Therefore, it should be considered the main reason for improved electrochemical performance and there are three guessable reasons. These parameters are described as below.

- a. Role as active materials: As mentioned above, CNTs have a lot chemical, physical, and electrochemical advantages. For these reasons, It can play a role as active material and it delivered a discharge capacity of ca. 180~200 mA h g⁻¹.
- b. A high electric conductivity of CNTs: One of advantage from CNTs is high electric conductivity. This feature decreases the internal resistance and develops reaction rate during charge/discharge process.
- c. Enhanced stability of Si-O-C: Silicon anode suffers volume change during intercalate/de-intercalate reaction, generating isolate silicon particles and increasing internal stress.

Despite a difference of discharge specific capacity, both Si-O-C composites show good coulomb efficiency over 98% for 100 cycles. This is a unique attribute of Si-O-C composites because of its thin thickness in comparison to typical graphite anode which has tens or hundreds μm of thickness (Si-O-C/Cu: $\sim 0.5 \mu\text{m}$, Si-O-C/CNTs/Cu: 5~6 μm before charge).

Figure 3.3.11 (b) indicates the discharge areal capacity of Si-O-C/Cu and Si-O-C/CNTs/Cu for 100 cycles. It was confirmed that Si-O-C/CNTs/Cu demonstrates a higher areal capacity of 0.10 and 0.06 mA h cm⁻² at the 1st and 100th cycle, respectively. Whereas, Si-O-C/Cu delivered a discharge areal capacity of 0.08 and 0.05 mA h cm⁻² at same cycle. The main reason of increased areal capacity of Si-O-C/CNTs/Cu is large deposited silicon amount because of enhanced electrodeposition efficiency by CNTs anchor layer.

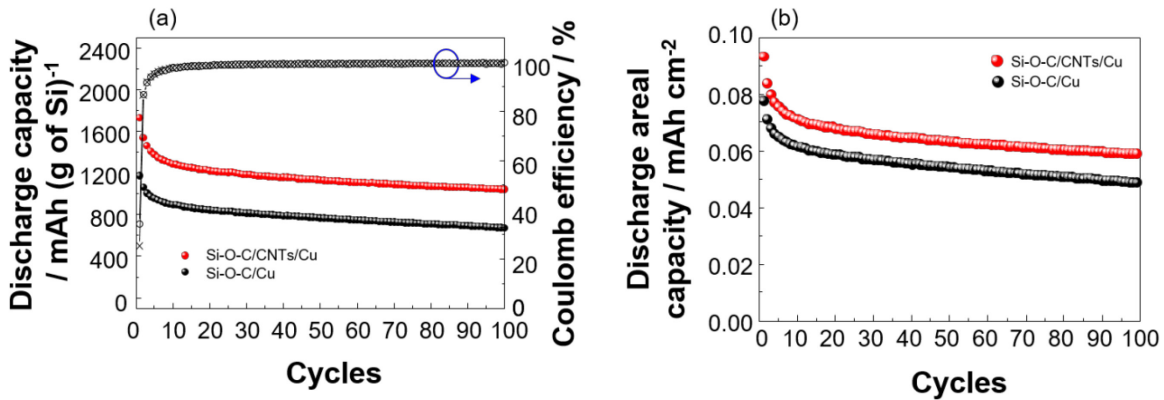


Figure 3.3.11 (a) The cycle ability of Si-O-C composites deposited on CNTs/Cu substrate and Cu substrate. (b) The discharge areal capacity of Si-O-C composites deposited on CNTs/Cu substrate and Cu substrate [21] Copyright © 2016 Elsevier B.V. All rights reserved.

To identify the effect of a high electric conductivity of CNTs anchor layer to electrochemical characteristics of Si-O-C composites, a C-rate performance of Si-O-C/Cu and Si-O-C/CNTs/Cu were tested and compared with various C-rate values from 0.1 to 1.0 C-rate and 0.1 C-rate again. Figure 3.3.12 (a) indicates the discharge specific capacity of both samples depending on C-rate values. Si-O-C/CNTs/Cu shows higher capacity than Si-O-C/Cu at all C-rate values. It is clear that Si-O-C/CNTs/Cu shows a higher specific capacity of ca. 1600 and 1200 mA h g⁻¹ at 0.1 and 1.0 C-rate, respectively. By contrast, Si-O-C/Cu delivered a discharge specific capacity of ca. 1180 and 600 mA h g⁻¹ at 0.1 and 1.0 C-rate, respectively. As explained above, it is possible that CNTs anchor layer can play a role as active material, resulting in a higher specific capacity of Si-O-C/CNTs/Cu across all C-rate condition.

To verify the determinate effect of CNTs, discharge capacity retention ratio of Si-O-C/Cu and Si-O-C/CNTs/Cu were calculated in Fig. 3.3.12 (b). At initial cycle, both samples have similar capacity retention ratio of ca. 100~95 %. However, capacity retention ratio of Si-O-C/Cu was rapidly decreased until 49 % depending on increasing of C-rate, by contrast, Si-O-C/CNTs/Cu has higher capacity retention ratio of 69 % at 1.0 C-rate. It means that CNTs anchor

layer influences a rapid intercalation/de-intercalation reaction of Si-O-C composites during charge/discharge process owing to its high electric conductivity.

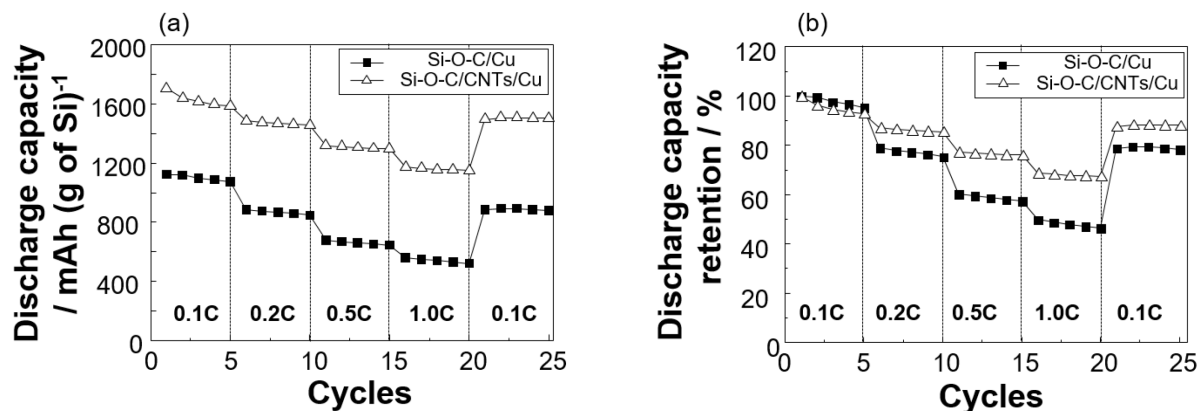


Figure 3.3.12 (a) The cycle ability and (b) discharge capacity retention ratio at various C-rates of Si-O-C composites deposited on CNTs/Cu substrate and Cu substrate [21]
Copyright © 2016 Elsevier B.V. All rights reserved.

3.3.3 Effect of enhance adhesion strength by CNTs anchor layer

As mentioned in introduction part, it is not easy to increase the deposited silicon amounts because of weak adhesion strength of 2D structure copper substrate, lead to peeling off Si-O-C composites from a substrate at a high quantity of electricity for electrodeposition. Loss of active material, i.e. silicon in Si-O-C composite, is the main reason of capacity fading and it causes a collapse of an anode structure during charge/discharge process, resulting in low cycle life.

In the previous report, it can be checked that surface modification of substrate increases the adhesion strength between Si-O-C composites and copper substrate, resulting in larger deposited silicon amount accompanying enhanced areal capacity by H. Tao. For this reason, it is guessable that CNTs anchor layer deposited on a copper substrate can enhance adhesion strength with an improvement of areal capacity. For a thorough investigation of adhesion strength change, a higher quantity of electricity for electrodeposition was applied from 2 to 15 coulomb cm⁻² for electrodeposition of Si-O-C composites. Figure 3.3.13 shows the comparison of deposited silicon amounts depending on a type of substrate, as-received copper, and CNTs/Cu substrate.

Until 4 coulomb cm^{-2} of passing charge, Si-O-C/Cu and Si-O-C/CNTs/Cu shows similarly deposited silicon amounts of ca. 0.10~0.12 mg cm^{-2} , indicating peeling off of Si-O-C composites has not occurred. However, at 8 coulomb cm^{-2} of passing charge, Si-O-C/Cu and Si-O-C/ CNTs/Cu shows different deposited silicon amounts of ca. 0.13 and 0.17 mg cm^{-2} , respectively. In the case of Si-O-C/Cu, the rate of increase in deposited silicon amounts was decreased than Si-O-C/CNTs/Cu. This behavior implies that peeling of Si-O-C composites was started partly not all area of Si-O-C composites.

The peeling off of Si-O-C composites from the as-received copper substrate was detected after 8 coulomb cm^{-2} of passing charge with deposited silicon amounts of ca. 0.11 mg cm^{-2} at 15 coulomb cm^{-2} of passing charge. This result demonstrates that the adhesion strength of an as-received copper substrate which has 2D structure properties can maintain until 8 coulomb cm^{-2} passing charge with maximum deposited silicon amounts of ca. 0.13 mg cm^{-2} . On the other hand, Si-O-C/CNTs/Cu shows still higher deposited silicon amounts of ca. 0.21 mg cm^{-2} . The major reason for the high deposited silicon amounts even at 15 coulomb cm^{-2} from Si-O-C/CNTs/Cu is enhanced adhesion strength between Si-O-C composites and a copper substrate by CNTs anchor layer. For this effect of CNTs anchor layer to deposited silicon amounts, improved discharge areal capacity is also can be expected.

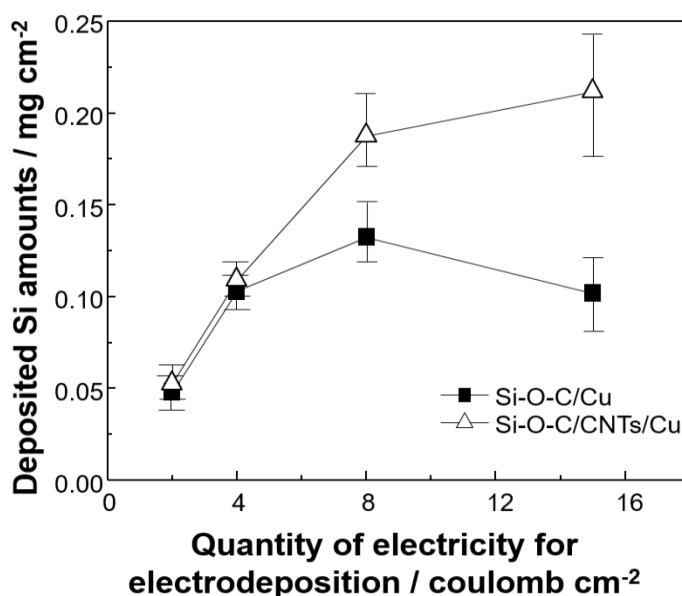


Figure 3.3.13 The deposited amounts of silicon depending on various quantities of electricity for electrodeposition [21] Copyright © 2016 Elsevier B.V. All rights reserved.

For optical verification about an effect of enhanced adhesion strength depending on the existence of CNTs anchor layer, plane views of Si-O-C/Cu and Si-O-C/CNTs/Cu were measured by FE-SEM depending on a quantity of electricity for electrodeposition from 2, 8, and 15 coulomb cm⁻² of passing charge. Figure 3.3.14 depicts the surface morphological characteristics of both samples. At the passing charge of 2 coulomb cm⁻², Si-O-C/Cu and Si-O-C/CNTs/Cu have typical surface properties of Si-O-C composites as reported before [18]. Incidentally, in the case of 4 coulomb cm⁻² of passing charge, morphological properties of both samples were same with in the case of 2 coulomb cm⁻² of passing charge, so it is not used here.

It was checked that the peeling off of Si-O-C composites from Si-O-C/Cu is started at 8 coulomb cm⁻² of passing charge by ICP measurement. By FE-SEM measurement, herein, the starting point of Si-O-C peeling off was observed at 8 coulomb cm⁻² of passing charge, and it is corresponding to ICP measurement in Fig. 3.3.13. In the SEM image of Si-O-C/Cu prepared at 8 coulomb cm⁻² of passing charge, it is clearly detected that structure of Si-O-C composites was collapsed, causing cracked Si-O-C composites. In addition, loss of Si-O-C composites was conjecturable can be speculated from this result.

After increasing the applied quantity of electricity for electrodeposition up to 15 coulomb

cm^{-2} of passing charge, it was confirmed that huge structural destruction of Si-O-C composites. As can see the SEM image of Si-O-C composites synthesized at $15 \text{ coulomb cm}^{-2}$ of passing charge in Fig. 3.3.14, a rolled up Si-O-C composites can be observed, indicating large quantities of Si-O-C composites peeled off from copper substrate. This result indicates that the Si-O-C composites deposited on the as-received copper substrate are easily detached from substrate because of weak adhesion strength. Moreover, it means that the copper substrate cannot provide enough amounts of silicon from Si-O-C composites, leading to the low possibility of realization the high energy density LIBs.

On the contrary to these results, Si-O-C/CNTs/Cu shows stable morphological properties from 2 to $15 \text{ coulomb cm}^{-2}$ of passing charge as shown in Fig. 3.3.14 (d)-(f). Electrodeposition technique is a one of a good way to synthesize a thin layer. In this dissertation, Si-O-C composites were also synthesis with thin thickness with micro-scale size. In Fig. 3.3.14 (a), Si-O-C composites were deposited on a surface of CNTs anchor layer very thin, therefore, Si-O-C/CNTs composites have CNTs shape. However, as increase, the quantity of electricity for electrodeposition, a thickness of Si-O-C composites were increased, forming film-like shape morphology. In addition, structural change or collapse was not detected because CNTs anchor layer might hold each Si-O-C composites to prevent peeling off from a substrate. For this reason, it can be expressed that CNTs anchor layer enhances adhesion strength between Si-O-C composites and copper substrate.

It should be identified that enhanced adhesion strength influences areal capacity, in practice, during charge/discharge process. Therefore, the comparisons of areal capacity depending on a quantity of electricity for electrodeposition of Si-O-C/Cu and Si-O-C/CNTs/Cu were compared and presented in Fig. 3.3.15. It demonstrates that Si-O-C/Cu shows the highest areal capacity of $0.12 \text{ mA h cm}^{-2}$ at $8 \text{ coulomb cm}^{-2}$ of passing charge, since then, areal capacity was decreased to $0.02 \text{ mA h cm}^{-2}$ at $15 \text{ coulomb cm}^{-2}$ of passing owing to peeling off of Si-O-C composites as described above. By contrast, Si-O-C composites deposited on CNTs anchor layer demonstrate ever-increasing areal capacity up to $0.49 \text{ mA h cm}^{-2}$. From those results by ICP, SEM, and charge/discharge test, it could be reasonably confident that CNTs anchor layer enhance the adhesion strength between Si-O-C composites and copper substrate, resulting in increased silicon amounts and higher areal capacity depending on a quantity of electricity for electrodeposition. In addition, Figure 3.3.16 shows the cycle ability of Si-O-C/Cu and Si-O-

C/CNTs/Cu prepared by 2, 8, and 15 coulomb cm^{-2} of passing charge for 20 cycles. In the case of Si-O-C/Cu, it could confirm that Si-O-C/Cu delivered a discharge areal capacity of 0.05, 0.07, and 0.01 mA h cm^{-2} at 20th cycle and these values are less overall than Si-O-C/CNTs/Cu. However, Si-O-C/CNTs/Cu shows enhanced the areal capacity of 0.06, 0.17, and 0.35 mA h cm^{-2} at 20th cycle. From this result, it was also discovered that Si-O-C/CNTs/Cu has not only enhanced areal capacity but also stable cycle abilities, indicating highly possible for high energy LIB full cell.

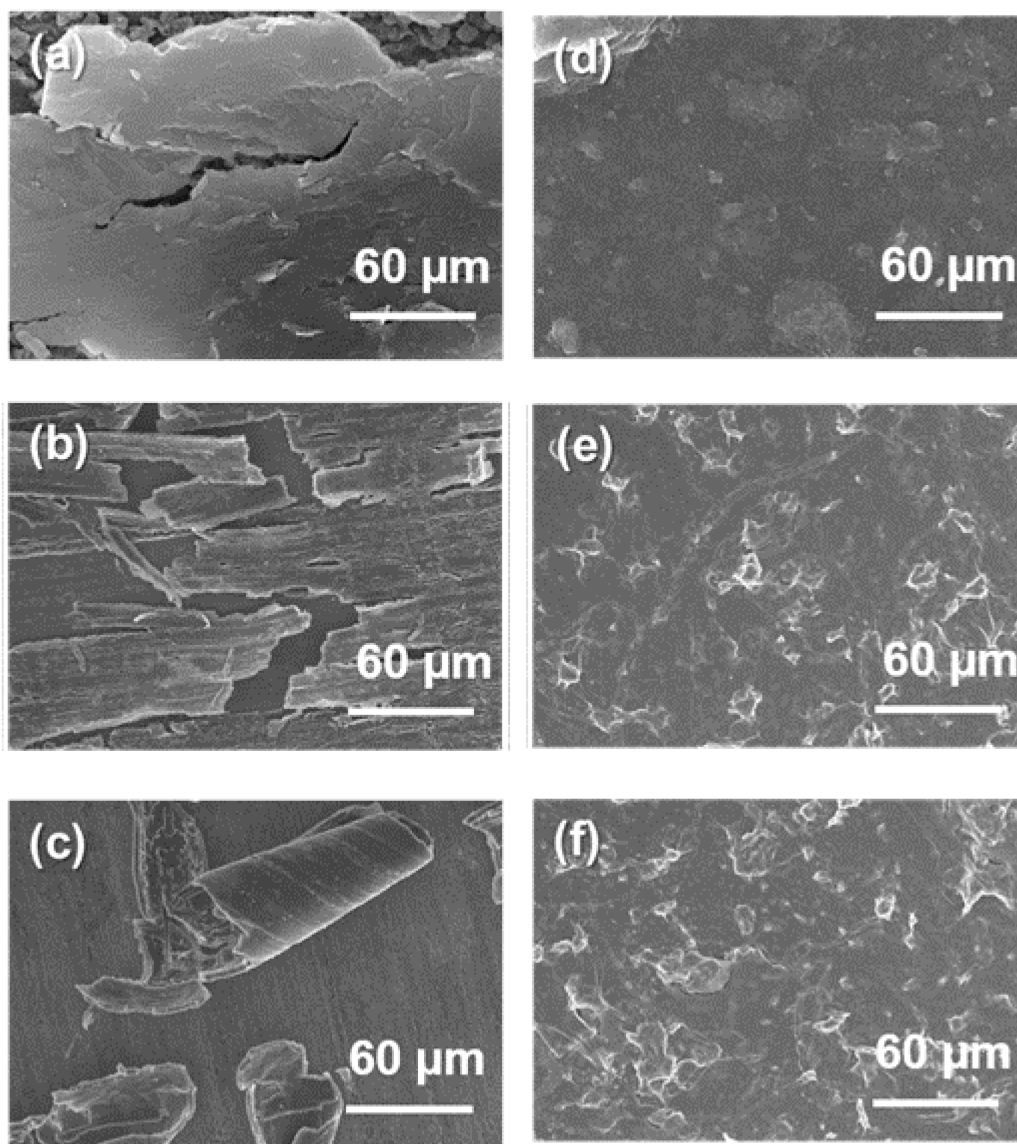


Figure 3.3.14 SEM images of Si-O-C/Cu depending on quantity of electricity for electrodeposition from (a) 2, (b) 8, and (c) 15 coulomb cm^{-2} of passing charge. SEM images of Si-O-C/CNTs/C depending on quantity of electricity for electrodeposition from (d) 2, (e) 8, and (f) 15 coulomb cm^{-2} of passing charge [21] Copyright © 2016 Elsevier B.V. All rights reserved.

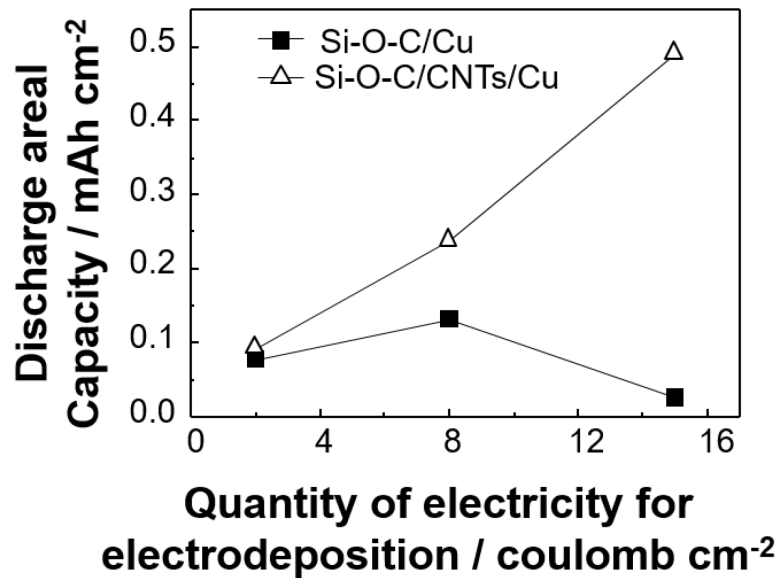


Figure 3.3.15 The comparisons of areal capacity depending on quantity of electricity for electrodeposition of Si-O-C/Cu and Si-O-C/CNTs/Cu [21] Copyright © 2016 Elsevier B.V. All rights reserved.

Furthermore, developed stability of Si-O-C composite was also identified. Figure 3.3.17 shows the plane view of Si-O-C/Cu and Si-O-C/CNTs/Cu prepared at 2 coulomb cm⁻² of passing

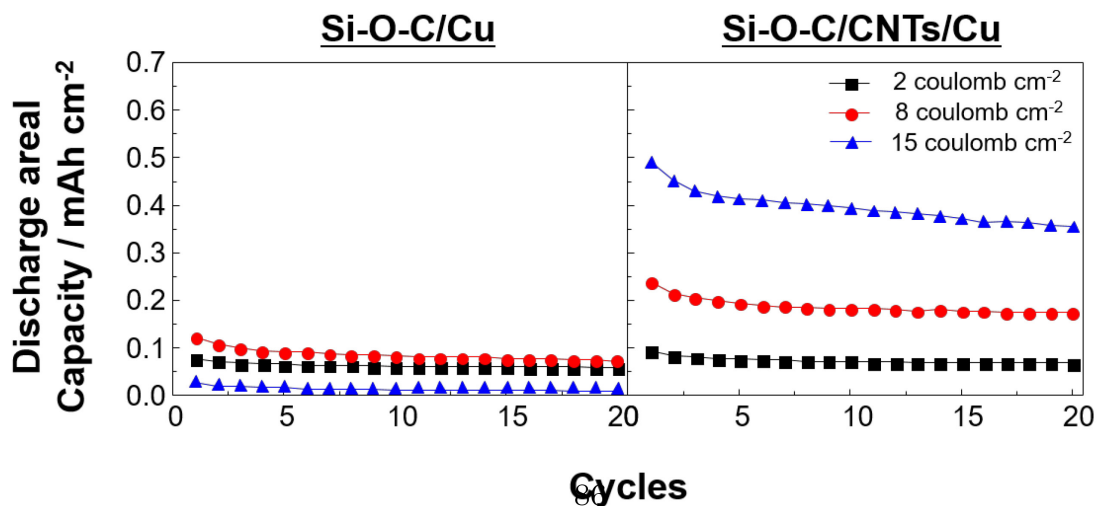


Figure 3.3.16 The cycle ability of Si-O-C/Cu and Si-O-C/CNTs/Cu prepared by 2, 8, and 15 coulomb cm⁻² of passing charge for 20 cycles.

charge after charge/discharge 100 cycles. It was already observed that Si-O-C composites were deposited on as-received copper and CNT/Cu substrate successfully at 2 coulomb cm^{-2} of passing charge without any structural damage on their surface before charge/discharge process. However, after charge/discharge test for 100 cycles, Si-O-C/Cu depicts cracked surface due to a volume change of silicon during lithiation and delithiation reaction. This structural damage caused by volume change occurs generation of isolated Si-O-C particles which cannot react with lithium ions as active materials, resulting in capacity fading during charge/discharge cycling. On the contrary, Si-O-C/CNTs/Cu shows non-cracked morphological properties ever after 100 cycles of charge/discharge process. It is supposed that CNTs anchor layer can play a role as a support layer to hold each Si-O-C composites, lead to developed structural stability. As a result, it is identified that CNTs anchor layer enhances not only adhesion strength between Si-O-C composites and copper substrate but also structural stability to prevent a destruction of Si-O-C composites by volume change.

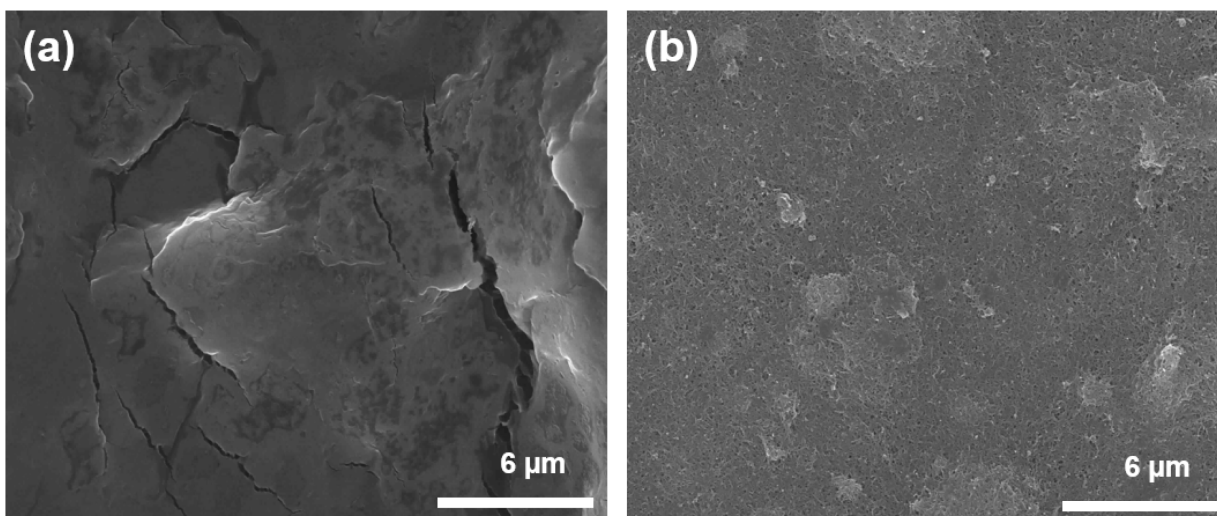


Figure 3.3.17 The plane view of Si-O-C/Cu and Si-O-C/CNTs/Cu prepared at 2 coulomb cm^{-2} of passing charge after 100th charge/discharge cycle [21] Copyright © 2016 Elsevier B.V. All rights reserved.

3.3.4 Electrochemical properties of LIBs full cell using Si-O-C anode

For full cell test, lithium cobalt oxide (LiCoO_2) and Si-O-C anode were used as cathode and anode, respectively. To realize the optimal performance of the full cell, cell balancing between cathode and anode is important because of their different theoretical and practical capacity. To fabricate cathode electrode, LiCoO_2 power (80wt %) acetylene black (10wt %), and polyvinylidene fluoride (10wt %) were used as an active material, conductivity additive, and a polymer binder, respectively. These three materials were mixed in organic solution, i.e. N-Methyl-2-pyrrolidone (NMP) and coated on an aluminum foil by doctor-blade with a thickness of 200, 400, 600, and 800 μm . Subsequently, those coated LiCoO_2 cathodes were dried for overnight in a dry room. After drying of LiCoO_2 cathodes, the thickness of each cathode was decreased 13, 40, 82, and 116 μm because of evaporation of NMP. The loading amounts of LiCoO_2 cathodes were 0.40, 2.28, 4.57, and 6.89 mg cm^{-2} . To identify the areal capacity of obtained LiCoO_2 cathodes, half-cell test was carried out with lithium metal as a counter electrode. As a result, it is revealed that each LiCoO_2 cathodes have discharge areal capacity of 0.08, 0.46, 0.85, and 1.25 mA h cm^{-2} tested with charge current density of 140 mA g^{-1} .

For cell balancing, the Si-O-C/Cu and Si-O-C/CNTs/Cu which have discharge areal of ca. 0.1 mA h cm^{-2} were used as an anode. Figure 3.3.18 (a) shows the each charge/discharge profile of LiCoO_2 cathodes (0.08 mA h cm^{-2}) and Si-O-C anode (0.093 mA h cm^{-2}) at 1st cycle. As mentioned above, the irreversible capacity of Si-O-C anode was detected because of conversion reaction of SiO_x and formation of SEI on its surface. The short cycle ability of cathode and anode is presented in Fig. 3.3.18 (b). From this result, despite a discharge areal capacity of Si-O-C anode was decreased slightly, those two electrodes have a similar areal capacity. Furthermore, it can be supposed that the LIBs full cell consists of LiCoO_2 cathodes and Si-O-C anode shows good electrochemical properties.

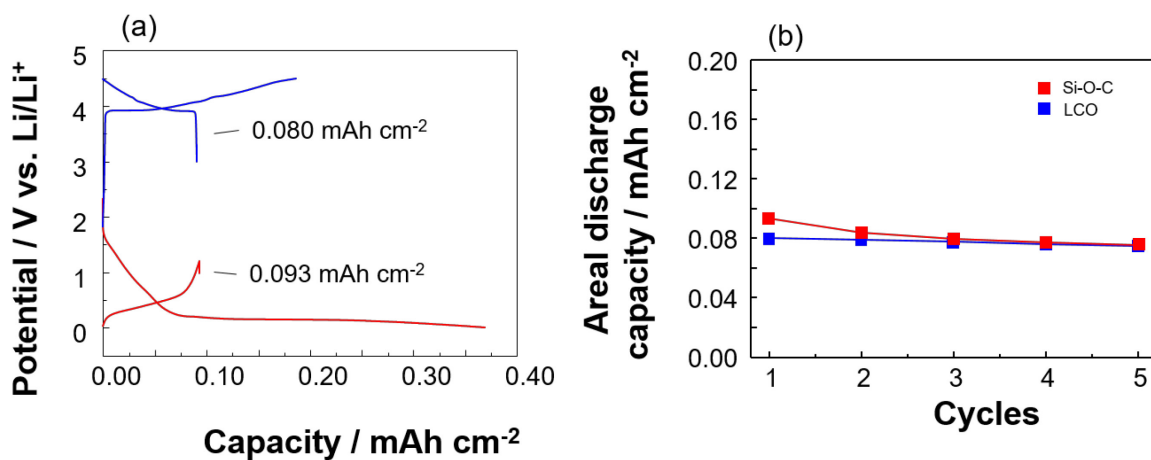


Figure 3.3.18 (a) The charge/discharge profile of LiCoO₂ cathodes (0.08 mA h cm⁻²) and Si-O-C anode (0.093 mA h cm⁻²) at 1st cycle. (b) The short cycle ability of both LiCoO₂ cathodes and Si-O-C anode.

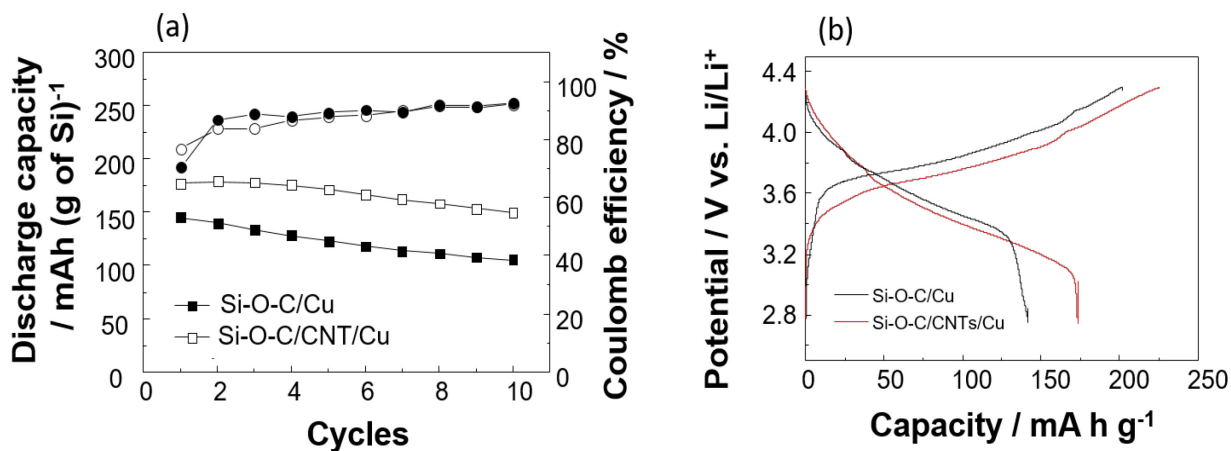


Figure 3.3.19 (a) The cycle ability depending on Si-O-C/Cu and Si-O-C/CNTs/Cu (b) The charge/discharge profile of LIB full cell in case of Si-O-C/Cu or Si-O-C/CNTs/Cu anode.

The LIBs full cell consists of a LiCoO_2 cathode and Si-O-C anode deposited on an as-received copper substrate and CNTs/Cu substrate were tested with a voltage range from 4.3 to 2.75 V. The cycle ability depending on Si-O-C/Cu and Si-O-C/CNTs/Cu are shown in Fig. 3.3.19 (a) for 10 cycles. The LIBs full cell using Si-O-C/CNTs/Cu has a higher capacity of 175, and 158 mA h g^{-1} at the 1st and 10th cycle and these values are corresponding to LiCoO_2 cathodes half-cell test. It means that cell balancing between LiCoO_2 cathode and Si-O-C anodes matched well by using the optimal performance of LiCoO_2 and Si-O-C as cathode and anode. In a case of LIBs full cell using Si-O-C/Cu composites as an anode, it shows a lower capacity than that of Si-O-C/CNTs/Cu. The reason for this different result is instable structural properties by a 2D copper substrate such as weak adhesion strength and instability of Si-O-C composites. Therefore, the full cell consists of Si-O-C/Cu demonstrates lower capacity than that of Si-O-C/CNTs/Cu. In addition, another possible supposition is decreased the internal stress of Si-O-C/CNTs/Cu composites during charge/discharge process because of a high electric conductivity of CNTs anchor layer. Figure 3.3.19 (b) shows charge/discharge profile of LIBs full cell in case of Si-O-C/Cu or Si-O-C/CNTs/Cu anode. It was confirmed that charge process of LIBs full cell using Si-O-C/CNTs/Cu as anode was started at 3.3 V vs. Li/Li^+ , whereas, LIBs full cell using Si-O-C/Cu has higher charge potential of 3.6 V vs. Li/Li^+ , and charge process of both samples was finished at 4.3 V vs. Li/Li^+ . This result implies that full cell consists of LiCoO_2 and Si-O-C/CNTs/Cu can use a larger potential range of 1.0 V vs. Li/Li^+ for charge process, in comparison to, using Si-O-C/Cu can use the smaller potential of 0.7 V vs. Li/Li^+ for charge process. For this reason, the discharge process of LIBs full cell consists of LiCoO_2 and Si-O-C/Cu was quickly finished. Consequentially, this behavior indicates that using CNTs anchor layer can reduce the internal stress during charge/discharge process, resulting in a higher capacity of LIBs full cell.

3.4 Summary

In chapter 2, it was confirmed that carbon paper which has 3D structure properties and good electric conductivity improved the electrochemical characteristics of Si-O-C composites as an anode. However, in the case of carbon paper, some demerits were discovered such as exfoliation of carbon paper and complicated experiment condition of EC/DEC. For this reason, in this chapter, the CNTs were used as supporting layer to enhance adhesion strength between Si-O-C composites and a copper substrate and structure instability of Si-O-C composites. The CNTs anchor layer was prepared by high voltage electrophoretic deposition using CoCl_2 as a metallic additive. The high surface area of CNTs/Cu substrate shows higher deposited silicon amounts than that of an as-received copper substrate, resulting in higher areal capacity (Si-O-C/Cu: $0.08 \text{ mA h cm}^{-2}$, Si-O-C/CNTs/Cu: $0.10 \text{ mA h cm}^{-2}$ at 1st cycle). In addition, the enhanced adhesion strength between Si-O-C composites and a copper substrate was confirmed through introducing of CNTs anchor layer. Si-O-C composites deposited on as-received copper substrate shows decreasing of deposited silicon amounts after $8 \text{ coulomb cm}^{-2}$ of passing charge because of weak adhesion strength by the smooth surface of copper. On the other hand, Si-O-C composites deposited CNTs/Cu substrate which has 3D structure properties demonstrate largely deposited silicon amounts even $15 \text{ coulomb cm}^{-2}$ of passing charge because CNTs anchor layer can hold Si-O-C composites during electrodeposition. Besides, an effect of CNTs anchor layer for LIB full cell was identified using LiCoO_2 cathode. For the LIBs full cell test, four kinds of LiCoO_2 cathodes were prepared and compared for cell balancing between a LiCoO_2 cathode and Si-O-C anode. The LIBs full cell using Si-O-C/CNTs/Cu shows good discharge capacity of 175 mA h g^{-1} , whereas, that of Si-O-C/Cu shows 158 mA h g^{-1} . From this results, it is clear that enhancement of adhesion strength by CNTs anchor layer leads to improvement of physical and electrochemical properties for high-performance LIBs.

3.5 References

1. S.R. Sivakkumar, and A.G. Pandolfo, *Electrochim. Acta*, 65 (2012) 280.
2. Y. Wang, L. Tian, A. Yao, F. Li, S. Li, and S. Ye, *Electrochim. Acta*, 163 (2015) 71.
3. H. F. Xiang, Z. D. Li, K. Xie, J. Z. Jiang, J. J. Chen, P. C. Lian, J. S. Wu, Y. Yu, and H. H. Wang, *RSC Adv.*, 2 (2012) 6792.
4. S. K. Ahn, J. J. Yang, H. I. Kim, H. Habazaki, and S. G. Park, *Chem. Lett.*, 43 (2014) 898.
5. B. J. Landi, M. J. Ganter, C. D. Cress, R. A. DiLeo, and R. P. Raffaele, *Energy Environ. Sci.*, 2 (2009) 638.
6. M. Yoshio, H. Wang, K. Fukuda, T. Umeno, T. Abebe, and Z. Ogumi, *J. Mater. Chem.*, 14 (2004) 1754.
7. B. -J. Kim, J. -S. Park, Y. -J. Hwang, and J. -S. Park, *Appl. Surf. Sci.*, 380 (2016) 2.
8. H. Zhao, H. Song, Z. Li, G. Yuan, and Y. Jin, *Appl. Surf. Sci.*, 251 (2005) 242.
9. B. Gao, G. Z. Yue, Q. Qiu, Y. Cheng, H. Shimoda, L. Fleming, and O. Zhou, *Adv. Mater.*, 13 (2001) 1770.
10. L. Wang, Y. Chen, T. Chen, W. Que, and Z. Sun, *Mater. Lett.*, 61 (2007) 1265.
11. M. S. Wu, C. Y. Huang, and K. H. Lin, *Electrochem. Solid St.*, 12 (2009) A129.
12. S. Santhanagopalan, F. Teng, and D. D. Meng, *Langmuir*, 27 (2010) 561.
13. C. V. Schenck, and J. G. Dillard, *J. Colloid Interface Sci.*, 95 (1983) 398.
14. B.A. Sexton, A.E. Hughes, and T.W. Turney, *Journal of Catalysis*, 97 (1986) 390.
15. J. C. Dupin, D. Gonbeau, H. B. Moudden, Ph. Vinatier, and A. Levasseur, *Thin Solid Films*, 384 (2001) 23.
16. A. A. Khassin, T. M. Yurieva, V. V. Kaichev, V. I. Bukhtiyarov, A. A. Budneva, E. A. Paukshtis, and V. N. PArmon, *J. Mol. Catal. A: Chem.*, 175 (2001) 189.
17. B. Ernst, A. Bensaddik, L. Hilaire, P. Chaumette, and A. Kiennemann, *Catalysis Today*, 39 (1998) 329.
18. H. Nara, T. Yokoshima, T. Momma, and Tetsuya Osaka, *Energy Environ. Sci.*, 5 (2012) 650.
19. T. Hang, H. Nara, T. Yokoshima, T. Momma, and T. Osaka, *J. Power. Sources*, 222 (2013) 503.

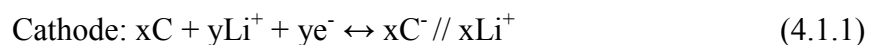
20. M. Jeong, Y. Yokoshima, H. Nara, Y. Momma, and T. Osaka, *J. Power Sources*, 275 (2015) 525.
21. S. Ahn, M. Jeong, T. Yokoshima, H. Nara, T. Momma, and T. Osaka, *J. Power Sources*, 336, (2016) 203.
22. Omer O. Van der Biest, and Luc J. Vandeperre, *Annu. Rev. Mater. Sci.*, 29 (1999) 327.

Chapter 4

Application of Si-O-C as anode for high rate lithium ion capacitor

4.1 Introduction

Energy storage devices such as lithium-ion batteries (LIBs), supercapacitor, and lithium ion capacitor (LIC) have been studied to reduce environmental pollutions for next generation as described in the introduction [1-4]. Among them, LIC consists of the anode from LIBs and cathode from supercapacitor has the strong possibility as a new type of energy storage devices because of its various advantages such as higher power density than non-aqueous batteries and higher energy density than supercapacitor in Fig. 4.1.1 [5-8]. This new type-energy storage device stores energy by two kinds of mechanism which can be described as below.



In equation (4.1.1), $xC^- // xLi^+$ indicates the double-layer charges by absorption of lithium ion on cathode surface prepared by carbon-based materials. In addition, in anode side, lithium ion can intercalate and de-intercalate into anode materials. From this reaction mechanism, it can be supposed that LIC has some merits such as enhanced power and energy density than LIBs and supercapacitor. Moreover, LIC has higher working voltage range than conventional supercapacitor owing to low intercalation and de-intercalation potential of an anode. Figure 4.1.2 depicts the schematics of charge/discharge profile of supercapacitor and LIC. As can see in Fig. 4.1.1, LIC consists of the anode which can be stored lithium ion during charge/discharge process. Therefore, it operates at lower potential range than conventional supercapacitor. By this feature, numerous studies related to anode materials from LIBs have been studied to apply it as an anode for high-energy LIC.

From chapter 2 and 3, it was revealed that Si-O-C composites have good electrochemical characteristics such as low potential range, high specific, and areal capacity. As a result, it is was confirmed that Si-O-C composites are a promising material. Thus, herein, Si-O-C composites were applied as an anode for LIC to evaluate its suitable for high rate performance LIC.

Electrochemically deposition method such as electrophoretic deposition and electrodeposition is known well as a way to synthesize thin film on a surface of a substrate. For this advantage, this technique was used to synthesize thin CNTs cathode and Si-O-C composites

as an anode by electrophoretic deposition, and electrodeposition, respectively. After preparation of CNTs cathode and Si-O-C anode, cell balancing between both electrodes was carried out to figure out appropriate amounts of active materials for LIC full cell test. Material and electrochemical characteristics of CNTs cathode, Si-O-C anode, and full cell consists of both electrodes were measured by various methods such as FE-SEM, XPS, and so on.

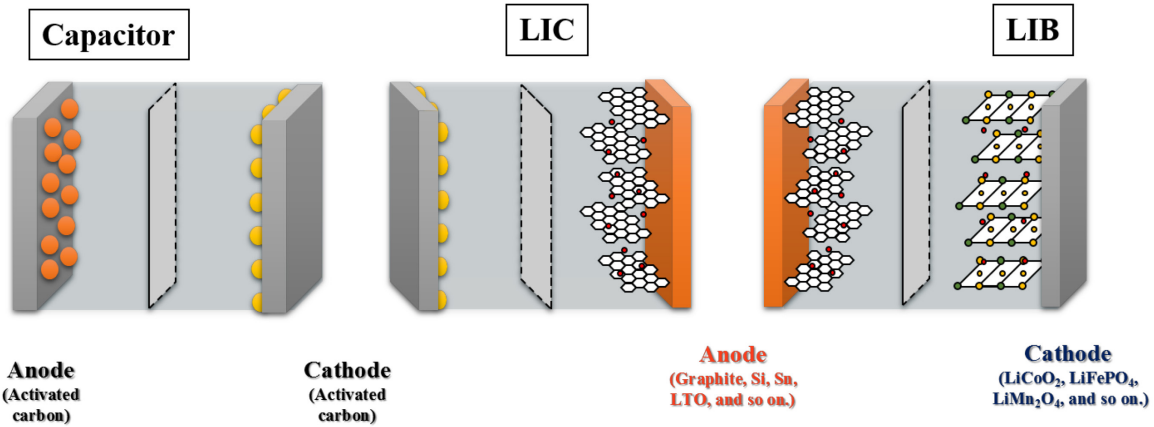
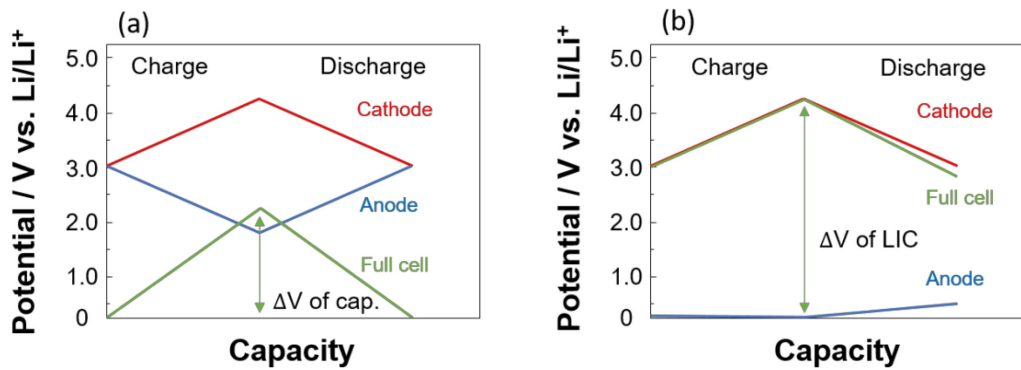


Figure 4.1.1 The schematics of charge/discharge profile of capacitor, LIC, and LIB with their components.



- Working voltage: ΔV of cap. < ΔV of LIC

Figure 4.1.2 The schematics of charge/discharge profile from (a) supercapacitor and (b) LIC.

4.2 Experiment

4.2.1 Fabrication of CNTs cathode by electrophoretic deposition

CNTs cathode was synthesized by electrophoretic deposition with cobalt dichloride (CoCl_2) in isopropyl alcohol (IPA). The purchased CNTs (Nanocyl -NC7000) were acid treated by mixed acid ($\text{H}_2\text{SO}_4/\text{HNO}_3$ mixed acid, 3:1; v/v, purity of 96.0 % and 60.0 %, respectively) to generate oxygen functional groups on surface of CNTs to enhance surface affinity and wettability with IPA and prevent aggregation of CNTs, forming CNTs bundle. After acid treatment, acid-treated CNTs were rinsed with distilled water and ethanol to be natural (Ph. 7), and then dried in vacuumed oven at 80 °C for 4 hours. Subsequently, acid-treated CNTs were dispersed in IPA by sonication for 30 min with CoCl_2 (0.5 mg ml^{-1}). For electrophoretic deposition of CNTs, aluminum foil (1x1 cm), platinum plate (2x2 cm), were employed as working and counter electrode. The electrophoretic deposition was carried out using DC power supply as a power source at -120 V for 10, 30, and 60 min to figure out appropriate time of electrophoretic deposition for high-performance CNTs cathode. After electrophoretic deposition, each CNTs cathodes were dried in a dry room overnight.

4.2.2 Synthesis of Si-O-C composites as anode by electrodeposition

For this procedure, an as-received copper substrate was used for Si-O-C composites. Before electrodeposition, an as-received copper substrate was surface treated using trichloroethylene and then ethanol by ultra-sonication for 20 min. After then, electrolytic degreasing was carried out for 30 sec with a constant current of 1 mA cm^{-2} in a water based electrolyte, containing 40 g L^{-1} of NaOH, 20 g L^{-1} of Na_2CO_3 , and 1 g L^{-1} of sodium dodecyl sulfate. Continually, a surface-treated copper substrate was rinsed by an acid solution with 10 % H_2SO_4 in distilled water. Afterward, electrochemical surface treatment was carried out in propylene carbonate (PC) containing 0.5 M of tetrabutylammonium perchlorate (Kanto Chemical) for 5 min. After then, electrodeposition was carried out in an Ar-filled glove box with a dew point of -90 °. A constant cathodic current of -1.0 mA cm^{-2} and various quantity of

electricity for electrodeposition from 0.3, 0.5, and 1.0 coulomb cm^{-2} was applied for thin layered Si-O-C composites.

4.2.3 Material characteristics of Si-O-C composites

Morphological properties of CNTs cathode and Si-O-C anode were measured by field emission scanning electron microscopy (FE-SEM, Hitachi, S-4800) with energy dispersive X-ray spectroscopy (SEM, Hitachi TM-3000). The elemental compositions on the surface of each electrode were analysis by X-ray photoelectron spectroscopy (XPS, JEOL, JPS-9010TR). In addition, inductively coupled plasma (ICP, Thermo Scientific, iCAP6500 Duo) analysis was used to measure deposited amounts of silicon from each Si-O-C composites.

4.2.4 Electrochemical characteristics of Si-O-C composites

A half-cell was assembled using coin typed cell (2032 type) with 1.0 mol dm^{-3} lithium perchlorate (LiClO_4) dissolved in propylene carbonate-ethylene carbonate (PC/EC = 1:1, v/v, Kishida). A cyclic voltammogram was used to measure the capacitance of CNTs cathode using a biologic machine (Hokuto Denko, HZ-5000). Electrochemical charge/discharge performance of each half-cell and LIC full cell was tested by constant current (CC) charge/discharge measurement.

4.3 Results and discussions

4.3.1 CNTs cathode prepared by electrophoretic deposition

For high rate performance of LIC, it was tried to obtain the thin layer of the cathode using CNTs. As mentioned above, electrophoretic deposition is a one of a good way to fabricate thin layer film on a substrate. Figure 4.3.1 (a) depicts the cross-section images of three kinds of CNTs cathode prepared by electrophoretic deposition at -120 V for 10, 30, and 60min. It is clear that CNTs were deposited on a surface pre-treated copper substrate by electrophoretic deposition and formed as a thin film in chapter 3. For this study, thickness and amounts of CNTs film were controlled by time of electrophoretic deposition in Fig. 4.3.1 (b). The deposited amounts of

CNTs were increased from 179 to 326 $\mu\text{g cm}^{-2}$ depending on increasing of electrophoretic deposition time from 10 to 60 min. In addition, a thickness of CNTs layer was also increased by electrophoretic deposition time from 2.68 to 8.55 μm .

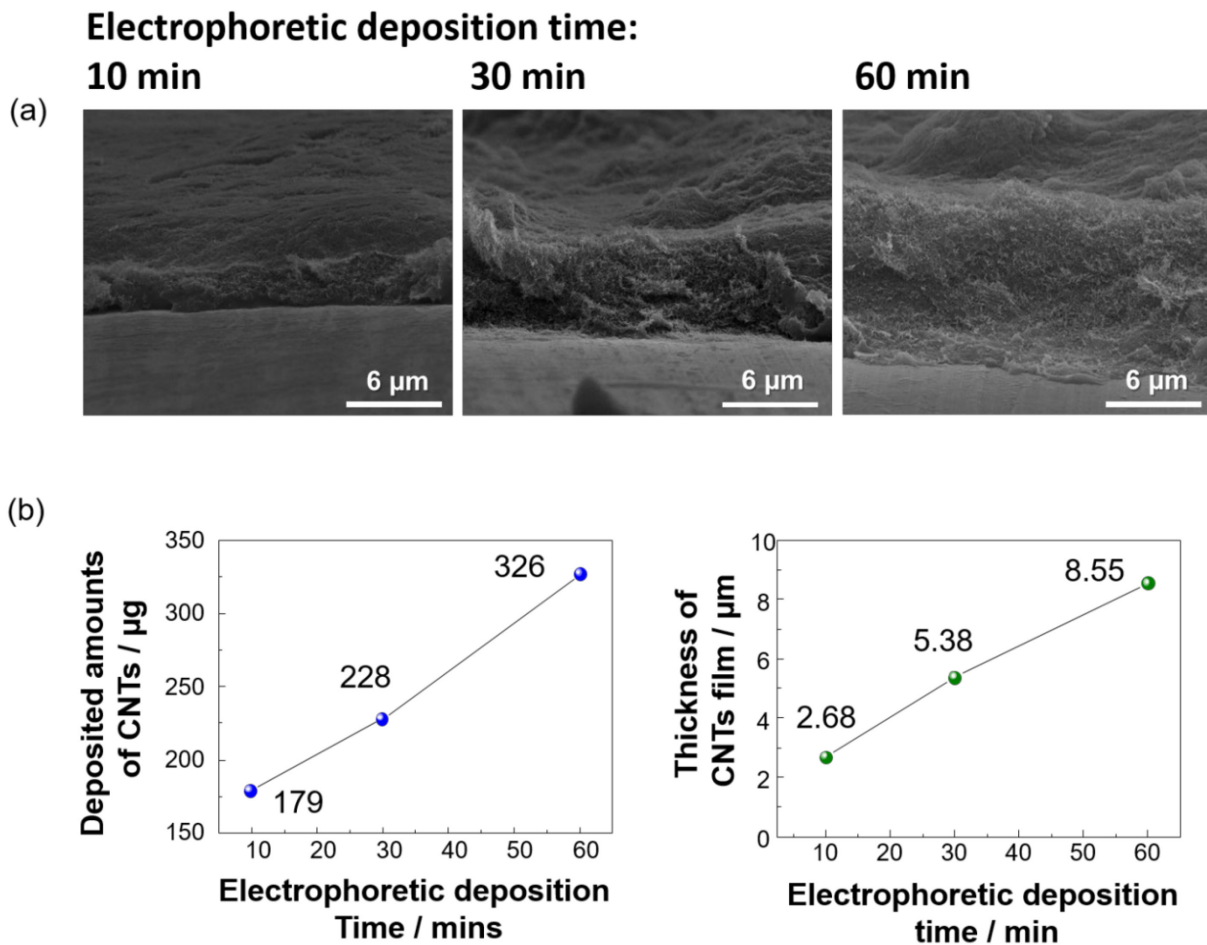


Figure 4.3.1 (a) The cross-section images of three kinds of CNTs cathode prepared by electrophoretic deposition at -120 V for 10, 30, and 60min. (b) Thickness and amounts of CNTs film with different time of electrophoretic deposition.

Another optical analysis of CNTs cathode was carried by FR-SEM measurement presented in Fig. 4.3.2. In low magnification, it was observed that CNTs were aggregated, forming CNTs particles on the surface depending on increasing of electrophoretic deposition time. The average diameter size of aggregated CNTs particles were 0.9 μm from CNTs cathode prepared by electrophoretic deposition for 10 min, and it was enlarged to 24 μm at 60 min. As a result, it was confirmed that the inordinate time for electrophoretic deposition generates aggregated particles, resulting in inhomogeneous surface properties. For the more thorough investigation, magnified SEM images of each CNTs cathode were shown in Fig. 4.3.2 (b). CNTs cathodes prepared for 10 and 30 min show typical optical properties of CNTs which is corresponding in chapter 3. On the other hand, CNT cathode fabricated by electrophoretic deposition for 60 min depicts thicker CNTs which were covered by unknown compounds on their surface, resulting in a thicker thickness of ca. 60 nm, whereas, CNTs cathode prepared for 10 and 30min have a thickness of ca. 28 nm.

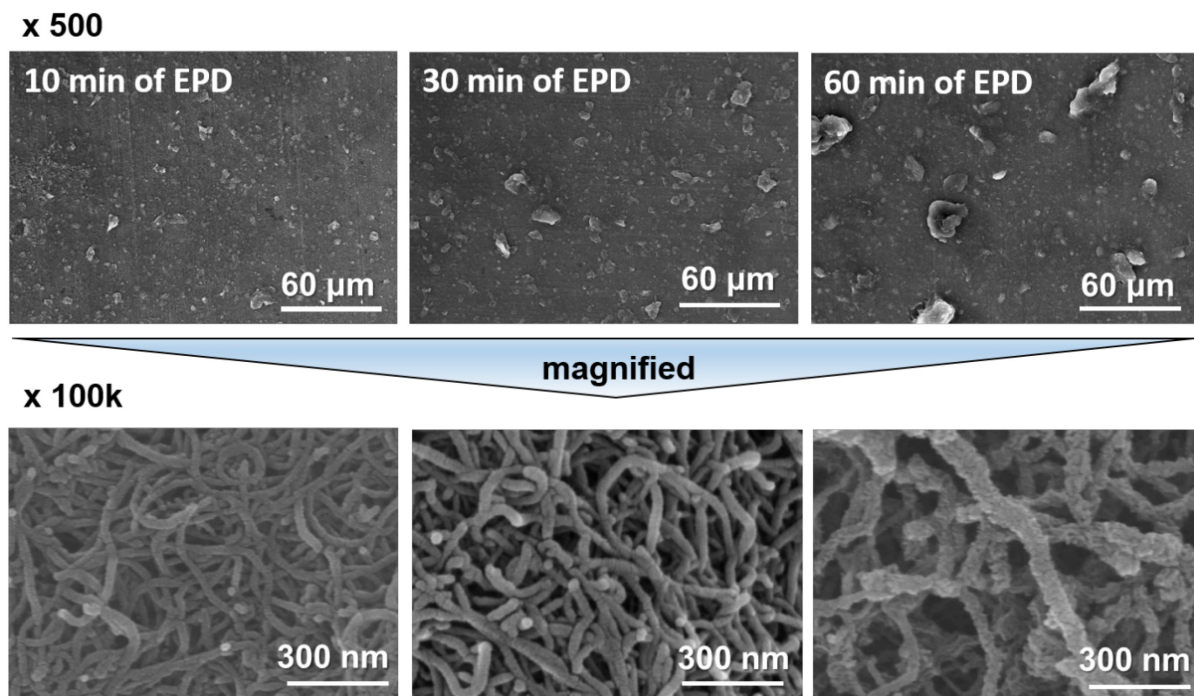
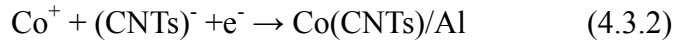


Figure 4.3.2 Plane views of CNTs cathode and their magnified images depending on electrophoretic deposition time, 10, 30, and 60 min.

To identify the unknown compounds deposited on CNTs surface, an elemental composition was examined by XPS measurement. Figure 4.3.3 demonstrates the wide and narrow spectrums of each CNTs cathode prepared by electrophoretic deposition for 10, 30, and 60 min. As can be seen in Fig. 4.3.3 (a), peaks related to cobalt oxide compounds appeared at a binding energy of 718, 782, and 787 eV which are attributed to Co LMM Auger peak, CoO, and Co₃O₄, respectively [9-12]. As described in chapter 3, CoCl₂ imparts positively charge on CNTs surface and migrates with CNTs toward on substrate. Afterward, cobalt ions are co-deposited on aluminum with CNTs to form CNTs layer. The reaction mechanisms of CNTs film formation are as below (equation 4.3.1 and 4.3.2).



In these equations, (CNTs)⁻ and /Cu mean that CNTs have negatively charge on their surface by acid-treatment and co-deposited on an aluminum substrate, respectively [13]. From a result of elemental composition analysis by XPS, it was believed that inordinate amount of time effect on not only aggregated CNTs particles but also cobalt oxide compounds on the surface of CNTs cathode.

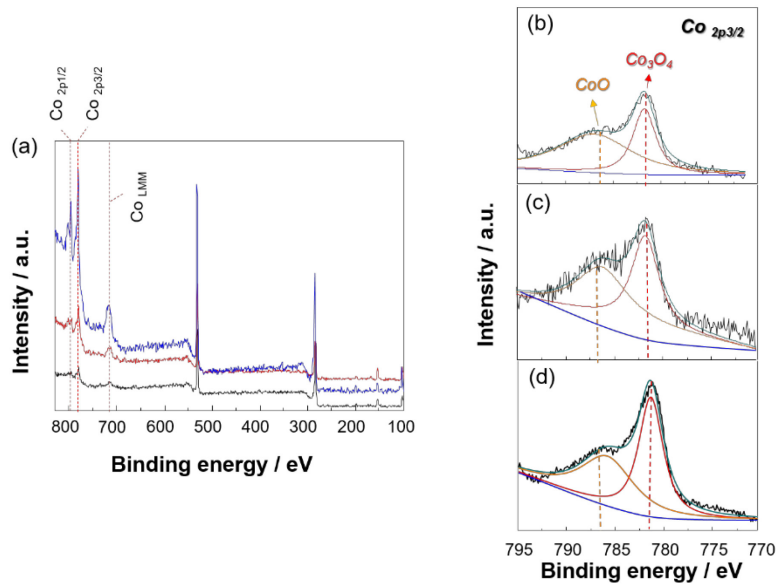


Figure 4.3.3 XPS spectrums of CNTs cathode with wide and narrow peaks of Co 2p_{3/2}.

For verification of electrochemical properties of CNTs cathodes, cycle voltammogram was carried out with a potential range from 4.3 to 2.8 V vs. Li/Li⁺ at various scan rate from 1 to 300 mV s⁻¹. Overall, three kinds of CNTs cathode show typical electric double layer behaviors, which have rectangle shape without any redox peaks during CV measurement in Fig. 4.3.4. (a)-(c). These results imply that CNTs cathode fabricated by electrophoretic deposition at -120 V using CoCl₂ can be employed as a cathode for supercapacitor or LIC. However, it was confirmed that rectangle shape of CNTs cathode prepared for 60 min of electrophoretic deposition time was started to become twisted according to increasing of scan rate, meaning inconsistency of CNTs/Al as a cathode for high rate performance of LIC. For easy understanding, CV results from three kinds of CNTs cathode measured at 300 mV s⁻¹ were presented in Fig. 4.3.4 (d). The capacitance of all CNTs cathode was calculated by following equation 4.3.3 (in Fig. 4.3.4. (e)).

$$C = I (dt/dv) \quad (4.3.3)$$

Where C is capacitance (F, farad), I is applied current (A), t is time (sec), v is a voltage difference between cathode and anode. Until scan rate of 5 mV s⁻¹, three CNTs electrodes show similar capacitance retention ratio over 60%. Afterward, CNTs cathode prepared for 30 min of electrophoretic deposition time demonstrates the highest capacitance retention ratio of 53%, whereas, other two CNTs cathode have capacitance retention ratio of ca. 40%. At a high scan rate of 300 mV s⁻¹, CNTs cathode (30 min of EPD time) shows a highest capacitance retention ratio of over 40%. On the other hand, CNTs cathode (60 min of EPD time) has lowest capacitance retention ratio because of cobalt oxide compounds deposited on the surface of CNTs. From there results, it is clear that cobalt oxide compounds effect on electrochemical properties of CNTs cathode as resistance, resulting in a decrease of capacitance retention ratio depending on scan rate. For full cell test, CNTs cathode prepared for 30 min was employed as a cathode for LIC full cell.

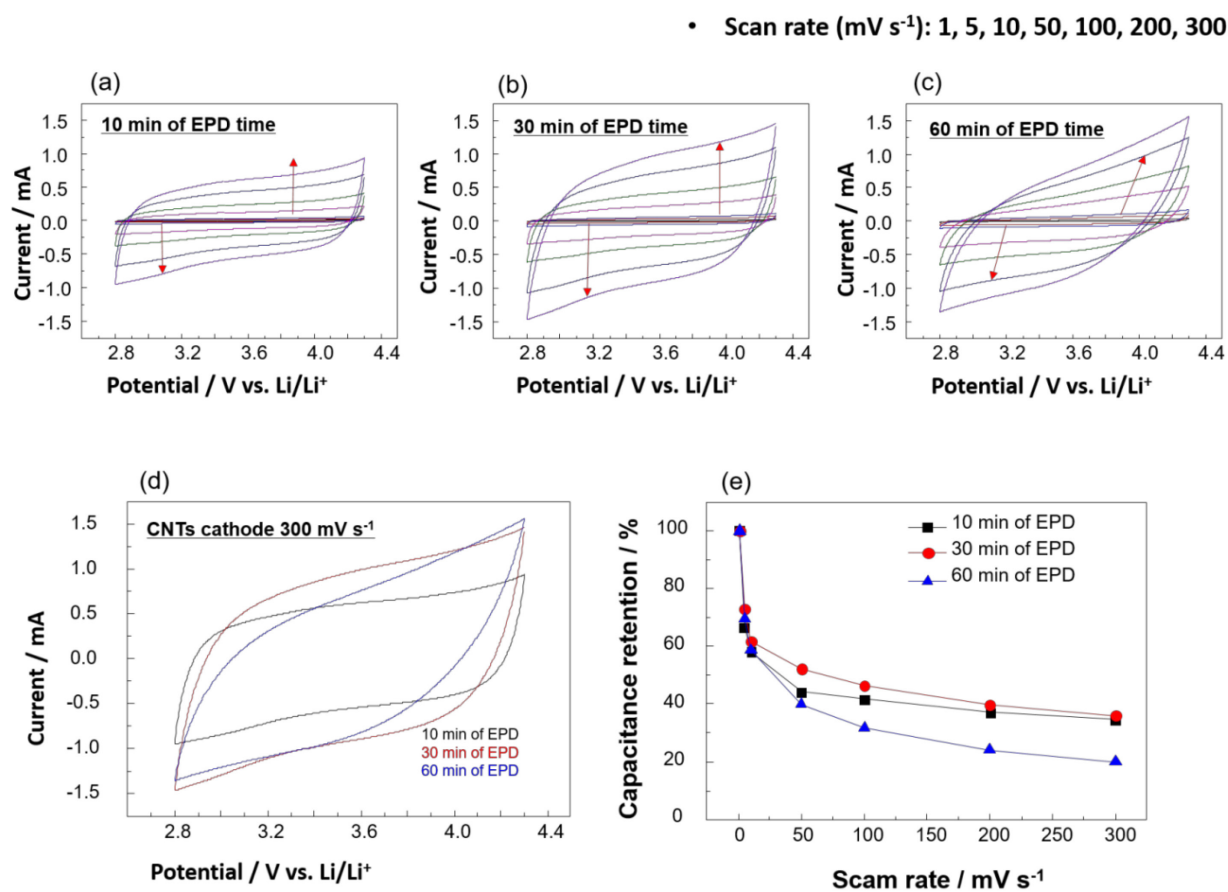


Figure 4.3.4 Cycle voltammogram of CNTs cathode with various scan rate from 1 to 300 mV s^{-1} and their capacitance retention ratio, electrophoretic deposition time (a) 10, (b) 30, (c) 60 min, and (d) comparison of each sample at scan rate of 300 mV s^{-1} and (e) its capacitance retention.

The cycle abilities of CNTs cathode was tested with constant current charge/discharge test with charge current of 100 mA g^{-1} in potential range of 4.3 to 2.8 vs. Li/Li^+ for 5000 cycles as shown in Fig. 4.3.5. At initial cycle, it has discharge capacitance of ca. 43, 41, and 36 F g^{-1} at 1st, 2nd, and 3rd cycle. The capacitance values at initial cycle are corresponding to discharge capacitance which was calculated from CV results.

However, the discharge capacitance of CNTs was decreased to 25 F g^{-1} from 1st to 20th cycle and it maintained up to 5000th cycle. The predictable reason of unstable capacitance at initial cycle is weak adhesion strength of CNTs on a surface of the cathode. After electrophoretic deposition, some of the CNTs were co-deposited on CNTs with a few amounts of Co ions, resulting in weak adhesion strength between CNTs bundles. These CNTs were started to detached from CNTs cathode, lead to capacitance fading for initial cycles. Despite this capacitance fading in the initial cycle, CNTs cathode shows outstanding cycle ability with 80% of capacitance retention ratio from 30th to 5000th cycle, as can be seen in Fig. 4.3.5. From this result, it was clear that CNTs cathode prepared electrophoretic deposition has the promising possibility as a cathode for high rate LIC.

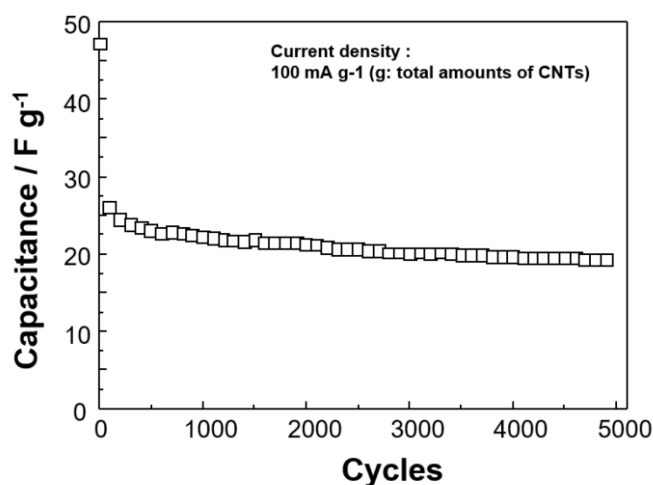


Figure 4.3.5 Cycle abilities of CNTs cathode prepared 30 min of electrophoretic deposition for 5000 cycles with current density of 100 mA g^{-1} .

4.3.2 Si-O-C anode deposited on copper substrate by electrodeposition

For this chapter, three kinds of Si-O-C composites were synthesized by electrodeposition depending on a quantity of electricity for electrodeposition for 0.3, 0.5, and 1.0 coulomb cm^{-2} of passing charge. The current transient curve during electrodeposition of Si-O-C composites was presented in Fig. 4.3.6 (a). Each sample show that electrodeposition of Si-O-C was carried out at ca. 1.2 V vs. Li/Li^+ and increased up to ca. 1.3 V vs. Li/Li^+ . It is typical silicon deposition plateau as reported previously [14-16]. It reveals that electrodeposition of Si-O-C composites was carried out an even low quantity of electricity for electrodeposition, supposing that these samples have thin thickness than our previous report (Si-O-C prepared at 2.0 coulomb cm^{-2} of passing charge: Thickness of 0.57 μm) [14]. The deposited silicon amounts depending on a quantity of electricity for electrodeposition were measured by ICP analysis. Figure 4.3.6 (b) shows the deposited silicon amounts depending on passing charge of 0.3, 0.5, and 1.0 coulomb cm^{-2} . These samples have deposited amounts of silicon of 9, 10, 19 $\mu\text{g cm}^{-2}$, respectively. Si-O-C composites at 0.3 and 0.5 coulomb cm^{-2} of passing charge have similar amounts of silicon, meaning that a few amounts of silicon can be deposited at an initial process. After 0.5 coulomb cm^{-2} of passing charge, deposited amounts of silicon were raised steeply.

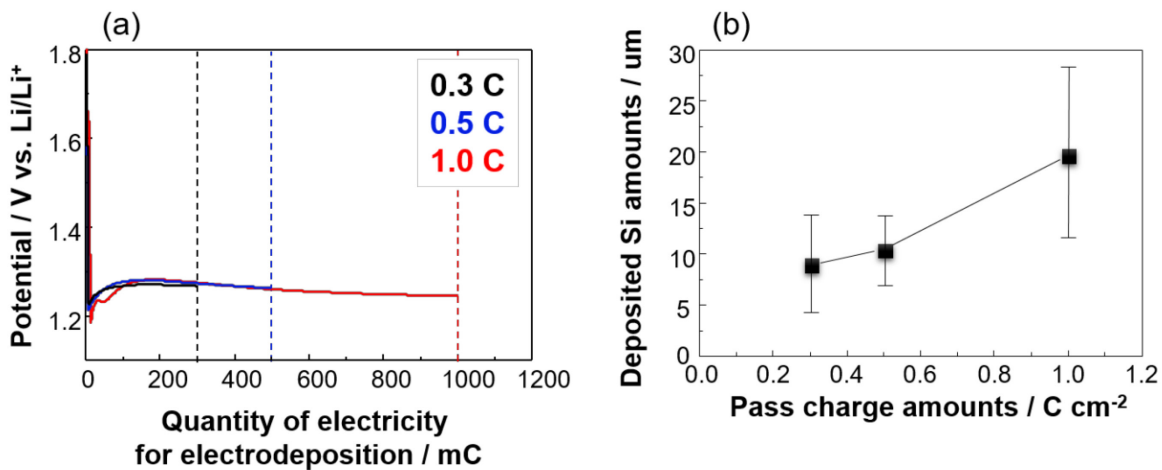


Figure 4.3.6 Current transient curves of Si-O-C anode depending on passing charge and deposited amounts of silicon.

Figure 4.3.7 depicts the EDX spectrum with elemental mapping of Si-O-C composites depending on a quantity of electricity for electrodeposition. In a case of 0.3 coulomb cm^{-2} of passing charge, amounts of silicon and copper were 4.48 and 79.48 %, respectively. As the quantity of electricity for electrodeposition increases, the percentage of silicon was increased up to 28.05 %, whereas, copper was decreased from 79.48 to 42.38 %. Though these results are not great discovery but it reveals that deposition rate of silicon was gradually increased even in a few quantity of electricity for electrodeposition at 0.3, 0.5 and 1.0 coulomb cm^{-2} of passing charge.

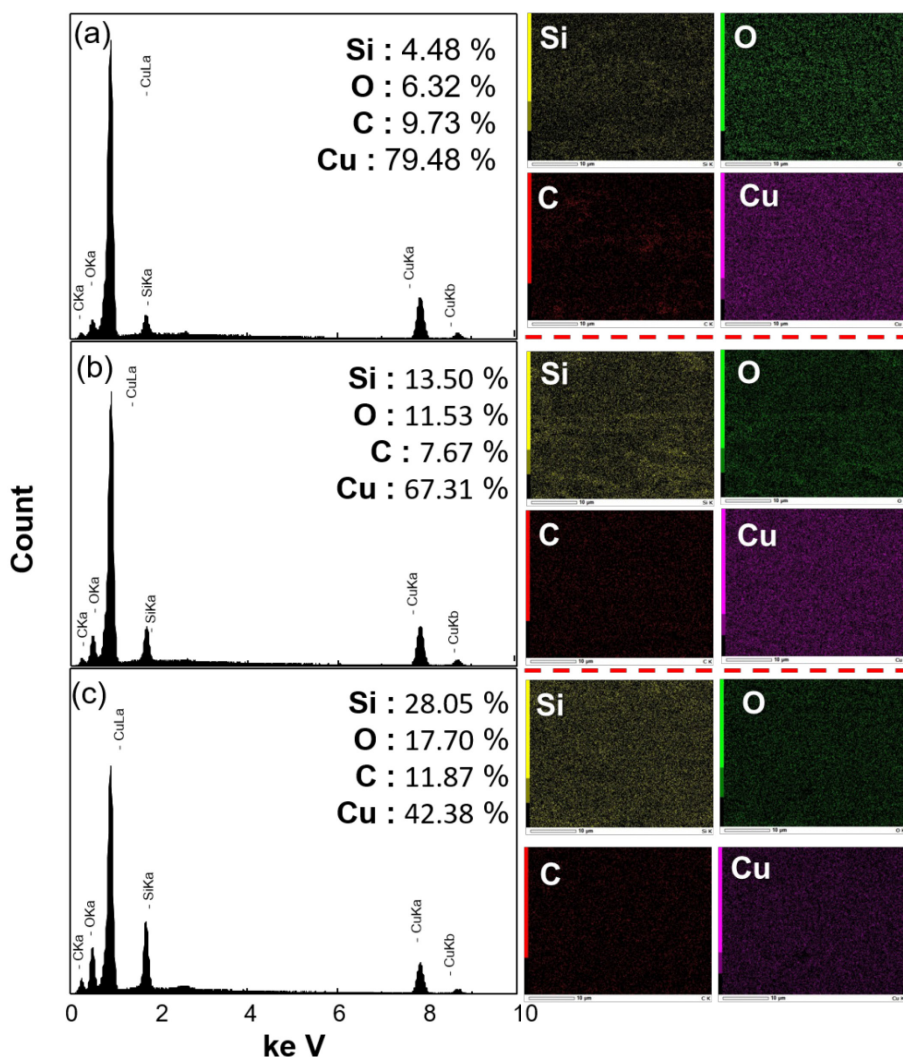


Figure 4.3.7 EDX spectrum with elemental mapping of Si-O-C composites depending on quantity of electricity for electrodeposition.

The XPS Peaks of the Si-O-C composite are shown in Fig. 4.3.8 depending on passing charge of 0.3, 0.5 and 1.0 coulomb cm^{-2} . The XPS peaks of $\text{Si}_{2p_{3/2}}$, C_{1s} , O_{1s} , and $\text{Cu}_{2p_{3/2}}$ were observed. The binding energies of $\text{Si}_{2p_{3/2}}$ located at ca. 103.2 and 101.7 eV was detected in three samples, which is attributed to deposited silicon, SiO_x/Si and SiO on a copper substrate. In addition, the peak of SiO located at ca. 101.7 eV was increased slightly depending on passing charge because the rate of silicon deposition was increased after 0.3 coulomb cm^{-2} of passing charge. In the spectrum of O_{1s} , three samples have similar peak located at ca. 532.3 eV, which is attributed to O in Si-O-Si bond by co-deposition with silicon and oxygen during electrodeposition. In addition, the peak of C_{1s} located at ca. 284.8 eV appeared from a C-O single bond. From peaks of O_{1s} and C_{1s} , it is obvious that oxygen and carbon are co-deposited on a copper substrate with silicon, which is corresponding to EDX mapping results. Moreover, $\text{Cu}_{2p_{3/2}}$ peak located at ca. 932.1 eV was observed only in Si-O-C composites prepared at 0.3 coulomb cm^{-2} of passing charge because of increased deposition rate of Si-O-C composites after 0.5 coulomb cm^{-2} of passing charge, which is good agreement with a peak of $\text{Si}_{2p_{3/2}}$.

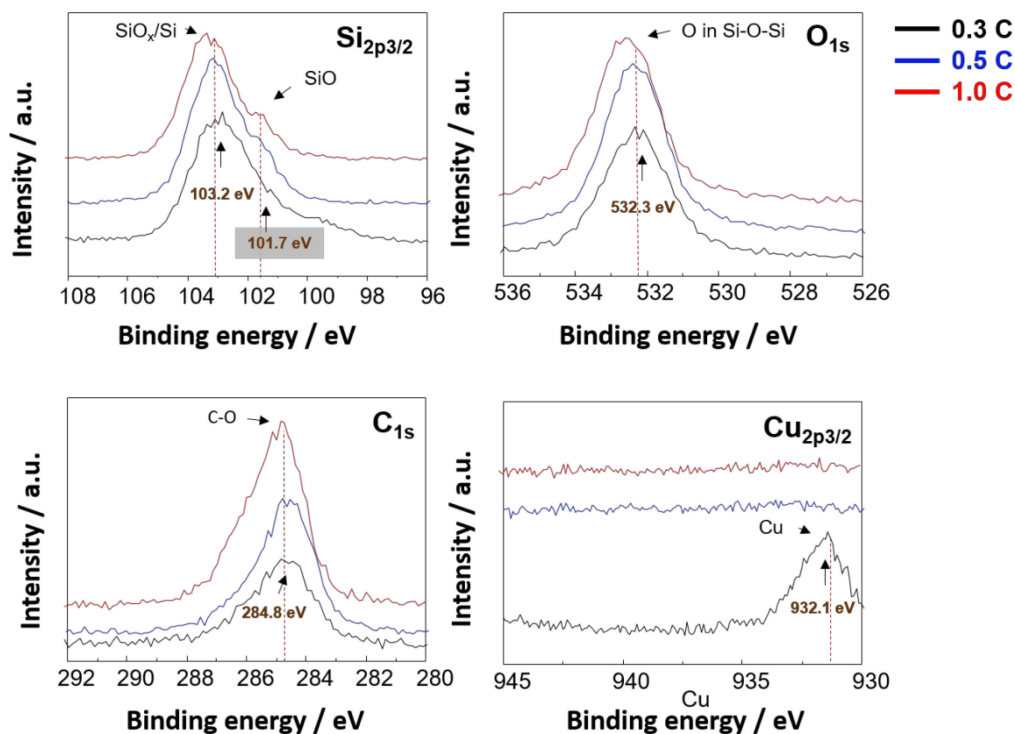


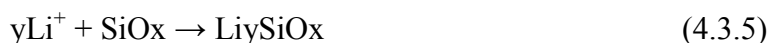
Figure 4.3.8 XPS peaks of $\text{Si}_{2p_{3/2}}$, C_{1s} , O_{1s} , and $\text{Cu}_{2p_{3/2}}$ of Si-O-C composites depending on passing charge of 0.3, 0.5, and 1.0 coulomb cm^{-2} .

4.3.3 Electrochemical investigation of LIC full cell

For cell balancing between CNT cathode and Si-O-C anode, charge/discharge test of each electrode was tested with charge current density of 100 mA g^{-1} . Figure 4.3.9 demonstrates the charge/discharge profile of CNTs cathode and three type of Si-O-C anode depending on passing charge. The CNTs cathode shows charge and discharges areal capacity of 25 and 22 uA h cm^{-2} , respectively. In addition, it was observed that CNTs cathode shows typical charge/discharge curve of a capacitor without intercalation/de-intercalation plateau.

Figure 4.3.9 (b) shows charge/discharge profile of Si-O-C composites depending on passing charge of 0.3 , 0.5 , and $1.0 \text{ coulomb cm}^{-2}$. Each sample has a huge irreversible capacity at charge process which is attributed to conversion reaction of SiO_x to Li_xSi_y and Li_2O and SEI formation of Si-O-C surface as described in chapter 3 and our previous report [14-16]. In addition, Si-O-C composites prepared at 0.3 , 0.5 , and $1.0 \text{ coulomb cm}^{-2}$ of passing charge delivered a discharge areal capacity of 9 , 14 , and 23 uA h cm^{-2} , respectively. CNTs cathode and a Si-O-C anode which have area capacity of 22 and 23 uA h cm^{-2} , respectively, were selected as cathode and anode for LIC full cell. Moreover, its individual charge/discharge profiles were presented in Fig. 4.3.9 (c). From this individual charge/discharge profile, it was confirmed that LIC full cell might be worked with potential range from 4.2 to $2.8 \text{ V vs. Li/Li}^+$.

Before full cell test of LIC consists of CNTs cathode and Si-O-C anode, lithium pre-lithiation of Si-O-C composites was carried out in 1M LiClO_4 dissolved in EC/PC solvent. The Si-O-C composites were lithiated by following reaction equation as mentioned in chapter 3. After pre-lithiation of Si-O-C anode, the color was changed from yellow to black, indicating completion of lithiation. Afterward, the cell was decomposed and re-assembled with CNTs cathode for full cell test.



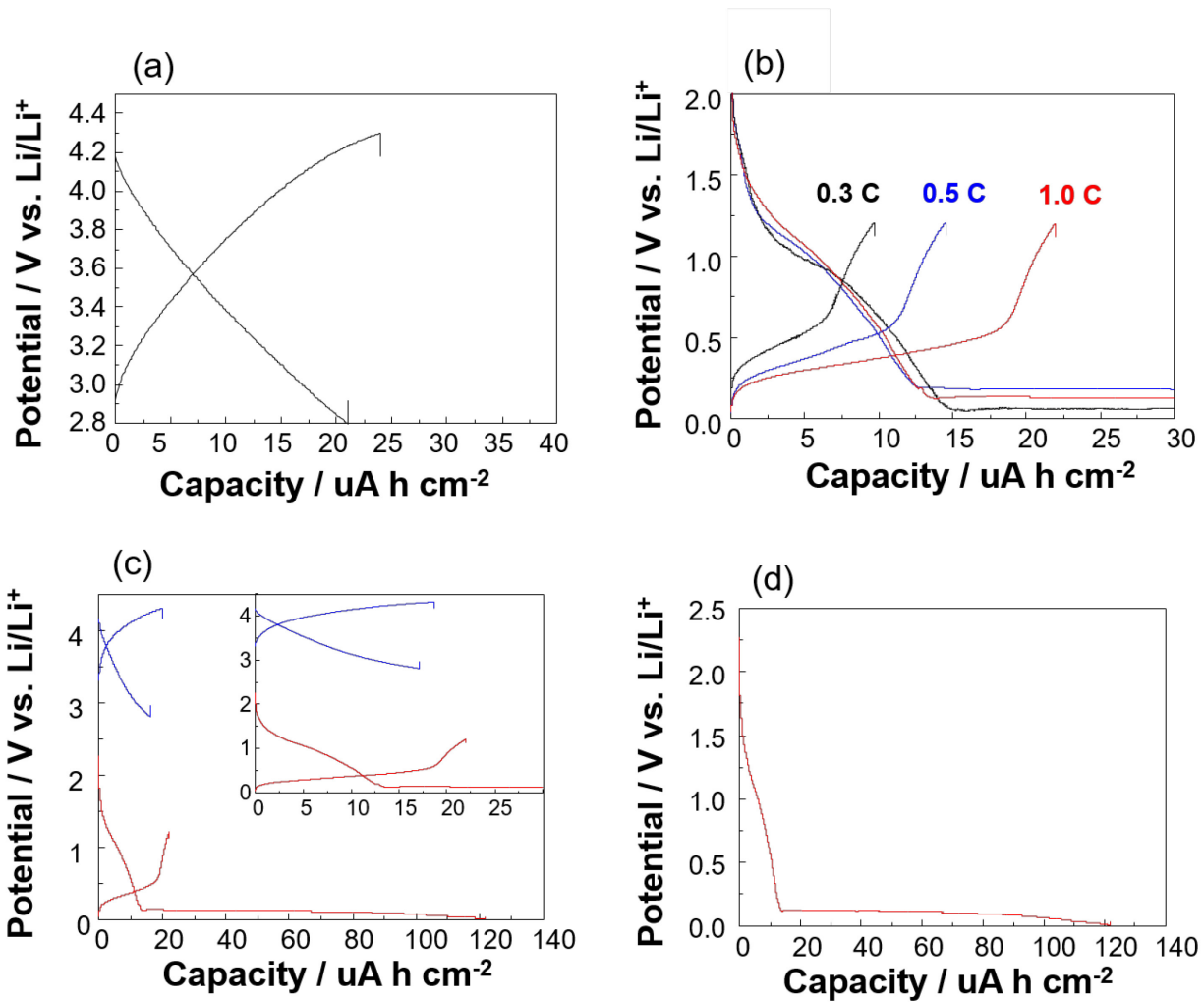


Figure 4.3.9 Charge/discharge profile of (a) CNTs cathode (30min of EPD time), (b) Si-O-C anode depending on passing charge of 0.3, 0.5, and 1.0 coulomb cm^{-2} , (c) individual charge/discharge curve of CNTs cathode and Si-O-C anode, and (d) Charge profile of Si-O-C pre-lithiation.

The cycle ability of LIC full cell consists of CNTs cathode (30min) and pre-lithiated Si-O-C anode ($1.0 \text{ coulomb cm}^{-2}$ of passing charge) for 300 cycles is shown in Fig. 4.3.10 (a). The discharge capacitance of LIC full cell is ca. 17, and 13 F g^{-1} at 1st and 10th cycles. As mentioned half-cell test of CNTs cathode, at the initial cycle, the capacitance was decreased slightly. However, after 10th cycle, the discharge capacitance of LIC full cell is ca. 12 F g^{-1} until 300th cycle. From this result, it was confirmed that LIC full cell shows outstanding cycle ability, which is meaning that Si-O-C anode has the strong possibility as an anode for high rate LIC.

The rate performance of LIC was measured with various current density. As described, the LIC was prepared with thin layer cathode and anode in order to high rate performance LIC. The capacitance retention of LIC was presented in Fig. 3.4.10 (b). Until ca. 100 C-rate, the LIC shows high capacitance retention of ca. 94 %. This high capacitance retention was maintained until ca. 138 C-rate of 88~89%. From this result, it was observed that LIC consists of CNTs cathode and Si-O-C anode has the strong possibility as high rate performance.

Despite the high rate performance, the LIC has low capacitance, indicating it shows low energy density. The main reason of this low capacitance is CNTs cathode. As explained, the CNTs cathode has low capacitance as presented in Fig. 4.3.9 (a). To increase the energy density of LIC, it should be replaced from CNTs cathode to activated carbon as a cathode for the higher energy density of LIC in future work.

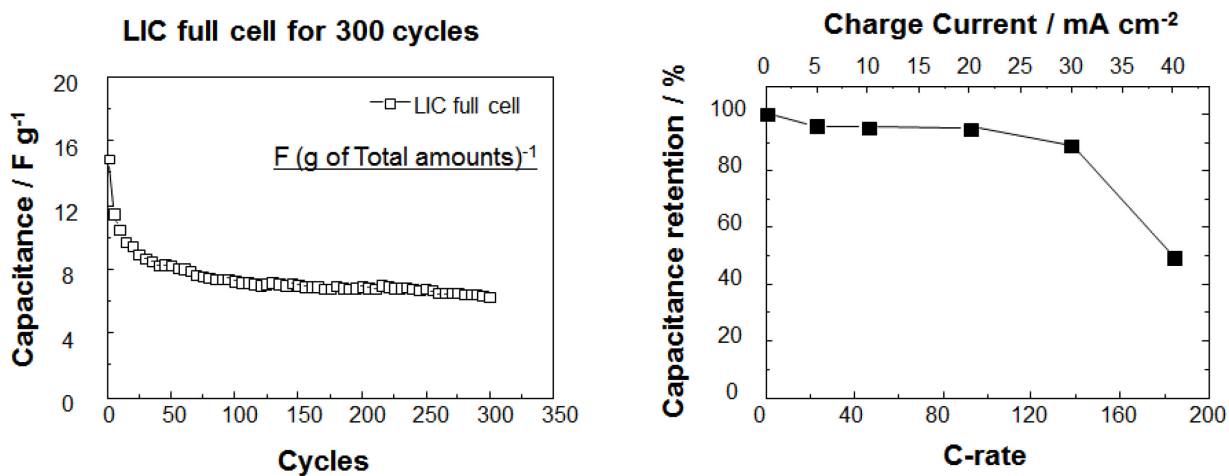


Figure 4.3.10 (a) Cycle abilities of CNTs/Si-O-C full cell for 200 cycles with current density of 100 mA g^{-1} , and (b) rate performance of LIC.

4.4 Summary

In this chapter, Si-O-C composites were applied as an anode for high rate lithium ion capacitor. For a high performance of cathode and anode, both electrodes were synthesized by an electrochemically deposition technique for a thin layered film. CNTs cathodes were fabricated by electrophoretic deposition for 10, 30, and 60 min. Each CNTs cathodes shows typical capacitor behavior of cyclic voltammogram with rectangular shape without any redox peaks. Among them, CNTs cathode prepare for 30 min of electrophoretic deposition shows the best performance as a cathode for LIC, whereas, CNTs by 60 min has the lowest capacitance because of cobalt oxide compounds on its surface and it might be internal resistance. Si-O-C anodes were prepared by electrodeposition at 0.3, 0.5, and 1.0 coulomb cm^{-2} of passing charge. From ICP and XPS result of each Si-O-C anode, it was revealed that deposition rate of Si-O-C composites was increased rapidly after 0.5 coulomb cm^{-2} of passing charge. For cell balancing between CNTs cathode and Si-O-C anode, each half-cell was tested by constant current charge/discharge test with a charge current of 100 mA g^{-1} . From cell balancing, CNTs cathode prepared for 30 min and Si-O-C anode synthesized at 1.0 coulomb cm^{-2} of passing charge were selected for assembling of full cell. The LIC full cell shows outstanding cycle ability for the 300th cycle and rate performance of ca. 88~89 % at 138 C-rate. Although LIC full cell shows not superb discharge capacitance compared with other reported papers, it could confirm that Si-O-C anode has the bright possibility as an anode for high rate LIC.

4.5 References

1. J.-J. Yang, C.-H. Choi, H.-B. Seo, H.-J. Kim, and S.-G. Park, *Electrochim. Acta*, 86 (2012) 277.
2. J.-j. Yang, J.-h. Choi, H.-j. Kim, M. Morita, and S.-g. Park, *J. Ind, Eng. Chem.*, 19 (2013) 1648.
3. T. Tsujikawa, K. Yabuta, T. Matsushita, T. Matsushima, K. Hayashi, and M. Arakawa, *J. Power Sources*, 189 (2009) 429.
4. K. Takano, K. Nozaki, Y. Saito, A. Negishi, K. Kato, and Y. Yamaguchi, *J. Power Sources*, 90 (2000) 214.
5. W. Qu, F. Han, A. Lu, C. Xing, M. Qiao, and W. Li, *J. Mater. Chem. A.*, 2 (2014) 6549.
6. S. R. Sivakkumar, and A. G. Pandolfe, *Electrochim. Acta*, 65 (2012) 280.
7. Q. Wang, Z. Wen, and J. Li, *Adv. Funct. Mater.*, 16 (2006) 2141.
8. J. Chen, K. Sheng, P. Luo, C. Li, and G. shi, *Adv. Mater.*, 24 (2012) 4569.
9. C. V. Schenck, and J. G. Dillard, *J Colloid Interface Sci.*, 95 (1983) 398.
10. B.A. Sexton, A.E. Hughes, and T.W. Turney, *Journal of Catalysis*, 97 (1986) 390.
11. J. C. Dupin, D. Gonbeau, H. B. Moudden, Ph. Vinatier, and A. Levasseur, *Thin Solid Films*, 384 (2001) 23.
12. A. A. Khassin, T. M. Yurieva, V. V. Kaichev, V. I. Bukhtiyarov, A. A. Budneva, E. A. Paushtis, and V. N. PArmon, *J. Mol. Catal. A: Chem.*, 175 (2001) 189.
13. S. Santhanagopalan, F. Teng, and D. D. Meng, *Langmuir*, 27 (2011) 561.
14. H. Nara, T. Yokoshima, T. Momma, and Tetsuya Osaka, *Energy Environ. Sci.*, 5 (2012) 6500.
15. T. Hang, H. Nara, T. Yokoshima, T. Momma, and T. Osaka, *J. Power. Sources*, 222 (2013) 503.
16. M. Jeong, Y. Yokoshima, H. Nara, Y. Momma, and T. Osaka, *J. Power. Sources*, 275 (2015) 525.
17. M. Jeong, S. Ahn, Yokoshima, H. Nara, Y. Momma, and T. Osaka, *Nano energy*, 28 (2016) 51.
18. T. Ohzuku, Y. Iwakishi, and K. Sawai, *J. Electrochem. Soc.*, 140 (1993) 9.
19. X. Wen, C. Ma, C. Du, J. Liu, X. Zhang, D. Qu, and Z Tang, *Electrochim. Acta*, 186

(2015).

Chapter 5

General conclusion

5.1 Conclusion

Lithium ion batteries (LIBs) are one of promising energy storage devices for an electric vehicle, home appliance, and numerous fields because of its many merits. For this reason, it was researched and discussed in this dissertation. Chapter 5 summarizes the results and discussions of this dissertation.

Chapter 1 introduced the history and operation mechanism about energy storage devices, in particular, LIBs. Furthermore, the major components of LIBs were discussed briefly. In addition, current issues about anode materials, in particular, Si-based anode material were described in this chapter. Si-based composites prepared by electrodeposition, namely Si-O-C composites, were introduced as a promising anode material because of its good electrochemical characteristics. Moreover, the motivations and strategies for the realization of high-performance LIBs using 3D structured carbonous substrates were suggested in this dissertation to increase deposited silicon amounts and areal capacity of Si-O-C composites.

In chapter 2, as 3D structured carbonous substrates, carbon paper was employed as a substrate for electrodeposition of Si-O-C composites. By SPM treatment, it could confirm that oxygen-containing functional groups generated on a surface of carbon paper enhance surface affinity and wettability between carbon paper and an organic solvent. As a result, higher deposited silicon amounts and discharge areal capacity could be obtained. Furthermore, exfoliation of a graphitic layer caused by PC molecule was discussed by Raman measurement. It is known well by other reports, PC molecule was decomposed at 1.0 V vs. Li/Li⁺ and co-intercalated into a graphitic layer with lithium ion during charge/discharge process, causing exfoliation of a graphitic layer. Likewise, this behavior was observed in this chapter. After electrodeposition, small amounts of PC remained in Si-O-C composites leads to exfoliation of a graphitic layer in carbon paper, resulting in low cycle abilities by rapid capacity fading of Si-O-C composites. To overcome low cycle ability, EC/DEC organic solvent was used as an electrolyte for electrodeposition of Si-O-C composites. As a result, it was achieved that improved cycle ability even high charge current density, in comparison to usage of PC organic solvent. Moreover, high amounts of areal capacity could be obtained by employing 3D structured carbon paper through this chapter. So far, discharge areal capacity of 0.7 mA g cm⁻² was reached as highest values by a nickel-copper substrate in our groups. However, higher discharge areal

capacity of $2.75 \text{ mA h cm}^{-2}$ could be obtained because of a higher surface area and good electric conductivity of carbon paper. From this attempt, it was obvious that usage of carbon paper which has 3D structure properties has a high possibility for high-energy lithium batteries.

In chapter 3, another attempt was introduced using 3D structured carbonous substrate using CNTs to enhance adhesion strength and stability of Si-O-C composites. The possibilities for improving deposition rate of Si-O-C composites and discharge areal capacity were confirmed through the usage of carbon paper in chapter 2. However, instability of Si-O-C composites was also observed by PC solvent. To overcome this problem, CNTs anchor layer was synthesized by electrophoretic deposition on a copper substrate as 3D structured characteristic. To control the electrophoretic depiction of CNTs anchor layer, appropriate amounts of CoCl_2 was used as an additive to impart positively charge on a surface of CNTs. As a result, 3D structured properties such as rough surface, a higher surface area could be obtained. The relationship between surface area and reactivity was discussed in this chapter by cyclic voltammogram. Therefore, it was confirmed that improved surface area by CNTs anchor layer is one of a reason for higher deposited amounts of silicon, in comparison to an as-received copper substrate. Enhanced rate performance of Si-O-C composites deposited on CNTs anchor layer was observed due to a high electric conductivity of CNTs, resulting in reduced internal stress during charge/discharge process. In addition, CNTs anchor layer enhances adhesion strength between Si-O-C composites and copper substrate. As a result, higher deposited amounts of silicon was obtained even at $15 \text{ coulomb cm}^{-2}$ of passing charge, whereas, as-received copper substrate shows peeling off of Si-O-C composites at $8 \text{ coulomb cm}^{-2}$ of passing charge because of its weak adhesion strength. Moreover, developed structural stability of Si-O-C composites also identified by surface morphological observation using FE-SEM measurement before and after 100 cycles of charge/discharge test. As a result, the non-cracked surface was detected from Si-O-C composites deposited on CNTs anchor layer, in comparison to as-received copper substrate shows cracked surface. From above results from optical and electrochemical measurement, it was revealed that CNTs anchor layer can play a role as not only electric pathway to reduce internal stress but also supporting material to prevent structural disintegration and enhanced adhesion strength between Si-O-C composites and copper substrate.

In chapter 4, Si-O-C composites were applied as an anode for high rate lithium ion capacitor.

For this chapter, CNTs cathode and Si-O-C anode were synthesized by electrochemically deposition, electrophoretic deposition for cathode and electrodeposition for an anode. These thin cathode and anode were employed for a lithium ion capacitor full cell. It was confirmed that excessive time of electrophoretic deposition lead to a formation of cobalt oxide compounds on the surface of CNTs and this compounds could play a role as resistances, resulting in low rate performance. The thin CNTs cathode prepared by electrophoretic deposition has discharge capacitance of ca. 20 F g⁻¹ and outstanding cycle ability for a 5000th cycle, meaning that electrophoretic deposition is a good way to fabricate thin composites as an electrode for energy storage devices. After cell balancing of CNTs cathode and Si-O-C anode, lithium ion capacitor full cell delivered a discharge capacitance of 10~12 F g⁻¹ for 300 cycles with good cycle abilities, which is corresponding to CNTs half-cell test. From this chapter, the applicability of Si-O-C composites for other energy storage devices was verified.

Throughout this dissertation, it is tried to realize high energy LIBs using two kinds of 3D structured carbonous substrate. One is the carbon paper which was used as a substrate for electrodeposition of Si-O-C composites and another one is CNTs anchor layer deposited on a copper substrate. These two kinds of substrate enhance deposited amounts of silicon and electrochemical characteristics, resulting in higher discharge areal capacity, in comparison to the as-received copper substrate. From material and electrochemical measurements, it is clear that usage of the 3D structure carbonous substrate is a remarkable attempt for improvement of LIBs. Moreover, the applicability of Si-O-C composites as an anode for lithium ion capacitor was discussed through this dissertation. This new approach demonstrates the various availability of Si-O-C composites toward other energy storage devices as anode active the material. Ultimately, it could be believed that high energy LIBs can be realized by above attempts for next generation energy storage device.

List of achievements

1. Publication

Original papers

1. Electrophoretically deposited carbon nanotube anchor layer to improve areal capacity of Si-O-C composite anode for lithium secondary batteries, *Journal of Power Sources*, 336 (2016) 203-211, S. Ahn, M. Jeong, T. Yokoshima, H. Nara, T. Momma, T. Osaka.
2. Development of areal capacity of Si-O-C composites as anode for lithium secondary batteries using 3D-structured carbon paper as current collector, *Journal of The Electrochemical Society*, 164 (2017) A355-A359, S. Ahn, M. Jeong, K. Miyamoto, T. Yokoshima, H. Nara, T. Momma, T. Osaka.
3. New Approach for Enhancing Electrical Conductivity of Electrodeposited Si-Based Anode Material for Li Secondary Batteries: Self-Incorporation of Nano Cu Metal in Si-O-C Composite, *Nano Energy*, 28 (2016) 51-62, M. Jeong, S. Ahn, T. Yokoshima, H. Nara, T. Momma, T. Osaka.

2. Presentation

Oral presentation

1. Electrochemical preparation of CNTs-coated Cu substrate for Si-O-C composite deposition and characteristics of Si-O-C/CNTs/Cu as an anode of Li secondary batteries, *ECS 228th meeting*, Phoenix, USA, October 2015, S. Ahn, M. Jeong, T. Yokoshima, H. Nara, T. Momma, T. Osaka.
2. Enhanced adhesion strength between Si-O-C composites and Cu substrate by introducing of CNTs layer via electrophoretic deposition, 第 57 回電池討論会, 千葉, 11 月 2016, S. Ahn, M. Jeong, T. Yokoshima, H. Nara, T. Momma, T. Osaka.

Poster presentation

1. Si-O-C composites prepared by electrodeposition on CNTs/Cu or carbon paper substrate and electrochemical performance for lithium ion battery, *PRIME 2016* 2016, S. Ahn, M. Jeong, T. Yokoshima, H. Nara, T. Momma, T. Osaka.
2. Electrodeposited Si-O-C Composite Anode with High Durability for Coming Lithium Secondary Batteries, *3rd Euro-Mediterranean Conference on Materials and Renewable Energies*, Marrakech, Moroko, November 2015, H. Nara, S. Ahn, T. Yokoshima, T. Momma, T. Osaka.
3. A study on the performance of Si-O-C anodes with CNTs/Cu substrates for lithium secondary batteries, *3rd DGIST-WASEDA workshop*, Tokyo, Japan, December 2015, S. Ahn, M. Jeong, T. Yokoshima, H. Nara, T. Momma, T. Osaka.

Acknowledgement

I was afraid when I decided to go to Japan for a doctoral degree because I didn't know well about electrochemistry and Japanese. However, there are too many good people in our laboratory, so I could do it well without big troubles. Thus, I would like to appreciate for a lot of people who help my journey for a doctoral degree in Waseda University.

At first, I would like to express my supervisor, Professor Dr. Toshiyuki Momma, for his supporting and advice. He gave me much of scientific idea for my research and greatly encouraged when I have some trouble including scientific and financial thing. In addition, he gave me a lot of chance to attend conferences in the world, so I could do my presentation in many countries. I think it is was a great lucky to be a student of his laboratory.

Also, I want to appreciate Professor Dr. Tetsuya Osaka. When I came here, I had a critical financial problem because of miss connection. So I worried seriously that I can continue my doctoral program for three years. However, I could do it due to his supporting and recommendation for MEXT scholarship. In addition, he showed me a lot of visions for the future as scientist and researcher. I cannot forget his warmth, passion, and acceptance when I belonged in this laboratory.

I would like to express my sincere appreciation to Professor Dr. Soo-Gil Park (Chungbuk National Univ.) for giving me many chances to go many countries as presentation, an exchange student, internship, and visiting research since I was bachelor student. Through many global activities, I'm able to learn various thing not only languages but also scientific knowledge.

I want to appreciate to Dr. Yoshiyuki Sugahara and Professor Dr. Takayuki Homma for reviewing my doctoral defense and thesis. The sensei's comments make my thesis better.

I also wish to express my appreciation to Dr. Tokihiko Yokoshima, Dr. Hiroki Nara, Dr. Sho Hideshima, Dr. Masahiro Kunimoto, and Dr. Norihiro Togasaki for their warmest advice. As teacher and senior, they help my papers, presentation, doctoral defense, and thesis. And I cannot forget the Japan life with my two Korean senior, Dr. Moongook Jeong, Dr. Jeongjin Yang. We have really good memories in Japan. So I want to say thank you them and their advice.

I want to appreciate the warmest gratitude to all colleagues in battery group in our laboratory

for sharing good memories and campus life, especially Mr. Shohei Seko, Mr. Taku Owada, Mr. Takahiro Kadoya and Mr. Tomohiro Inoue, and Mr. Yusuke Nakamura in silicon group. In addition, I would like to thank all doctoral candidates in our group, Mr. Yoshiki Fujihira, and Ms. Yunwen Wu.

And last but not least, herein, I would like to thank for my beloved family, my parents and young sister for encourages my decision, supporting my Japan life, and raising me through happy and difficult times alike. Sometimes there was a hard time, but now I am happy as my parent's son and one of my Family. Thank you again, my father, mother, and my little sister.

February 2017
Seongki Ahn